

**UNCLASSIFIED**

**AD** **407 584**

**DEFENSE DOCUMENTATION CENTER**

**FOR**

**SCIENTIFIC AND TECHNICAL INFORMATION**

**CAMERON STATION, ALEXANDRIA, VIRGINIA**



**UNCLASSIFIED**

**NOTICE:** When government or other drawings, specifications or other data are used for any purpose other than in connection with a definitely related government procurement operation, the U. S. Government thereby incurs no responsibility, nor any obligation whatsoever; and the fact that the Government may have formulated, furnished, or in any way supplied the said drawings, specifications, or other data is not to be regarded by implication or otherwise as in any manner licensing the holder or any other person or corporation, or conveying any rights or permission to manufacture, use or sell any patented invention that may in any way be related thereto.

**AD No 407584**

**DDC FILE COPY**

**407 584**

FINAL TECHNICAL REPORT  
FEASIBILITY STUDY OF  
TERRAIN SENSORS AND TERRAIN SENSING  
Contract No. DA-04-495-ORD-3569

**DDC**  
**REC'D**  
**JUN 20 1963**  
**TISIA A**

**\$ 15.50**

**Best  
Available  
Copy**

(4) #15.5, (5) 298 440

(9) ~~FINAL TECHNICAL REPORT~~

(15) CONTRACT No. DA-04-495-ORD-3569

Ordnance Project No. \_\_\_\_\_

(1) FEASIBILITY STUDY OF  
TERRAIN SENSORS AND TERRAIN SENSING

(12) by  
Harry F. Gilmore, Jr.,  
Richard C. Ramsey  
and  
Thomas R. Fahy.

Spectral Technology and Applied  
Research Division  
Emerson Electric Manufacturing Company  
322 Palm Avenue, Santa Barbara, California

Performed Under the Technical Supervision of the  
Research and Engineering Directorate  
Army Tank-Automotive Command, and the  
Compliance of the Los Angeles Procurement District, U.S. Army

(11) 28 December 1962

(7) NA  
(8) NA  
(12) 22 x 10.  
(13) NA  
(14) NA  
(16) NA  
(17) NA  
(18) NA  
(19) NA  
(20) U  
(21) NA

A.C.

ABSTRACT CARD

- 1) AD \_\_\_\_\_ ACCESSION \_\_\_\_\_
- 2) Prepared by: Emerson Electric, STAR Division, Santa Barbara, California
- 3) Final Technical Report, Feasibility Study of Terrain Sensors and Terrain Sensing (U)
- 4) Authors: Harry F. Gilmore, Jr., Richard C. Ramsey, Thomas R. Fahy
- 5) 228 pages, 0 text illustrations (40 sheets), 1 table
- 6) Contract No. DA-04-495-ORD-3569
- 7) Department of the Army Project No. \_\_\_\_\_.
- 8) Research and Engineering Directorate, Army Tank-Automotive Command
9. 28 December 1962
10. Optical techniques were studied for application in a terrain sensor which measures the profile and consistency of the terrain ahead of a cross-country military vehicle and provides information for the actuation of an active vehicle suspension system. Automatic optical ranging techniques were found to be eminently suitable for terrain profile sensing. Optical methods of spatial and spectral analysis of an image of the terrain were shown to have considerable promise for consistency determination. Preliminary designs for equipment for terrain profile and consistency sensing are used as a basis for performance evaluation.
11. (Information needed on categories available)
12. Report is unclassified
13. Abstract card is unclassified

ABSTRACT

Optical techniques were studied for application in a terrain sensor which measures the profile and consistency of the terrain ahead of a cross-country military vehicle and provides information for the actuation of an active vehicle suspension system. Automatic optical ranging techniques were found to be ~~adequately~~ suitable for terrain profile sensing. Optical methods of spatial and spectral analysis of an image of the terrain were shown to have considerable promise for consistency determination. Preliminary designs for equipment for terrain profile and consistency sensing are used as a basis for performance evaluation.

## TABLE OF CONTENTS

	<u>Page</u>
OBJECT	1
SUMMARY	3
CONCLUSIONS AND RECOMMENDATIONS	10
Major Conclusions	10
Recommendation	10
INTRODUCTION	11
SENSOR REQUIREMENTS	15
General Requirements	15
Geometrical Model	21
Performance Requirements	23
OPTICAL RANGING METHODS	39
Active C-W Rangefinder	40
Image-Plane Rangefinding	58
Triangulation Tracking	77
Triangulation Tracking Using Correlation	82
Laser Rangefinding	84
STABILIZATION AND COMPUTATION REQUIREMENTS	87
Assumptions	87
Stabilization Problems	87
Computation Requirements	92
CONSISTENCY DETERMINATION	112
Consistency Model of Terrain	114
Consistency Measurements	115
Spatial Detail Analysis	116

## TABLE OF CONTENTS

	<u>Page</u>
Spectral Reflectance Analysis	117
Wet Objects	127
Ditches	129
Snow	131
Measurements Program	133
Conclusions	142
PRELIMINARY DESIGN	143
Choice of Ranging Technique	143
Choice of Computation Method	144
Preliminary Optical Design	147
Computation Equations for Preliminary Design	150
Preliminary System Block Diagram	155
Consistency Sensor Design	158
Optical Considerations	166
Modulation In the Terrain Sensor	177
LIMITS ON SENSOR OPERATION	182
Introduction	182
Effect of Atmospheric Turbulence	182
Effect of Climatic Conditions	187
Day or Night Operation	192
Range Limitations	193
HUMAN FACTORS ENGINEERING	196
APPENDIXES:	197
A. Derivation of Equations for Active C-W Ranger	197
B. The Multiplier Phototube	200
C. Experimental Data on Rangefinding by Image - Plane Location	211

## ILLUSTRATIONS

<u>Fig. No.</u>	<u>Page</u>
1. Geometrical Model for Study	22
2. Reaction Time vs. Speed for Geometrical Model	22
3. Representation of Simple Obstacle	26
4. $p(t)$ vs. $t$ for Simple Obstacle and Constant $v$	26
5. $\beta(t)$ and $L \{ p(t) \}$ vs. $t$ for Simple Obstacle and Constant $v$ .	29
6. Computed Profile for Simple Obstacle for Various Values of Averaging Time, $a$ .	29
7. Beam-Ground Geometry	32
8. Effect of Range Error $\Delta R$	32
9. Axle Path for 2-ft.-radius Wheel and 1-ft-square obstacle	35
10. Effective Shape of Obstacle for Conditions of Figure 9.	35
11. Sensor Shadow Geometry	37
12. Terrain Variations Giving Differing Axle Response but Same Sensor Response	37
13. Geometry for Axle-Error Computation	38
14. Axle Error vs. Obstacle Height for Wheels of 1-ft and 2-ft. radius.	38
15. Parameters $\Omega$ , $D_0$ , $w$ to Determine $f_{\max}$ (cps), for Use in Figure 18 to Find $\Delta R$ .	54
16. Relationship Between Parameters $f_{\max}$ and $R$ for Use in Figure 18 to Find $\Delta R$ .	55
17. Relationship Among Parameters $\rho$ , $b_H$ , $D_R$ for Use in Figure 19 to Find $\Delta R$ .	56

## ILLUSTRATIONS

<u>Fig. No.</u>	<u>Page</u>
18. Determination of $\Delta R$ (inches)	57
19. Energy Distribution Near Focus, and Resulting Waveform	66
20. Tracker Geometry	81
21. Illuminated Portion of Terrain as Seen by Tracker	81
22. Simple Geometry for Range Measurement	89
23. Effect of Cant on Terrain Measurement	89
24. Parameters Used for Terrain Measurement	95
25. Functional Block Diagram of Computation Process	98
26. Error in Calculated Value of $y$ for Sine Wave Terrain Input, for Various Values of $y_{pk}$ Produced by Constant 45 deg Slope.	107
27. Functional Block Diagram of Alternate Computation Process	110
28. Spectral Reflectance for Eleven Types of Natural Objects as Measured by Krinov	119
29. Three-Color Diagram for Sunlight Reflected From Natural Objects	122
30. Three-Color Diagram for 3000°K Incandescent Tungsten Light Reflected From Natural Objects	123
31. Three-Color Diagram for Sunlight and Corrected Values for Artificial Light Reflected From Natural Objects	124
32. Suggested Laboratory Setup for Spectral-Spatial Analysis	137
33. Field Test Equipment	140
34. Preliminary Optical Design	148
35. Dual-Thickness Chopper	149
36. Terrain Sensor Geometry	151
37. Pitch-Axis Geometry	151
38. System Functional Block Diagram	156

## ILLUSTRATIONS

<u>Fig. No.</u>	<u>Page</u>
39. Rotating Filter Wheel for Spectral Analysis	159
40. Rotating Chopper Wheel for Texture Analysis	161
41. Consistency Sensor Optics and Detector	163
42. Hypothetical Chopping Disk	164
43. Block Diagram of Data Processing System	165
44. Fraction of Total Energy Emitted by a Blackbody at Temperature T Observable by Multiplier Phototubes With 5-11 and 5-20 Phosphors, and by The standard Observer.	206
45. Relative Spectral Response of Multiplier Phototubes with 5-11 and 5-20 Phosphors, and of the Standard Observer ( $K_\lambda$ ).	208
46. Total Illumination on the Horizontal Plane, $I_{H\lambda}$ , From Direct Sunlight and Skylight, Versus Solar Altitude,	209-a
47. Measured Relative Signal Response as a Function of Chopper Position for the Laboratory System	215
48. Theoretical Curve of Relative Signal Response as a Function of Chopper Position for the Laboratory System	221
49. Measured Relative Signal Response as a Function of Chopper Position for the Laboratory System With Sharply Defined Field Stop	223
50. Measured Relative Signal Response as a Function of Chopper Position for the Laboratory System Without Sharply Defined Field Stop	224

## OBJECT

The object of Contract No. DA-04-495-ORD-3569 is the conduct of a feasibility study of the techniques and processes required to provide a system for gathering and presenting terrain intelligence data, in accordance with the requirements specified in Research and Engineering Purchase Description No. 62-32.

The ultimate objective of this program is to allow Ordnance military vehicles to maintain greatly increased speeds over cross-country terrain. This objective can be accomplished through the use of an active suspension system. Such a suspension system requires four separate components: a terrain sensor, a sensor suspension computer, a suspension controller, and an active suspension system. The present study is devoted to the terrain sensor component.

It is required that:

1. The sensor or sensors shall operate without any mechanical part between the vehicle and the terrain being sensed.
2. The sensor, or sensors, shall not be based on inertial techniques.
3. The final technical report shall include the following information on each technique:
  - a. Limitations on sensing distance from the vehicle.
  - b. Limitations imposed on sensors by climatic conditions.
  - c. Limitations of sensors on obtaining accurate information on obstacle size and shape.
  - d. Limitation of sensors on obtaining accurate information on

consistency of obstacle or terrain.

The specific object of the study conducted by Emerson Electric is the preliminary design of a sensor embodying optical ranging, together with a detailed analysis of its effectiveness in determining terrain contour and consistency under various climatic, tactical, and terrain conditions.

## SUMMARY

The study of optical ranging techniques for the determination of terrain profile and of optical techniques for determining terrain consistency requires first the analysis of the tactical, climatic, and environmental requirements on the terrain sensor, and the specification of the desired performance characteristics. The most important of these requirements are:

1. No restrictions exist on the use of active optical systems.
2. The aperture in the vehicle must be less than 6 inches in diameter.
3. The sensor is mounted 5 feet above the terrain.
4. A vertical axis in the vehicle is held to within  $5^{\circ}$  of vertical in pitch and  $15^{\circ}$  in cant by the active suspension system.
5. The measured terrain profile should be within two inches of the true profile.
6. Maximum vehicle speed is 50 mph.
7. The post-sensor system has a reaction time of 1/2 second.
8. The effect of turns is not considered during this study.

On the basis of these restrictions, the following requirements were placed on the terrain sensor:

1. Obstacles in the two tracks of the vehicle must be measured individually, so two sensors are required.
2. The horizontal distance from the sensors to the points at which their line-of-sight intersects level terrain is 44 feet.

3. The vertical field of view of the sensor should be about 5 milliradians; the horizontal field of view should be about 20 milliradians.
4. The electrical bandwidth of the system should be 16 cps; a trade-off can be made between bandwidth and the vertical field of view of the sensor.
5. Range to the terrain should be measured to an accuracy of  $\pm 2$  inches.

Various optical ranging techniques were evaluated for this application. These included ranging by image plane location (passive), phase comparison (active), triangulation tracking (active), triangulation using image correlation (passive), and pulsed lasers (active). It was found that the first two had adequate range accuracy for this application. Ranging by image plane location was selected as most suitable for the following reasons:

1. This method has a greater inherent accuracy and thus is less affected by adverse conditions than other techniques investigated.
2. The system is passive under normal daylight operation, leading to simplicity and security.
3. Only one station is required for each track (two per vehicle) as required by active systems and those based on triangulation. This leads to simplicity of installation and alignment.
4. For night operation a source of light on the vehicle is required for any of the systems. The system permits a considerable freedom of choice, since the source may be either a very narrow

beam boresighted with the sensor, which leads to good security, or may cover a broad area as do conventional headlamps.

5. This ranging method is based on well-known optical principles and does not require the development of a technique.
6. Certain of the parameters have already been investigated experimentally to verify calculations.
7. The equipment configuration is relatively simple - apparently as simple as the equipment for any other method. This leads to low cost and high reliability.

The stabilization and computation necessary for terrain sensing were studied within the framework established by the previous requirements.

It was determined that the following stabilization errors were allowable:

1. The r.m.s. error in knowledge of the elevation of the terrain sensor above the terrain is 1.0 inch.
2. The r.m.s. error in knowledge of the elevation of the terrain with respect to a vertical reference level is 1.0 inch. (This and the previous error may be combined to imply that the elevation of the terrain sensor above the vertical reference level must be known with an r.m.s. error of 1.4 inches.)
3. The r.m.s. error in the terrain sensor depression angle must be less than 0.11 degree.
4. Under worst conditions, 2 degrees of cant is allowable; with proper vehicular mounting, considerably greater errors can be tolerated.

The computation process was studied by writing the equations which must be solved in order to determine the terrain profile a fixed distance ahead of the vehicle from the range-to-terrain measurements made by the sensor. Two techniques were considered. In the first the terrain sensor looks out with a fixed depression angle and measures range-to-terrain. This technique requires a buffer storage element, because measurements are made at varying distances ahead of the vehicle. The second technique consists of adjusting the depression angle so that range is always measured to a point a fixed horizontal distance ahead of the vehicle. This process does not require a buffer storage, and while it does require adjusting the depression angle, such an adjustment is required for pitch stabilization in any case. Hence the latter method was chosen as most appropriate.

The analysis of the computation process showed that deriving an accurate terrain profile required an independent measure of the actual vertical motion of the sensor. This may be provided with the required degree of accuracy by an accelerometer incorporated as an integral part of the sensor.

In order to determine consistency by reflected optical radiation it is necessary to classify objects which may be encountered according to their consistency, and then attempt to discover properties of the reflected optical energy which correlate with the assigned consistencies. This process was first studied qualitatively by listing a number of obstacles and considering how they differed optically; it was decided

that many different obstacles could be distinguished on the basis of color and texture. Adequate data was discovered to demonstrate convincingly that measurable spectral differences exist between different types of terrain. No quantitative information on texture differences was discovered; however, everyday experience leads to the conclusion that equally pronounced texture differences exist. Therefore it appears that a combination of spectral and texture analysis can be used as a basis for the design of a useful consistency sensor.

Using the above choices of ranging and computation methods, a preliminary sensor design was produced. The essential parts of the contour sensor are:

1. A flat elliptical mirror, about 3-1/2 inches by 4 inches, which directs energy onto a folding mirror and then onto the primary mirror, and which can be rocked to adjust the depression angle.
2. A 3-inch-diameter parabolic primary mirror.
3. A chopper which interrupts the incident radiation in such a way as to provide an unambiguous indication of the location of the image plane.
4. A photomultiplier which generates an electrical signal as a function of the incident radiation.
5. Electronics to derive error signals from the photomultiplier output.
6. Mechanical components to rapidly adjust the flat elliptical mirror to reduce the error signals to zero.
7. Electrical readout components, which convert the resulting angular position of the flat elliptical mirror to terrain

elevation a fixed distance ahead of the vehicle.

8. Sensors of vertical acceleration and pitch which allow the optical system and the output to be adjusted for these effects.

The terrain sensor also contains a consistency sensor which uses spatial and spectral analysis to automatically determine the nature of obstacles; this is described in less detail.

The requirements on the various optical elements are specified; all of the elements are within the current state-of-the-art.

It is observed that in the design of an automatic ranging system based on image plane location, field chopping, which results in a spurious signal independent of the location of the image plane, must be held to a minimum. Also, the modulating frequencies must be chosen outside the range of frequencies generated by motion of the terrain through the field of view of the instrument.

Atmospheric conditions limit the operation of the terrain sensor. Atmospheric turbulence and its effects in producing scintillation, image motion, and image blur are considered. Because of the short ranges involved and the moderate resolution requirements on the optical system, no significant degradation in performance is anticipated as a result of atmospheric turbulence. Atmospheric climatic conditions, fog, haze, dust, rain, and snow reduce atmospheric transmission and thus degrade the

performance of optical instruments. Calculations made of the effects of these conditions on the terrain sensor indicate that adequate terrain contour measurements can be made when the visual range is only about 50 feet. Thus the terrain sensor will be effective under most climatic conditions.

The possibility of extending the range of the terrain sensor is considered. If the same actual field of view is maintained, the terrain sensor has a 2-inch range accuracy at 220 feet. However, using terrain information obtained at long ranges may require very accurate velocity information, increases the effect of vehicle maneuvers, and accentuates the shadow problem (the effect of high terrain points concealing lower parts of the terrain behind them).

Finally, independently conducted laboratory experiments on range-finding by image plane location are discussed. These experiments verify the signal-to-noise ratio calculations made in analyzing the ranging technique, and demonstrate the rate at which the detector output falls off as the chopper moves out of the plane of best focus. They also illustrate the effect of field chopping mentioned above.

## CONCLUSIONS AND RECOMMENDATIONS

### MAJOR CONCLUSIONS

1. An effective contour sensor making use of automatic optical range-finding and meeting tactical and environmental requirements is feasible.
2. Optical techniques for consistency determination, based on spatial and spectral analysis of an optical image of the terrain, are extremely promising.
3. Contour sensing, consistency sensing, and the required data handling circuitry can be combined in a single, relatively small equipment.

### RECOMMENDATIONS

It is recommended that a measurements program be conducted to acquire data which will lead to the most effective optical technique for consistency determination.

## INTRODUCTION

This is the final technical report under Contract No. DA-04-495-ORD-3569 for a Feasibility Study of Terrain Sensors and Terrain Sensing.

The contract calls for a six-month feasibility study of the techniques and processes required to provide a system for gathering and presenting terrain intelligence data in accordance with the requirements specified in Research and Engineering Purchase Description No. 62-32. Work under the contract began in July, and was completed in December of 1962. The work was performed by personnel of Emerson Electric's Spectral Technology and Applied Research (STAR) Division, at Santa Barbara, California, under the direction of Mr. M. L. Michaelson of the Army Tank Automotive Command, who contributed much information and many helpful suggestions.

The ultimate objective of this program is to allow military vehicles to maintain greatly increased speeds over rough terrain. This objective can be accomplished through the use of an active suspension system. Such a suspension system requires four separate components: a terrain sensor, a terrain suspension computer, a suspension controller, and an active suspension system. The present study is devoted to the terrain sensor component.

The approach to the terrain sensing problem involves the use of an automatic optical rangefinder operating in the visible spectral region. The rangefinder continuously measures the distance from the vehicle to the terrain ahead of the vehicle along a depressed line of sight; knowledge

of this range, the depression angle, and the distance of the sensor above the terrain at the time of measurement allows a continuous profile of the ground ahead of the vehicle to be produced as the vehicle moves. Additional information about the consistency of the terrain and obstacles is obtained by spatial and spectral analysis of the radiation received from the terrain.

The results of the study show that terrain profile data to the required degree of accuracy can be obtained by optical ranging. The study also shows that optical methods hold excellent promise of providing information on the consistency of the terrain and obstacles to be traversed; however, the detailed field data necessary to provide definitive results is not currently available.

The following section of this report presents an analysis of the tactical, climatic, and environmental requirements on the terrain sensor, and sets forth the performance characteristics desired from the sensor in terms of the terrain information that is needed, including resolution, range accuracy, information rate, and security. This information provides the essential framework for the study.

Next, consideration is given to the various types of optical range-finding methods that might be useful in the terrain sensor system, and to a number of computational procedures that could be used to derive terrain profile information. Optical methods for terrain consistency determination are then examined.

From the various possible approaches, a terrain-sensor system is then selected based on passive ranging (image-plane location) and a computation process that requires varying the depression angle in such a way that the horizontal distance to the point measured is always constant. This combination is recommended as providing the simplest and most reliable approach to a practical terrain-sensor system. A preliminary design for a system incorporating the features recommended is then presented.

The final section of the report provides a performance analysis of the system adopted in the preliminary design, including the limitations on sensing distance from the vehicle, on obtaining accurate information on obstacle size and shape, on obtaining accurate information on the consistency of obstacles or terrain, and on operation under various climatic conditions. The directions in which performance can be extended are indicated. A brief discussion of human factors is also included.

The appendixes include a number of detailed technical discussions which it was felt would interfere with the continuity of the narrative if presented in the body of the report. Also included as an appendix is a report on the results of a laboratory study of certain aspects of passive ranging conducted by Emerson Electric under its company-sponsored research program. This laboratory data is included here because it provides strong confirmatory evidence that the ranging method adopted in the preliminary design can attain the predicted level of performance.

It is required by the contract that this final report shall include the following information on each technique investigated:

- a. Limitations on sensing distance from the vehicle.
- b. Limitations imposed on sensors by climatic conditions.
- c. Limitations of sensors on obtaining accurate information on obstacle size and shape.
- d. Limitations of sensors on obtaining accurate information on consistency of obstacles or terrain.

This information cannot be adequately summarized here, but will be found in the following sections of this report entitled:

- a. Limits on Sensor Operation -- Range Limitations.
- b. Limits on Sensor Operation -- Effect of Climatic Conditions.
- c. Sensor Requirements.
- d. Consistency Measurements.

## SENSOR REQUIREMENTS

### GENERAL REQUIREMENTS

In order to provide a framework for the study, it is necessary to analyze the tactical, climatic, and environmental requirements on the terrain sensor and to specify the desired performance characteristics in terms of the terrain information which is needed, including resolution, range accuracy, information rate, and security.

As a first step in accomplishing this, a list of questions was drawn up; the answers to these questions establish reasonable requirements for a terrain sensor system meeting the aims expressed in the REPD.

The questions fall into four categories: 1) those on shock, vibration, heat, and other environmental requirements; 2) those concerned with climate and use times; 3) questions of vehicle security; and 4) a number of questions concerning the use of the device which may be grouped under the heading of geometry.

Since at this stage we are not concerned with actual design of equipment, the only specific question on environment which is important at present is the amount of vibrational displacement of the sensor from a smooth path in space, since this displacement may interfere with the required measurement.

With respect to climatic requirements it is desired to know the range

of ambient light levels within which the equipment is to operate, and the effects of climatic conditions on atmospheric transmission and on the optical characteristics of various terrain features.

The two questions on security are 1) how large an aperture in the vehicle can be allowed, and 2) is there any restriction on the use of an active system operating in a) the visible region, and b) the infrared region?

A number of questions related to geometry may be asked. These are:

1. What is the vehicle type - track laying or non-track laying?
2. What is the elevation above the terrain of the sensor location?
3. How much pitch and cant of the vehicle hull may be expected?  
(This is related to the question on vibration given earlier.)
4. How much short-term vertical motion of the sensor with respect to a fixed reference level may be expected? (This and the above question relate to the expected effectiveness of the active suspension system.)
5. How accurately is the elevation of the sensor above the terrain known? (It is expected that this knowledge is required for terrain computation.)
6. How large an obstacle is important?
7. How accurately must the profile be determined?
8. Is it desirable to measure the obstacles in the two tracks of the vehicle individually? (These last three questions are fundamental to determining the resolution of the system.)

9. What is the speed of the vehicle?
10. What reaction time is required?
11. What maneuvers may be expected, can they be anticipated, and how important is maintaining information during maneuvers?
12. Is the sensor to be used for choosing a route? (The answers to the last three questions affect the areas of the terrain to be covered.)

It should be noted that the set of answers to these questions constitutes a set of design requirements. However, the answers are to a considerable extent arbitrary. Thus, these requirements must be understood as doing no more than describing performance believed at present to be satisfactory. Further tactical consideration may suggest changes in the requirements; also, design analysis may show that they cannot be met, but that different performance characteristics will provide satisfactory equipment.

The following answers have been adopted for these questions, and were reviewed in a meeting between Mr. H. W. Courtney of Emerson Electric and Mr. M. Michaelson of OTAC in July, 1962. The answers have been used as a set of ground rules for the conduct of the study.

It will be assumed that the vibration environment experienced by the hull is represented by the following informal data obtained from OTAC:

<u>Type of Operation</u>	<u>Vertical Vibration</u>		<u>Longitudinal Vibration</u>		<u>Transverse Vibration</u>	
	<u>g</u>	<u>cps</u>	<u>g</u>	<u>cps</u>	<u>g</u>	<u>cps</u>
High Speed, Hard Road	4	500	3.8	500	2.3	520
Medium Speed, Off Road	2.3	540	2	520	0.6	430

Although these values are representative of vibration encountered in vehicles with conventional suspension, it appears that 4 g at 500 cps must be expected even in a vehicle employing an active system. This peak acceleration results from a peak displacement, A, of

$$A = \frac{9.78}{f^2} \quad g = 1.56 \times 10^{-4} \text{ inch,}$$

where f is the frequency and g the acceleration in g's.

With respect to climatic conditions, it has been assumed that the system is to be independent of ambient light levels, but that with low ambient illumination the terrain ahead of the vehicle may be illuminated by visual headlamps. As a program objective, the sensor is to operate under all climatic conditions.

With respect to security, it has been assumed that no restrictions exist on the use of active systems using beams of visible or infrared lights. (This is reasonable because of the rather narrow beamwidths involved.) It has also been assumed that not more than a 6-inch aperture in the vehicle is permitted.

The following answers to the questions on geometry have been adopted for the study:

1. Vehicle type - not considered important at present stage.
2. Elevation of sensor - assumed to be 5 feet above level terrain.
3. Pitch and cant - it has been supposed that a vertical axis in the vehicle will be held to within  $5^\circ$  of vertical in pitch and  $15^\circ$  in cant by the active suspension system.
4. Short-term vertical motion has been assumed to be negligible.
5. The elevation of the sensor above the terrain is assumed to be known to within 1 inch.
6. Size of obstacles - in order to have a model for design and comparison purposes, it has been assumed initially that the vehicle traverses a smooth level surface. Randomly positioned on this surface are fixed obstacles of irregular shapes having minimum dimensions of 2 inches or greater. These can be approximately spherical, cubical, or long cylinders. In addition, it has been supposed that the surface contains long holes or depressions which may be as large as 10 feet across and 3 feet deep.
7. It has been assumed that knowledge of the profile to within 2 inches is desirable. This in effect leaves 2-inch bumps to be handled by the passive suspension system.
8. It appears on the basis of this model and the last requirement above, that obstacles in the two tracks must be measured individually.

9. The maximum speed of the vehicle is taken as 50 mph.
10. A 1/2-second reaction time is assumed to be an attainable goal for the post-sensor system, with 1-second unquestionably attainable.
11. The sensor is not initially to be used for choosing a route.
12. For the purposes of the study, it has been assumed that the vehicle travels a straight path. This guideline was adopted to remove the complexities of considering the effects of turns until such a time as it could be established that the basic approach would be successful.

## GEOMETRICAL MODEL

Based on the requirements outlined above, a model of the sensor-terrain geometry has been established to form a framework for the study. In this model, a pair of sensors is assumed, each mounted at a position 5 feet above the ground directly over the contact points of the leading wheels. The sensors look forward along the paths of their respective wheels at a fixed depression angle  $\alpha$ , and with horizontal and vertical beamwidths of  $\phi$  and  $\theta$  respectively. The horizontal distance from the sensors to the points at which their beam axes intersect level terrain is 44 feet, permitting 1 second reaction time for the active suspension system at 30 mph, and 0.6 second at the maximum velocity of 50 mph. Figure 1 shows the geometry of this model for a single sensor.

The values selected above represent an initial trade-off among 1) the requirement to maintain a reasonable reaction time (which favors greater horizontal distances), 2) maintenance of good signal-to-noise ratios (which favors minimum slant range), 3) maintenance of large values of depression angle to minimize the shadow problem (which favors large elevations and short horizontal distances), 4) reduction of the probability that the vehicle will turn and so depart from the actual wheel tracks (which favors short horizontal distances), and 5) reduction of the accuracy with which vehicle velocity must be known in order to make correct use of terrain information (which favors short horizontal distances.) The major factor preventing adoption of an even shorter horizontal viewing distance in this model is the restriction on wheel-reaction time by the active suspension system. Figure 2 shows the resulting reaction-time vs. vehicle-speed curve for this model.

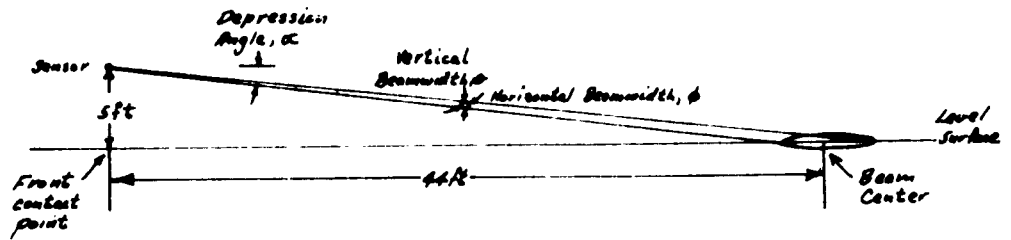


Figure 1. Geometrical Model for Study

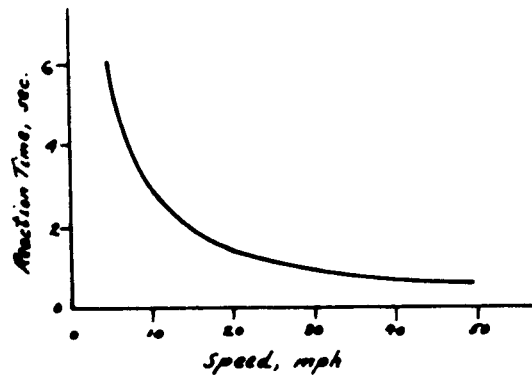


Figure 2. Reaction Time vs. Speed for Geometrical Model

## PERFORMANCE REQUIREMENTS

The terrain and sensor-geometry models described above place performance requirements on the sensor. The questions considered here are the required vertical field of view of the instrument, the system bandwidth, and the range accuracy.

In order to determine these, an obstacle on level terrain will be considered; this will be taken as a step up of height  $h$  to a second level surface. If  $h$  is taken as 1 foot, this step corresponds to the leading edge of a typical 1-foot obstacle. Figure 3 represents such a step occurring at  $x = 0$ , with the zero height reference ( $y = 0$ ) at the lower of the two levels.

In considering that the system requirements are determined by the response to this obstacle, several factors are neglected. Among these are the effect of steps down, and the effect of a narrow obstacle (one extending across only part of the horizontal field of view of the sensor). The vertical step up, however, is considered to represent the most serious of the possible obstacles, and thus to be of primary importance in the sensor design.

The vertical field of view and the system bandwidth limitation are both averaging processes having similar effects on the measured ranges, and therefore on the computed terrain profile. Thus, the first step is to examine the effect of such averaging processes.

In figure 3, suppose that the range to the terrain,  $R(x)$  is measured along a line of sight making an angle  $\alpha$  with respect to the horizontal. Let  $x$  be the horizontal distance from the vertical step to the point at which this line of sight would intersect the lower level. It is convenient to suppose that  $p(x)$ , as shown in the figure, is actually determined by this measurement. Then, for  $x > 0$ ,

$$p(x) = R_0 - R(x),$$

where  $R_0$  is the (fixed) range from the sensor to the extension of the lower level. Similarly, if  $R(x)$  is a function of time we may write

$$p(t) = R_0 - R(t).$$

Any linear operation (such as averaging) performed on  $p(t)$  corresponds directly to an identical operation performed on  $R(t)$ .

If  $p(t)$  is measured, the  $x$  and  $y$  coordinates of the surface intersection of the line of sight are

$$\begin{aligned} x(t) &= x_0(t) - p(t) \cos \alpha \\ y(t) &= p(t) \sin \alpha. \end{aligned}$$

where  $x_0$  is the coordinate of the intersection of the line of sight with the terrain.

When  $\alpha$  is small, as it is for the model ( $\alpha = 0.114$  radian or 6.5 deg),

$$x(t) = vt - p(t)$$

$$y(t) = \alpha p(t)$$

Suppose now that the time varying signal is subjected to a linear process  $L$ . Then the computed values of  $x$  and  $y$  will be

$$x_c(t) = vt - L \{ p(t) \}$$

$$y_c(t) = \alpha L \{ p(t) \} .$$

Suppose that  $L$  consists of averaging  $p$  over a period of time  $a$ . This may be due to the beamwidth causing the ranges which would ideally be measured over different times to be measured at the same time and averaged, or to the integration due to finite amplifier bandwidth. Thus

$$L \{ p(t) \} = \frac{1}{a} \int_{t-\frac{a}{2}}^{t+\frac{a}{2}} p(u) du .$$

Consider the effect of this on a step input. Values of  $p(t)$  can easily be seen to be represented by the curve of figure 4 (or deduced from the parametric equations for  $x$  and  $y$  given earlier).

Thus if the step is

$$y = 0 \text{ for } x < 0$$

$$y = h \text{ for } 0 < x$$

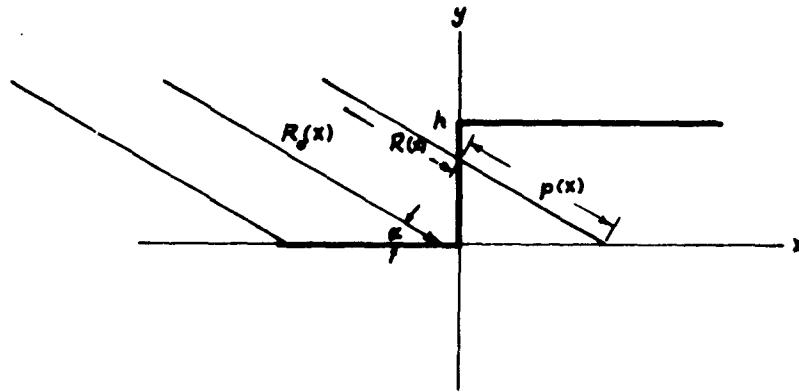


Figure 3. Representation of Simple Obstacle

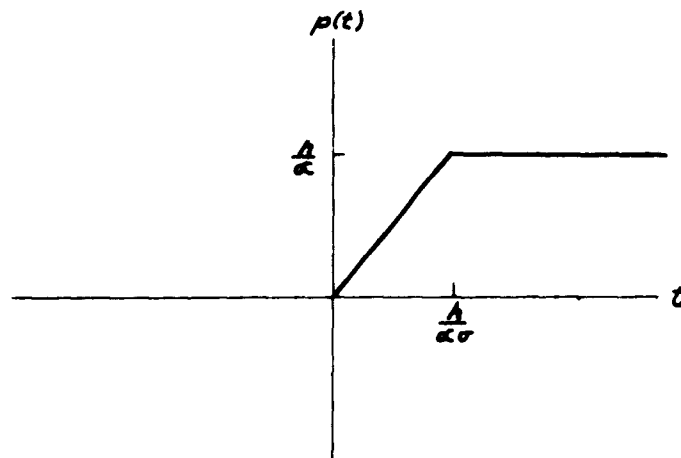


Figure 4.  $p(t)$  vs.  $t$  for Simple Obstacle and Constant  $v$ .

Then

$$p(t) = 0 \text{ for } t < 0$$

$$p(t) = tv \text{ for } 0 < t < \frac{h}{v}$$

$$p(t) = \frac{h}{\alpha} \text{ for } \frac{h}{v\alpha} < t$$

If this is averaged over time  $a \leq \frac{h}{\alpha v}$ , the result is

$$L \left\{ p(t) \right\} = 0$$

$$t < -\frac{a}{2}$$

$$= \frac{v}{2a} \left( t + \frac{a}{2} \right)^2$$

$$-\frac{a}{2} < t < \frac{a}{2}$$

$$= vt$$

$$\frac{a}{2} < t < \frac{h}{\alpha v} - \frac{a}{2}$$

$$= \frac{h}{\alpha} - \frac{v}{2a} \left[ \frac{h}{\alpha v} - t + \frac{a}{2} \right]^2$$

$$\frac{h}{\alpha v} - \frac{a}{2} < t < \frac{h}{\alpha v} + \frac{a}{2}$$

$$= \frac{h}{\alpha}$$

$$\frac{h}{\alpha v} + \frac{a}{2} < t$$

This is sketched in figure 5. Note that the waveforms are **symmetrical** at the top and bottom, and that the maximum error in range occurs when  $t = 0$  and when  $t = \frac{h}{\alpha v}$ .

Now what does this range curve do to the computed contour?

Since

$$\begin{aligned} x_c(t) &= vt - L \left\{ p(t) \right\} \\ y_c(t) &= \alpha L \left\{ p(t) \right\} \end{aligned} ,$$

for the step, the y error is  $y_c(t)$  whenever  $x_c(t) < 0$ , and  $y_c(t) - h$  when  $x_c(t) > 0$ .  $x_c$  is negative when  $vt - L \left\{ p(t) \right\} < 0$ ; inspection of figure 5 or the corresponding equations shows that this is the case until  $t = \frac{a}{2}$ . During this time

$$y_c = \frac{\alpha v}{2a} \left( t + \frac{a}{2} \right)^2$$

increases, and is largest at  $t = \frac{a}{2}$ , when  $y_c = \frac{\alpha v a}{2} =$  largest error before the step.

Similarly, at the top of the step, corresponding to  $x_c > 0$ , the error is

$$\alpha \left[ \frac{h}{\alpha v} - \frac{v}{2a} \left( \frac{h}{\alpha v} - t + \frac{a}{2} \right)^2 \right] - h = - \frac{\alpha v}{2a} \left( \frac{h}{\alpha v} + \frac{a}{2} - t \right)^2$$

This expression is zero at  $t = \frac{h}{\alpha v} + \frac{a}{2}$ , and is more and more negative for smaller  $t$ . Thus the largest error occurs at  $t = \frac{h}{\alpha v} - \frac{a}{2}$ , where it has the value  $- \frac{\alpha v a}{2}$  as before. The effect of averaging time,  $a$ , on the computed profile is shown in figure 6. For the maximum velocity of 50 mph and the geometrical model adopted previously, the averaging time,  $a$ , for a 2-inch maximum error is

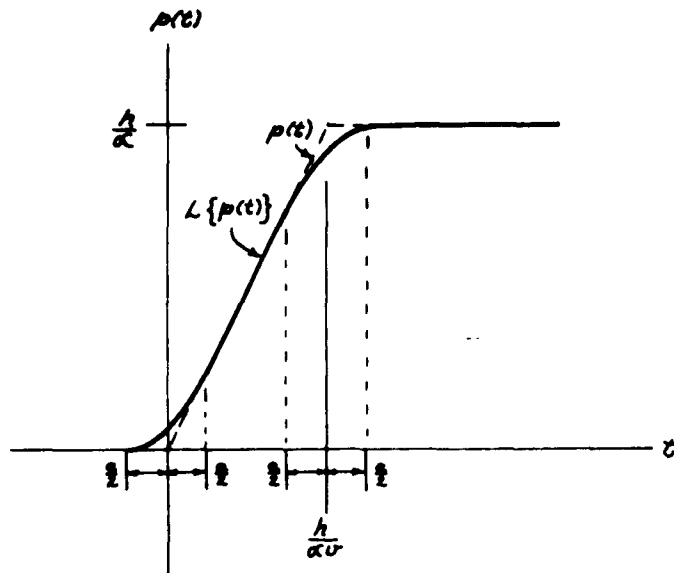


Figure 5.  $p(t)$  and  $L\{p(t)\}$  vs.  $t$  for Simple Obstacle and Constant  $v$ .

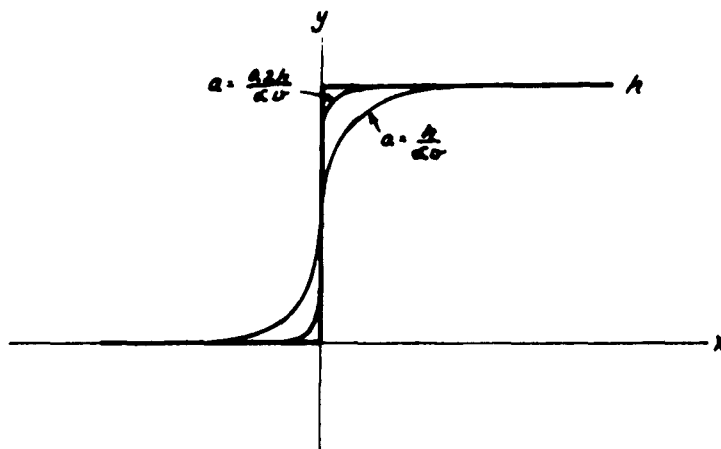


Figure 6. Computed Profile for Simple Obstacle for Various Values of Averaging Time,  $a$ .

$$a = \frac{4}{(0.114)(880)} = 0.040 \text{ sec.}$$

The averaging time,  $a$ , must now be described in terms of the vertical beamwidth of the optical system and the characteristics of the amplifier.

To determine the vertical beam, it is only required to determine the relation between the beam averaging time,  $a_1$ , and the vertical beamwidth,  $b$ .

It can be seen from figure 7 that when  $\alpha$  is small the distance along the ground lying within the beam is about  $d = \frac{b}{\alpha}$ . Since the averaging time is  $\frac{d}{v}$ ,  $a_1 = \frac{b}{v \alpha}$ . Here, for  $v \alpha = 8.3$  foot/sec and  $a_1 = 0.040$  second,  $b = .33$  foot.

It may be pointed out that since the allowable error is

$$\frac{\alpha \sqrt{a}}{2} = \frac{\alpha v}{2} \frac{b}{\alpha v}$$

$b$  is just twice the allowable error, independent of the product  $\alpha v$ .

This value (4 inches) requires a beamwidth of  $\frac{1}{3 \times 44} = 7.6$  milliradians, assuming that measurements are to be made at 44 feet.

In considering an amplifier following optical elements it is convenient for calculation to define a quantity  $a_2$  called the integration time of the amplifier. This is defined as 1.25 times the 10-90% rise

time of the amplifier. Integration times add in the root square, and the integration time-bandwidth product is 0.44 for typical systems. The averaging time,  $a$ , considered above represents the integration time of the system. For the specific system considered,

$$B = \frac{.44}{.040} = 11 \text{ cps.}$$

It may be concluded that the vertical beam should be about 7.6 milliradians wide and that the amplifier bandwidth should be 11 cps, if either were the only source of error. Since both are involved, each error must be somewhat smaller. Suppose  $B = 25$  cps, then  $a_2 = \frac{.44}{25}$ , and

$$a_1 = \sqrt{(.040)^2 - \left(\frac{.44}{25}\right)^2} = .036$$

and  $b = (.036) (8.3) = 0.30$  foot, which corresponds to 6.8 milliradians.

This choice is probably better than decreasing the originally computed  $a_1$  and  $a_2$  by  $\sqrt{2}$ , since it is easier to increase the system bandwidth than to narrow the sensing beam.

The next question to be considered is allowable range errors. This requires less analysis than the foregoing. It can be seen from figure 8 that a range error of  $\Delta R$  results in the corresponding computed coordinates being shifted along the line of sight by the amount of the range error.

When the line of sight makes a small angle  $\alpha$  with the horizontal,

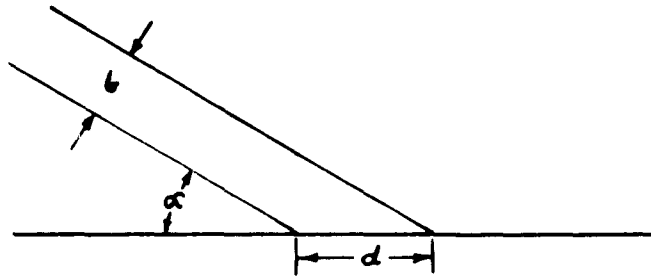


Figure 7. Beam-Ground Geometry

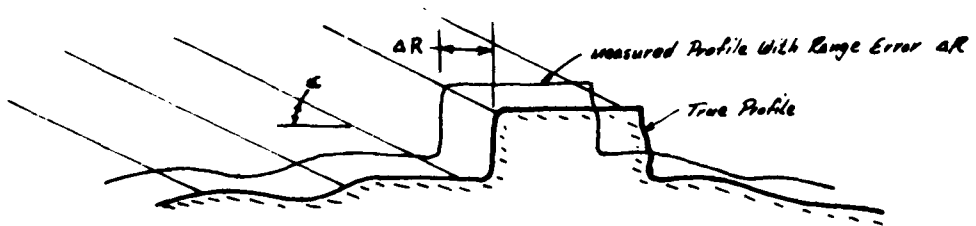


Figure 8. Effect of Range Error  $\Delta R$

range errors thus show up as horizontal shifts in the computed terrain. The corresponding vertical error is thus a maximum when observing an obstacle which is perpendicular to the line of sight (or approximately perpendicular to the terrain) and under these conditions is equal to the height of the obstacle.

Since it is assumed that the sensor is to function against small obstacles on a level surface, this situation must be taken as determining the allowable range error. Clearly any range error may result in a vertical error exceeding the 2-inch allowance previously established. And it cannot be expected that the sensor will measure range with no error. Hence an arbitrary choice must be made.

It is reasonable to set the allowable range error at 2 inches. This allows an error in the location of a vertical obstacle of 2 inches along the terrain; it is considered that the effect of such an error in the vehicle suspension will not be critical. Incidentally, in order to make use of knowledge of an obstacle to this degree of accuracy requires knowledge of the velocity of the vehicle to the same accuracy as the range, or to within 0.38%. A one percent error in knowledge of velocity yields a .44 foot error (5.3 inches).

Since we are considering abrupt obstacles on a level surface as one type of environment in which the sensor is to function, some initial consideration may be given to the effect of such an obstacle on the motion of the vehicle hull when the obstacle is encountered. Because of the curvature of the wheel or track, the axle of the vehicle does not follow

the obstacle exactly. This effect will be considered here in the idealized form of a rigid wheel having a two-foot radius rolling over a hard obstacle having a square cross-section one foot on a side.

As shown in figure 9, the axle of the vehicle traverses a path considerably different from the shape of the obstacle. In a sense, the wheel or track of a vehicle smooths small abrupt obstacles. Thus, for the case considered, the obstacle of figure 10 is effectively equivalent to that of figure 9.

In this particular case, at least, the axle never moves directly vertically unless the obstacle is a hole having a depth greater than the radius of the wheel, and the vehicle is moving very slowly so that the trajectory effects can be ignored.

This has some effect on the shadow problem. As suggested by figure 11, a sensor looking at an angle  $\alpha$  cannot distinguish between the contour ABCD and the contour ABD. Any contour lying between these lines gives the same output. The effect of this lack of information on the vehicle depends on the difference in axle paths that would result from the two extreme contours responsible for this sensor indication.

As can be seen in figure 9, the axle motion resulting from the square obstacle is the same as would result from the rounded obstacle of figure 10. Thus the possible terrain variations which would result in different axle responses and yet give the same sensor response are

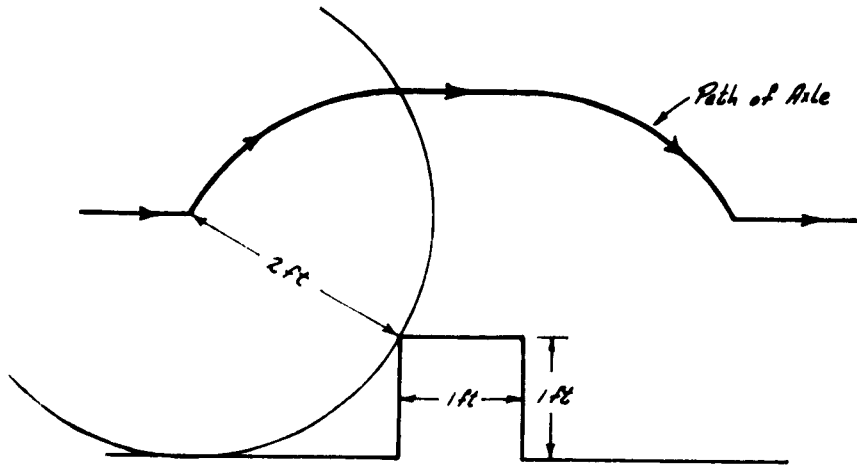


Figure 9. Axle Path for 2-ft-radius Wheel and 1-ft-square Obstacle



Figure 10. Effective Shape of Obstacle for Conditions of Figure 9.

as shown by the dotted area in figure 12. It might be assumed that the actual contour was intermediate between these two, as shown by the dotted line in figure 12. This yields an axle error which depends on the height of the drop-off and the radius of the wheel. It can be seen from figure 13 that the maximum difference in axle locations occurs at a distance  $\sqrt{2Wh - h^2}$  after the brink of the drop-off, where  $W$  represents the wheel radius and  $h$  is the drop height. If  $X$  is the maximum distance between the axle locations for the two extreme contours,  $X = (W+h) - (W+y)$ . When  $\alpha$  is small, and when  $h$  is not too small,  $y$  is approximately

$$y \approx \alpha \sqrt{2Wh - h^2},$$

and hence

$$X = h - \alpha \sqrt{2Wh - h^2}.$$

The maximum axle error is  $(1/2)X$ , if the terrain is assumed to lie midway between the extreme possible paths. This has been plotted in figure 14 for values of the wheel radius  $W$  of one foot and two feet. It can be seen that for obstacles of 6 inches or less, the error is within the 2-inch limit required. Of course, to this error will be added those resulting from errors in measurement.

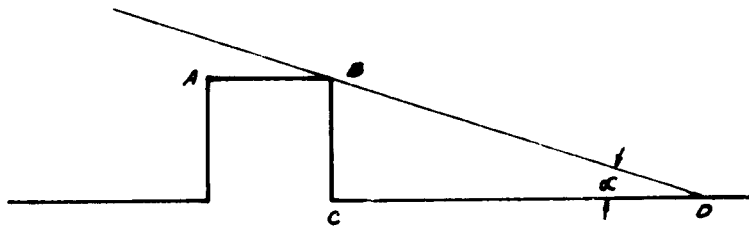


Figure 11 Sensor Shadow Geometry



Figure 12. Terrain Variations Giving Differing Aisle Response but Same Sensor Response.

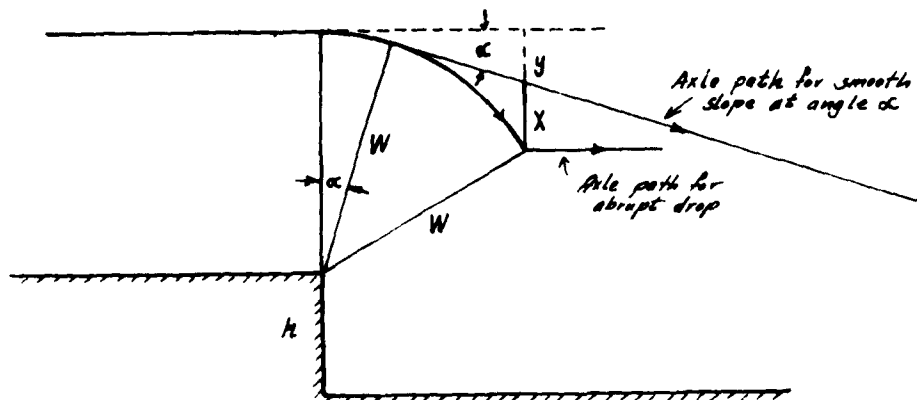


Fig 13 Geometry for Axle-Error Computation

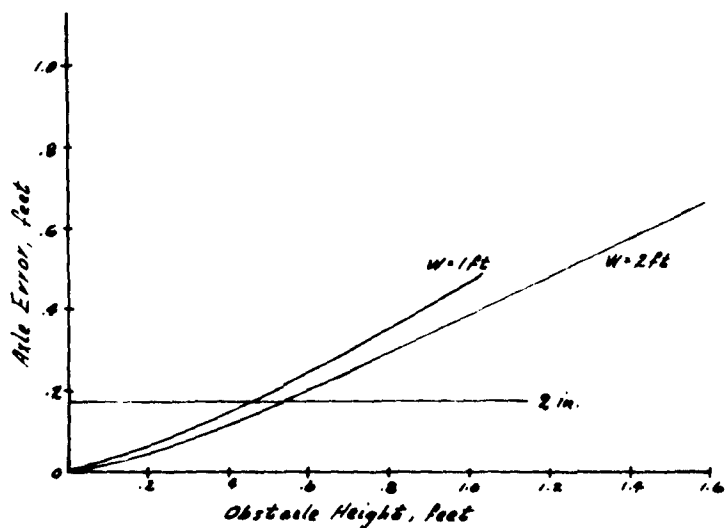


Figure 14. Axle Error vs Obstacle Height for Wheels of 1-ft. and 2-ft. Radius

## OPTICAL RANGING METHODS

The type of sensor system under consideration derives terrain contour information from optical range measurements. These measurements are made from a point on the vehicle a known height above the local terrain, along a line of sight with known depression angle. In the previous section, the allowable range error was chosen to be 2 inches, and a nominal value of range-to-terrain on level ground of 44 feet was adopted. The ranging device must thus be accurate enough to provide the required resolution at ranges of a few tens of feet, and must respond rapidly enough to changes in range to be compatible with the system bandwidth, somewhat greater than 11 cps, calculated earlier.

Five different types of optical rangefinders, both active and passive, have been studied for the terrain sensor application. Of these, an active system using c-w transmission, and a passive system using image-plane location have shown the greatest promise and have been studied in most detail. The ranging methods considered are described below.

A note on the terminology used in this report is in order. Active systems are considered to be those in which modulated energy is transmitted from the vehicle, reflected from the terrain, detected at the vehicle, and processed to derive range from travel-time effects on the modulation waveform. Passive systems are considered to be those that make use of radiated or reflected energy and do not require a modulated source; in this sense, a system that operates in the daytime by detecting reflected sunlight and at night by detecting reflected light from a simple unmodulated beam is considered to be "passive," even though under some

conditions of operation a simple source may be required to provide adequate energy for operation.

#### ACTIVE C-W RANGEFINDER

The first ranging system studied was of the type described in the original proposal. This system uses visible or infrared energy intensity modulated at a fixed frequency. Energy reflected from the terrain is collected, and the phase of the resulting modulation is compared with that of the transmitted energy. The phase shift resulting from two-way transit time gives a measure of range to the target. It is shown below that a system meeting the assumed accuracy requirements is feasible in a package of reasonable size, and can be designed without requiring extensions in the present state of the art.

Derivations of the equations given below for calculating the effectiveness of this type of system are found in appendix A.

Equations

The basic factor used to evaluate the range-finding capability of the system is the noise-equivalent range increment,  $\Delta R$ . This factor is a measure of the change in range that is required to produce a change in output equal to system noise (including noise-in-signal) and is thus a good indication of the limiting value of range resolution which can reasonably be expected from a well-designed system. For this type of active ranger, the governing equation is

$$\Delta R = \frac{2 R_{\max} P \sqrt{2 B} R^2}{W A_t A_c \rho \omega \epsilon}$$

(1)

where

$R_{\max}$  = maximum unambiguous range

$P$  = multiplier phototube noise equivalent power (NEP) 1 cps bandwidth

$B$  = integration bandwidth

$R$  = range

$W$  = transmitter radiated power

$A_t$  = area of transmitting aperture

$A_c$  = area of collecting aperture

$\rho$  = reflectivity of target area

$\omega$  = solid angular field of view

$\epsilon$  = optical efficiency

As noted earlier, a value of 2.0 inches for  $\Delta R$  at a range,  $R$ , of 44 feet is considered to be satisfactory.

The equations required to derive the factors  $R_{\max}$  and  $P$  of equation (1) from the various system parameters are as follows:

$$R_{\max} = C/4 f_{\max} \quad (2)$$

where

$C$  = velocity of light

$f_{\max}$  = maximum modulation frequency, and

$$P = \left[ \frac{2Ge}{S} \left( \frac{i}{S} + 0.625Et + E_b \right) \right]^{1/2} \quad (3)$$

where

$G$  = multiplier phototube gain

$e$  = charge on electron

$i$  = multiplier phototube dark current

$E_t$  = power collected from target area from transmitted beam

$E_b$  = background power collected from target area from incident ambient radiation

$S$  = multiplier phototube responsivity

The factors  $E_t$  and  $E_b$  may be derived from

$$E_t = \frac{WA_t A_c \rho W E}{\pi R^2},$$

and

(4)

$$E_b = Y \rho \omega A_c,$$

(5)

where Y = ambient power reflected by target with unit reflectivity.

(The ambient energy considered here is direct and scattered sunlight.)

#### Values For Parameters

Reasonable values for the parameters necessary for solution of the equations given above have been selected, based on the types of components and techniques presently available. As shown below, these give an acceptable value of  $\Delta R$  even under adverse operating conditions.

Transmitter Radiated Power, W. The transmitted radiated power, W, enters into the denominator of equation (1), and thus must be maximized to obtain minimum  $\Delta R$ . The power of interest is that which lies within the range of spectral sensitivity of the receiver, so that the color temperature as well as the brightness of the source must be taken into consideration in calculating the effective value of W.

The brightest source commercially available is an arc lamp provided with permanent electrodes sealed into an argon-filled glass bulb. This device is several times brighter than a conventional tungsten-filament lamp, and operates at a color temperature of 3200°K. A typical value of brightness is 46 candles per square millimeter, for a source diameter of 0.110 inch. To convert these values to effective watts in the spectral bandwidth of the receiver, it is necessary to use the following relationships, given for multiplier phototubes with S-11 and S-20 responses.\*

$$(S-20); W = \frac{4600 \text{ lumens}}{\text{cm}^2 \text{ - ster}} \times 0.00147 \times \frac{\eta [S-20, 3200^\circ K] \text{ watt}}{\eta [K_\lambda, 3200^\circ K] \text{ lumen}}$$

$$= 4600 \times .00147 \times .065 \times .040^{-1} = 11.0 \text{ watt cm}^{-2} \text{ ster}^{-1}$$

$$(S-11); W = 4600 \times .00147 \times .036 \times .040^{-1} = 6.1 \text{ watt cm}^{-2} \text{ ster}^{-1}$$

Values for  $\eta$  are given in figure

\* A detailed description of the characteristics of these multiplier phototubes is given in Appendix B, together with derivations of the conversion factors from lumens to watts.

Background Radiation,  $E_b$ . The factor  $E_b$  is the power collected from the ambient radiation incident on the terrain. Figure indicates that the worst background condition yields a terrain illumination of about 11,000 foot-candles. Thus, Y, the sun power reflected from the terrain (for  $\rho = 1.0$ ), is

$$(S-20); Y = \frac{11.0 \times 10^3 \text{ lumens}}{\pi (30.48 \text{ cm})^2} \times .00147 \frac{\eta [S-20 \lambda, 5900^\circ \text{K}] \text{ watts}}{\eta [K \lambda, 5900^\circ \text{K}] \text{ lumen}}$$

$$= \frac{11.8}{\pi} \times .00147 \times .316 \times .137^{-1} = 1.28 \times 10^{-2} \text{ watt cm}^{-2} \text{ ster}^{-1}$$

$$(S-11); Y = \frac{11.8}{\pi} \times .00147 \times .246 \times .137^{-1} = 1.00 \times 10^{-2} \text{ watt cm}^{-2} \text{ ster}^{-1}$$

where it is assumed that the sunlight is scattered according to the cosine law. The above values of  $\eta$  were obtained from figure

It is thus possible to calculate  $E_b$ , the power on the detector collected from the ambient radiation scattered from the terrain (equation 5). A value of 0.13 is assumed for  $\rho$ , the average terrain reflectivity. If the terrain were very smooth, little transmitted energy would be returned, since the transmitted beam would strike the ground near the grazing angle. However, surface roughness and the presence of vegetation combine to insure a relatively large and constant return from such a beam. It should also be noted that for very smooth terrain (e.g., improved roads) the active suspension system would not be required for maintenance of high vehicle speeds.

The solid angular field of view,  $\omega$ , is a function of the vertical and horizontal beamwidths. For an electrical bandwidth of 25 cps, a value of 6.8 milliradians for the vertical beamwidth was calculated previously. A value of 22.7 milliradians for the horizontal beamwidth is equivalent to a 1-foot-wide beam at a range of 44 feet, to give a reasonably wide pattern on the ground. Thus the solid angle  $\omega$  equals  $.0068 \times .0227 = 1.54 \times 10^{-4}$  steradian.

$A_c$  is the clear aperture area of the collector optics. A value of  $125 \text{ cm}^2$  for  $A_c$  corresponds to an unobstructed circular aperture of approximately 5-inch diameter. This aperture size will give good performance in a relatively small-sized system.

From these values, we can compute  $E_b$  as follows:

$$(S-20); E_b = 1.28 \times 10^{-2} \times 0.18 \times 1.54 \times 10^{-4} \times 125 = 4.43 \times 10^{-5} \text{ watt}$$

$$(S-11); E_b = \quad \quad \quad = 3.46 \times 10^{-5} \text{ watt}$$

Target Radiation,  $E_t$ . The remaining value necessary for the solution of equation (3) is the value of  $E_t$ , the power returned from the target as a result of illumination by the transmitter. The remaining quantities not yet chosen are  $A_t$ , the area of the transmitting aperture, and  $\epsilon$ , the optical efficiency. Again, a value of  $125 \text{ cm}^2$  is practical for  $A_t$ , and a value of  $\epsilon$  of 0.5 is reasonable. Thus,

$$(S-20); E_t = \frac{11.0 \times 125 \times 125 \times 0.18 \times 1.54 \times 10^{-4} \times 0.5}{(44 \times 30.48)^2} = 4.21 \times 10^{-7} \text{ watt}$$

$$(S-11); E_t = 2.33 \times 10^{-7} \text{ watt}$$

Multiplier Phototube NEP. From the values derived above and the known device characteristics, it is thus possible to evaluate equation 3 for the multiplier phototube NEP,  $P$ . In Appendix B, a simplified relationship is shown to be valid for tubes with both S-20 and S-11 phosphors. This relationship is

$$P = \left[ 5.3 \times 10^{-18} E_t \right]^{1/2} \text{ watts,} \quad (6)$$

with the simplification arising from the fact that the contributions from

the values of  $i/S$  and  $E_c$  (as computed above) are negligible compared to those arising from  $E_b$ . During nighttime\* operation  $E_c$  will predominate and  $P$  will have to be recomputed for this situation. However, night operation is not the limiting case, and the purpose of this section is the calculation of  $\Delta R$  under the most adverse conditions. Thus we can evaluate the multiplier phototube NEP as

$$(S-20); P \approx 1.53 \times 10^{-11} \text{ watt}$$

$$(S-11); P \approx 1.35 \times 10^{-11} \text{ watt}$$

Maximum Unambiguous Range,  $R_{max}$ . Equation 2 yields the value of  $R_{max}$ , the maximum unambiguous range. It is a function of  $f_{max}$ , the maximum chopping frequency which should be as high as practical to minimize  $R_{max}$  and thus  $\Delta R$ . A spoke-type reticle of alternate opaque and transparent lines of equal width is the most practical for this application. In order to obtain a value of  $f_{max}$  equal to  $2 \times 10^6$  cps, assume that the reticle is formed on a disk of 10-inch circumference and is rotated at 18,000 rpm. This rotational speed is achievable. (Actually, a second stationary disk of identical shape is necessary to perform the chopping.) The width of the lines on the disks become

$$\frac{10}{2} \text{ inch} \times 300 \frac{\text{rev}}{\text{sec}} \div 2 \times 10^6 = .00075 \text{ inch.}$$

During nighttime operation,  $P \sim E_c^{1/2}$ , and since the above calculated ratios of  $E_c/E_b \approx 100$ ,  $\Delta R$  is a factor of 10 better than during daytime operation.

An investigation of the present state-of-the-art in the manufacture of reticles indicates that the above value is achievable. Thus an  $f_{\max}$  of  $2 \times 10^6$  cps and an  $R_{\max}$  of  $3.75 \times 10^3$  cm (123 feet) are attainable values.

Calculation of  $\Delta R$ . Equations 1 and 4 combine to give

$$R = \frac{2 R_{\max} P \sqrt{2B}}{\pi E_t} \quad (7)$$

A value of B, the amplifier bandwidth, of 25 cps was calculated previously. Since  $\Delta R$  is to be minimized, the S-20 photocathode provides improved operation over the S-11, since

$$(S-20); \frac{P}{E_t} = 3.63 \times 10^{-5}$$

$$(S-11); \frac{P}{E_t} = 5.79 \times 10^{-5}$$

so that the S-20 type is better than the S-11 by a factor of 1.6.

Before  $\Delta R$  is calculated, one more factor must be applied. Since the source is chopped, only one-half of the total emitted energy, W, is transmitted, so that  $E_t$  should be reduced by one-half. Thus

$$R = \frac{2 \times 3.75 \times 10^3 \times 1.53 \times 10^{-11} \sqrt{2 \times 25}}{\pi \times 4.21 \times 10^{-7}/2} = 1.23 \text{ cm} = 0.50 \text{ in.},$$

when the S-20 multiplier phototube is used in a system having the characteristics selected above.

This calculated value of  $\Delta R$  is a factor-of-four better than the assumed maximum allowable error of 2 inches at a range of 44 feet. It is felt that the assumptions made in the preceding calculations were conservative, and represent achievable values. The value of 0.5 inch provides a sufficiently large margin of error to give a good degree of confidence that this type of active range finder will perform the necessary function.

### Tradeoff Analysis

Although preliminary design calculations can provide a reasonably accurate estimate of system performance, many of the critical parameters can only be determined exactly after the system is built, and it is often necessary as the design progresses to make various trade-offs as practical difficulties are encountered or specific portions of the design are frozen. Based on the equations presented earlier, and with reasonable assumptions as to the reliance that can be placed on various factors, a set of charts has been constructed to permit rapid analysis of the effects of changes in several of the more important parameters. The charts are based on the following analytical approach.

Equation 1 may be rewritten in terms of all the basic parameters as:

$$\begin{aligned}\Delta R &= \frac{2c [2GeY\rho\omega A_c/S]^{\frac{1}{2}} \sqrt{2B} R^2}{4 f_{\max} [W/2] A_t A_c \rho \omega \epsilon} \\ &= \frac{c [2GeY/S]^{\frac{1}{2}} \sqrt{2B} R^2}{f_{\max} W A_t A_c^{\frac{1}{2}} \rho^{\frac{1}{2}} \omega^{\frac{1}{2}} \epsilon}\end{aligned}$$

(8)

If we then assume that the transmitter and receiver clear apertures are equal, so that

$$A_t = A_c = \pi D_a^2/4$$

51

where  $D_a$  is the diameter of the apertures, and that

$$\omega = \theta \cdot \phi = \theta b_H / R,$$

where  $\theta$  and  $\phi$  are the vertical and horizontal beamwidths, respectively, and  $b_H$  is the linear width of the horizontal beam pattern at range  $R$ , we may write equation (8) as

$$\Delta R = \frac{4c(2GeY/S)^{\frac{1}{2}} \sqrt{2B} R^{\frac{5}{2}}}{f_{max} W \pi D_a^3 \rho^{\frac{1}{2}} \theta^{\frac{1}{2}} b_H^{\frac{1}{2}} \epsilon}$$

(9)

Certain of the above parameters are more reliably known than others.

These are

$Y$  = 11,000/ $\pi$  foot candle

$\theta$  = .0068 radian

$B$  = 25 cps

$W$  = 11.0 watt  $\text{cm}^{-2}$  ster $^{-1}$

$\epsilon$  = 0.5

If these values and the known values of  $G$  and  $C$  for a multiplier phototube with 8-20 photocathodes are substituted into equation (9), we may write

$$\Delta R = \frac{4.14 \cdot 10^3 [R(ft)]^{5/2}}{f_{max} [D_a(in)]^3 [\rho]^{1/2} [b_H(ft)]^{1/2}}$$

(10)

The value of  $\Delta R$  is thus given in terms of the range,  $R$ ; the maximum chopping frequency,  $f_{max}$ ; the aperture diameters,  $D_a$ ; the terrain reflectivity,  $\rho$ ; and the linear horizontal beamwidth at range  $R$ ,  $b_H$ .

The maximum chopping frequency,  $f_{max}$ , may be written as

$$f_{max} = 26.2 D_D (in) \Omega (rpm)/w (in) \quad (11)$$

where  $D$  is the chopping disk diameter,  $\Omega$  is the rotation rate of the chopper disk, and  $w$  is the width of the opaque and transmitting lines in the chopper.

Based on these equations, figures 15, 16, 17, and 18 have been constructed to permit rapid graphical solution for assessment of tradeoffs or evaluation of the effects of various changes in the system. A set of "typical" construction lines is given on the figures, representing the current best estimate for a practical system design meeting program objectives.

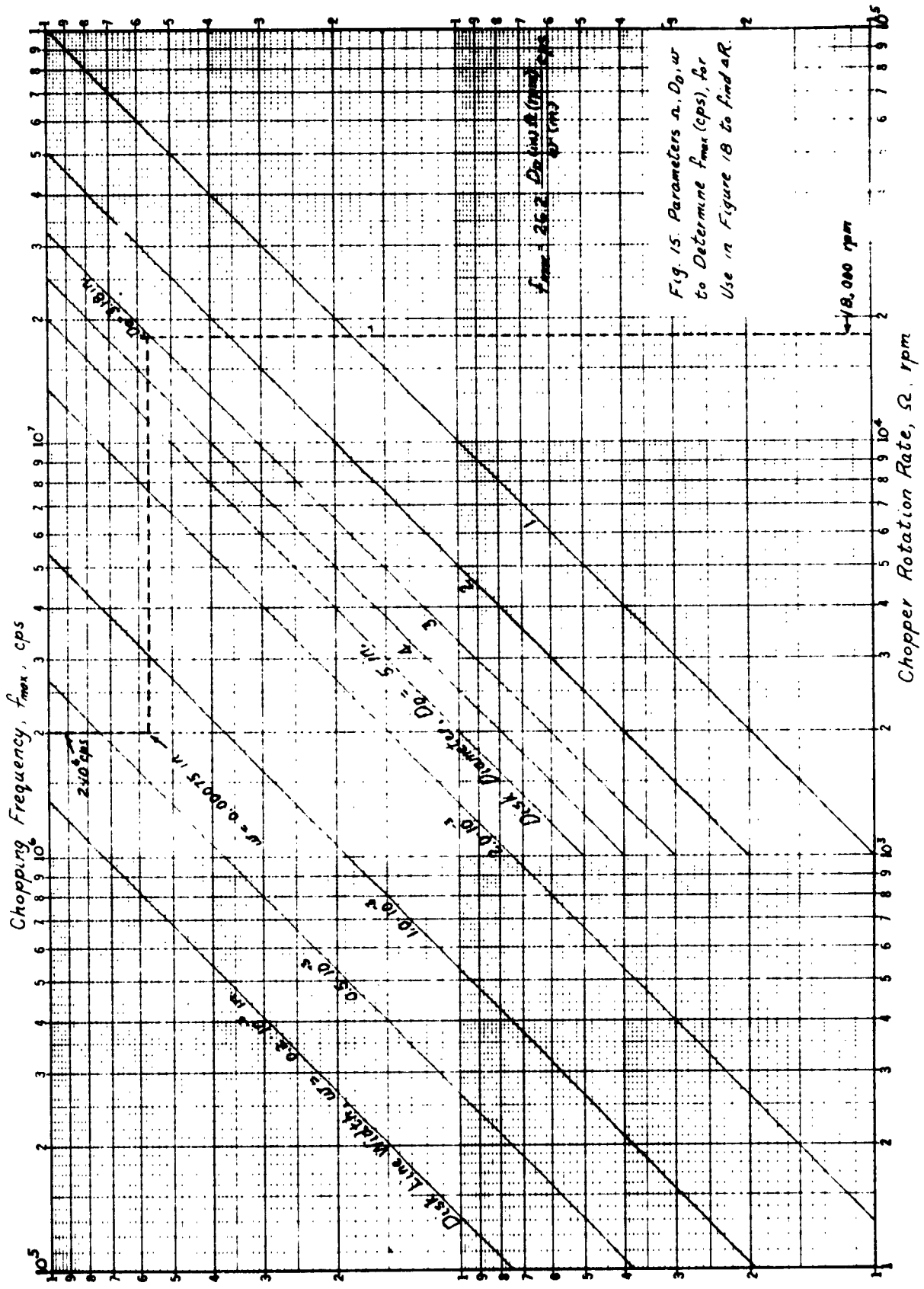


Fig. 15. Parameters  $n, D, w$  to Determine  $f_{max}$  (cps), for Use in Figure 18 to find  $\Delta R$ .

$f_{max} = 2.5 \times 10^6$  cps  
 $D = 5$  in.  
 $w = 0.25$  in.

$\Omega = 1.8 \times 10^4$  rpm

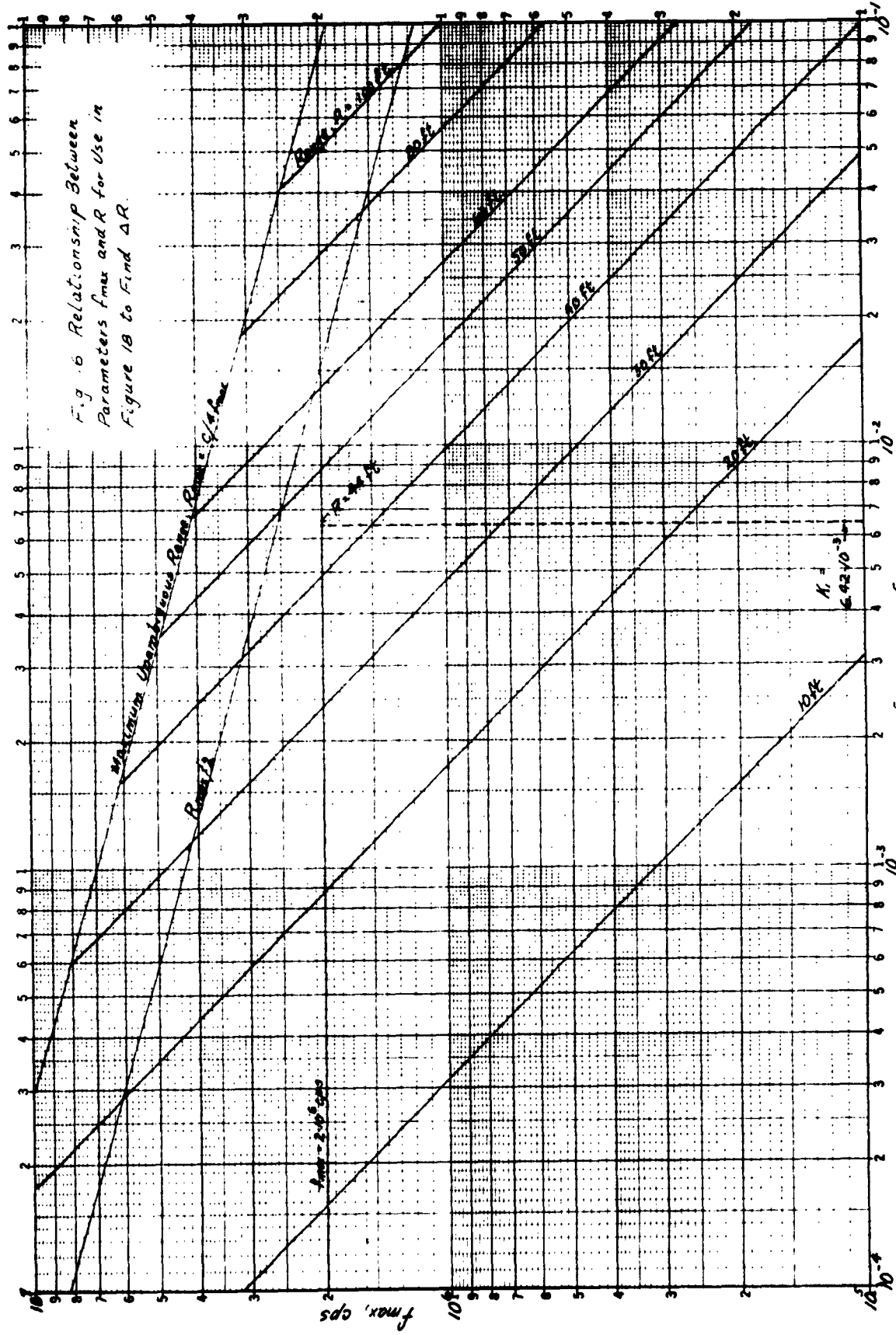


Fig. 6 Relationship Between Parameters  $f_{max}$  and  $R$  for Use in Figure 1B to Find  $\Delta R$ .

$$R_1 = R \frac{f}{f_{max}}, \quad f \frac{f}{\text{cps}}$$

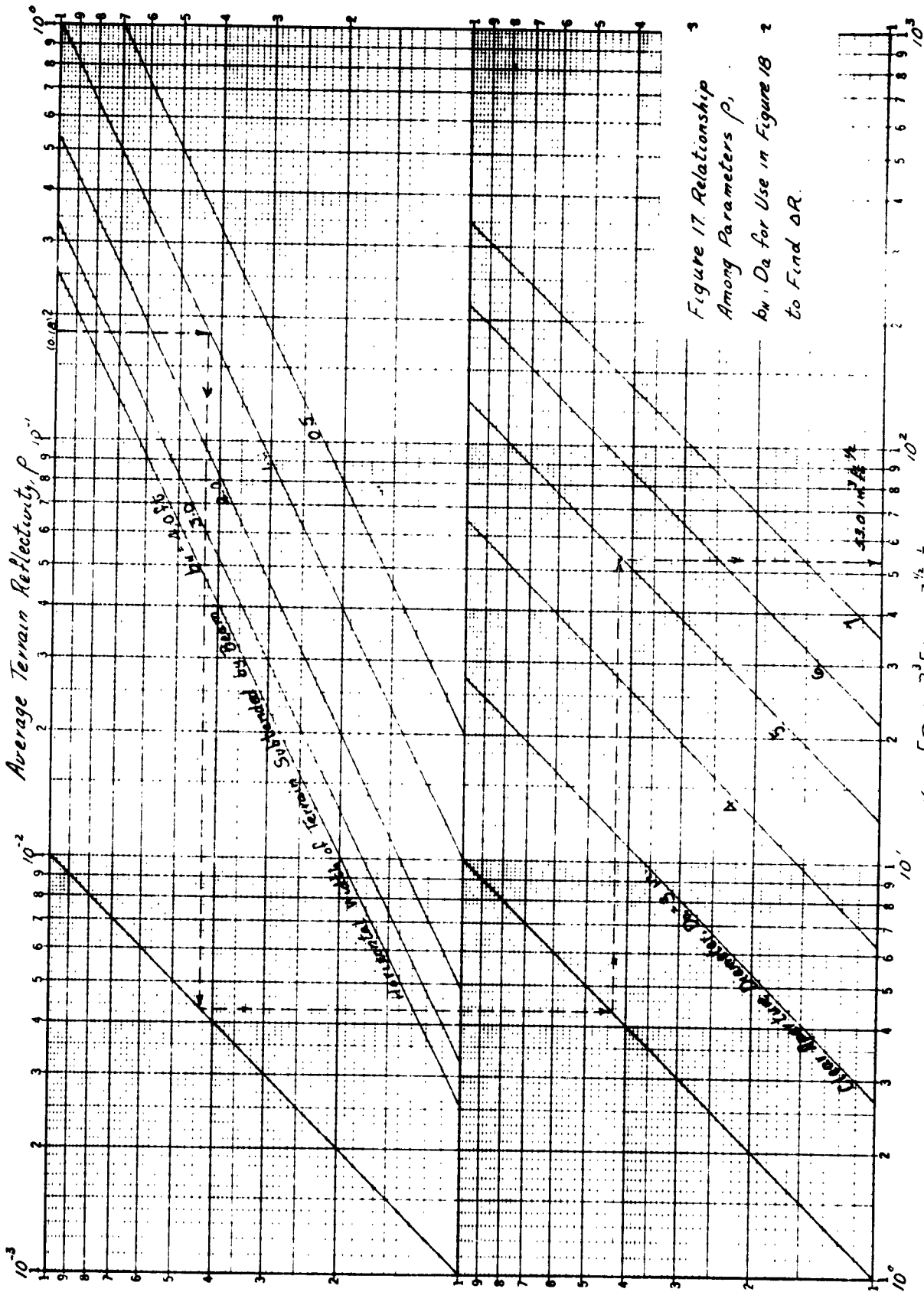


Figure 17. Relationship  
 Among Parameters  $\rho$ ,  
 $b_w$ ,  $D_e$  for Use in Figure 18  
 to Find  $\Delta R$ .

$$k_2 = [D_e(m)]^3 [b_w(ft)]^{1/2} \rho^{1/2}$$

2

FREDERICK POST COMPANY  
 321223 - FULL LOGARITHMIC - 233 5-1/2" CYCLES

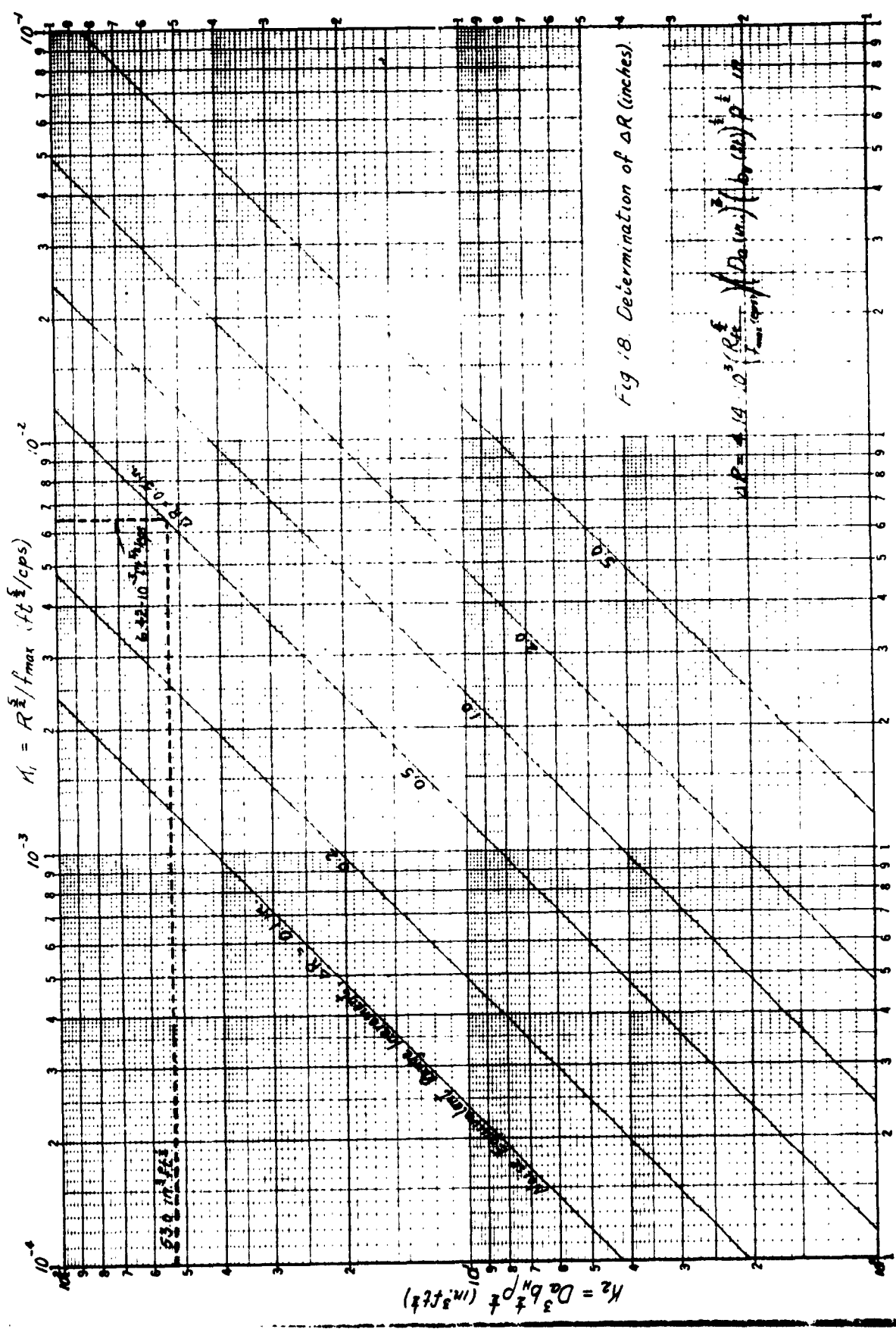


Fig 18. Determination of ΔR (inches).

## IMAGE-PLANE RANGEFINDING

In this section passive optical ranging by means of image plane location is examined. The basic concept behind this ranging technique is that of aiming an optical system at the object to which range is to be measured and determining the position of the image plane of sharpest focus. Knowledge of the location of this plane of sharpest focus permits the object distance to be calculated.

This process can be made automatic by various means. For example, if a photomultiplier or other radiation detector is placed on the optical axis, with a rotating chopper wheel in front of it, and the chopper wheel is moved along the optical axis, maximum modulation occurs when the chopper is in the plane of sharpest focus. Slightly more complicated methods than this may present sufficient advantages to warrant their adoption.

The present discussion of such systems contains two parts. The first is a brief presentation of the mathematics required for a complete analysis of such systems. This presentation is included only for completeness, since, as it will be seen, actual numerical calculations require data which is not available. However, this part does serve as a guide for the second part of the discussion, which is an analysis of a particular system; the minimum detectable change in range is calculated for this special case.

### System Analysis

The following is a brief outline of the steps required for the complete analysis of ranging by image plane location.

We describe the image space by an intensity distribution  $I(x, y, z)$  where  $z$  represents distance along the optical axis. The field stop and chopper together constitute a time-varying space filter  $W(x, y, t)$ ; when this is located at  $(x_0, y_0, z)$  in image space the time-varying output,  $O(x, y, z, t)$ , is

$$O(x, y, z, t) = \iint_{\infty} W(x_0, y_0, t) I(x_0 + x, y_0 + y, z, t) dx_0 dy_0.$$

The mean square value of the resulting electrical output (neglecting a constant factor for gain) is

$$P(x, y, z) = \lim_{T \rightarrow \infty} \frac{1}{2T} \int_{-T}^T \{O(x, y, z, t)\}^2 dt$$

Now if  $x$  and  $y$  are allowed to vary, the average value of  $P(x, y, z) = \bar{P}(z)$  may be taken as the expected electrical output as a function of position along the optical axis. This quantity  $\bar{P}(z)$  will have a maximum at the position of sharpest focus,  $z_0$ , and the average minimum detectable change in focus,  $\Delta z$ , will be such that

$$\bar{P}(z_0) - \bar{P}(z_0 + \Delta z) = N, \text{ where } N \text{ is the noise power in the system.}$$

There are two mathematical problems involved in actually carrying

out the required calculations. The first is this: it must be supposed that the intensity distribution in the image plane results from the action of the optical system on an intensity distribution in object space, and that this intensity distribution is not given explicitly, but only its statistical structure is available; this structure may be expressed in terms of two-dimensional Wiener spectra, for example.

The second problem is that of calculating  $W(x,y,t)$  from the known characteristics of the chopper and field stop.

Briefly, the first problem is handled by considering that the object space is a plane located a fixed distance from the optical system\*, and is described by a Wiener spectrum  $B(k_1, k_2)$ . Then the statistical properties of the image space are given by the Wiener spectrum

$$I(k_1, k_2, z) = | H(k_1, k_2, z) |^2 B(k_1, k_2)$$

where  $H(k_1, k_2, z)$  is the transfer function of the optical system.

If the expression for  $\bar{P}(z)$  is written out as

$$\bar{P}(z) = \lim_{R \rightarrow \infty} \frac{1}{4R^2} \iint_{-R}^R dx dy \left[ \lim_{T \rightarrow \infty} \frac{1}{2T} \int_{-T}^T \{ O(x, y, z, t) \}^2 dt \right]$$

\*The additional complications introduced by considering a three-dimensional object space are not warranted at this stage of the study.

then it may be shown that

$$\bar{P}(z) = \iint_{\infty} dk_1 dk_2 \left[ |H(k_1, k_2, z)|^2 B(k_1, k_2) \lim_{T \rightarrow \infty} \frac{1}{2T} \int_{-T}^T dt |W(k_1, k_2, t)|^2 \right].$$

In this expression  $H(k_1, k_2, z)$  can be found by analyzing the optical system, and, as will be shown below,  $W(k_1, k_2, t)$  can be calculated from the characteristics of the field stop and chopper, and so if the nature of the background  $B(k_1, k_2)$  is known,  $\bar{P}(z)$  can be calculated. Of course, the limitation on this approach is the specification of  $B(k_1, k_2)$ . The many background studies which have been conducted have been concerned with very much lower resolution information than is required for this problem, and so the necessary data does not exist.

To complete the discussion, the relation of  $W(k_1, k_2, t)$  to the characteristics of the field stop and chopper will be indicated.

If the chopper has a weighting function  $C(x, y)$  and the field stop has a weighting function  $F(x, y)$ , the resulting combined weighting function when the relative displacement between the chopper and field stop is  $x_1, y_1$  is

$$W(x, y, x_1, y_1) = F(x, y) C(x + x_1, y + y_1)$$

If  $x_1$  and  $y_1$  are functions of time, then the time-varying weighting function  $W(x, y, t)$  is given by

$$W(x,y,t) = F(x,y) C(x + x_1(t), y + y_1(t)).$$

The transform of this product is the convolution of the transforms,  
and so

$$W(k_1, k_2, t) = \frac{1}{4\pi^2} \iint_{\infty} F(k_1 + k_1', k_2 + k_2') C(-k_1', -k_2') e^{-j[k_1' x_1(t) + k_2' y_1(t)]} dk_1' dk_2'$$

Thus, as stated above,  $W(k_1, k_2, t)$  can be computed from the known characteristics of the chopper and field stop.

Instead of following the above generalized approach, a specific case will be analyzed. Comparison will show that each step described above appears in the calculations, but the results lack a generality that they might have if more data on the terrain background were available. On the other hand, the calculations for this specific case are relatively simple.

Optimization of System and Noise Equivalent Range Accuracy

Suppose that a fine-grained optical chopper is rotated in the image space of an optical system, and then the energy passing through the chopper is allowed to fall on a detector. The detector output will contain an a-c signal resulting from the chopping of small detail in the image. If the chopper is located in the image plane, this a-c signal will be a maximum; as the chopper is moved away from this plane, the amplitude of the a-c signal falls off, slowly at first and then faster. (This phenomenon is evident in the experimental results discussed in Appendix C.)

In order to determine the location of the plane of sharpest focus the chopper may be moved periodically back and forth along the optical axis by a small fixed amount, and the amplitude of the signals obtained in the two positions compared. The mean position of the chopper is moved in the direction of the larger signal; when the signals are balanced, the plane of sharpest focus is located half-way between the two positions of the optical chopper.

In order to design such a system, the process of determining best focus may be described in slightly different terms which lead to a quantitative treatment.

It may be considered that the rotational motion of the chopper gives a relatively constant frequency signal in the presence of detail in the image; this signal is thought of as a carrier (in the radio-frequency sense) which is amplitude modulated by the back-and-forth motion of the chopper.

This modulated carrier is rectified and filtered (demodulated) to get the modulation envelope, and this envelope is synchronously rectified to determine which direction to move the mean position of the chopper. The synchronous rectification results in a d-c level, and the sensitivity of the system can be measured by the amount of modulation of the carrier which is necessary to make this output equal to r.m.s. noise in the system.

Calculation shows that for such a system, if the input signal has the form

$$S(t) = S_0 (1 + \epsilon \cos 2\pi p t) \cos 2\pi f_c t$$

where  $S_0$  is the carrier amplitude,

$\epsilon$  is the fractional modulation,

$p$  is the modulation frequency, and

$f_c$  is the carrier frequency, and

if the input carrier signal-to-noise ratio is high, then the minimum detectable modulation  $\epsilon_{\min}$  (that is, the fractional modulation which results in a final d-c level equal to r.m.s. noise) is given by

$$\epsilon_{\min} = \frac{2\sigma}{S_0} (\Delta f)^{1/2},$$

where  $\sigma$  is the r.m.s. noise power per unit bandwidth, and  $\Delta f$  is the bandwidth of the system at the output.

This formula can be used to calculate the accuracy with which the location of the plane of best focus can be determined, and this can be

related to the accuracy with which range can be measured with such a system.

In order to do this the quantities  $\epsilon$ ,  $S_0$ ,  $\sigma$ , and so on must be related to the various parameters of the optical system.

A point near the focus of the optical system is sketched in Figure 19. The double cone represents the volume of space through which energy passes from a point target. This cone of energy is chopped at A and then at B; the detector output might be as shown, where the a-c signal generated at position B is less than that generated at A because the chopper is further from the focal plane at B.

Suppose that the amplitude of a narrow band a-c signal generated at a point  $\Delta$  away from the plane of best focus is  $Q(\Delta)$ . Then the difference between the carrier amplitudes at  $\Delta = \eta + \Delta_1$  and  $\Delta = \eta - \Delta_1$  is  $Q(\eta - \Delta_1) - Q(\eta + \Delta_1)$ . Here  $2\Delta_1$  represents the fixed distance between the two positions of the chopper, and  $\eta$  represents a small shift in the location of the plane of best focus away from the midpoint of the chopper positions. For  $\eta$  small,

$$Q(\eta - \Delta_1) - Q(\eta + \Delta_1) \cong 2\eta \frac{dQ(\Delta)}{d\Delta}$$

then in the expression

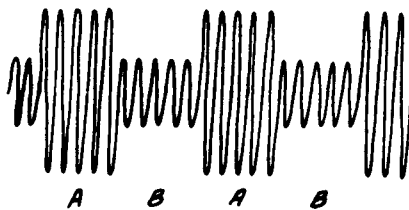
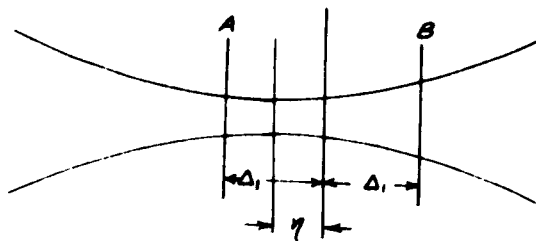


Figure 19. Energy Distribution Near Focus, and Resulting Waveform.

$$\epsilon_{min} = \frac{2\sigma}{S_0} (\Delta f)^{1/2}$$

we can write for the left hand side

$$\epsilon_{min} = 1.27 \eta_{min} \left| \frac{dQ(\Delta_i)}{d\Delta} \right| \frac{1}{Q(\Delta_i)},$$

because  $S_0 = Q(\Delta_i)$ . The factor  $1.27 = \frac{4}{\pi}$  is used because in the system under consideration the carrier is modulated with a square wave; only the fundamental of this square wave is detected and the amplitude of this fundamental is  $\frac{\pi}{4}$  times the amplitude of the square wave. The factor  $\Delta f$  is simply the system bandwidth measured at the output, and  $\sigma = P$ , the noise equivalent power of the system, if all of the amplitudes in question are measured in terms of input power to the detector. This leads to the equation

$$1.27 \eta_{min} \left| \frac{dQ(\Delta_i)}{d\Delta} \right| \frac{1}{Q(\Delta_i)} = \frac{2P}{Q(\Delta_i)} (\Delta f)^{1/2},$$

or

$$\eta_{min} = 1.57 \frac{P(\Delta f)^{1/2}}{\left| \frac{dQ(\Delta_i)}{d\Delta} \right|}.$$

The value of  $\eta_{min}$  now represents the minimum detectable image shift.

This can be related to the minimum detectable object shift  $(\Delta x)_{min}$

by differentiating the expression  $x x' = f^2$ , where  $x$  is the object distance (measured from the front and back focal points of the optical system) and  $f$  is the focal length of the optical system. It is found that

$$\eta_{\min} = (\Delta x)_{\min} \frac{f^2}{x^2} .$$

Hence the minimum detectable shift in object position is

$$(\Delta x)_{\min} = \frac{x^2}{f^2} \frac{1.57 P(\Delta f)^{1/2}}{\left| \frac{dQ(\Delta)}{d\Delta} \right|} .$$

It is now necessary to determine the function  $Q(\Delta)$ . Then in order to optimize the system  $\Delta$ , and the other parameters affecting  $Q(\Delta)$  must be adjusted to maximize  $\left| \frac{dQ(\Delta)}{d\Delta} \right|$ . Finally, substitution in the above expression allows the ranging accuracy to be determined.

To determine the function  $Q(\Delta)$ , we begin by imaging an ideal optical system which forms a perfect image of the field of view, and assume that the optical chopper is located in the image plane of this optical system. Let the total energy falling on the image of the field of view be  $E$ , and suppose that the chopper has these three characteristics: 1) On the average it transmits half of the energy. 2) The fundamental spatial frequency it responds to is  $k$  cycles per radian. (If the chopper moves past the field of view with velocity  $v_c$ , and if the focal length of the system is  $f$ , the principal electrical frequency appearing in the output of the detector is  $kv_c/f$  cycles per second; this is the carrier

frequency used above, and so  $f_c = kv_c/f_o$ .) 3) The fractional modulation of the energy E produced by the chopper in the image plane of this ideal optical system is m. The fractional modulation is defined as the r.m.s. value of the a-c fluctuations in the power falling on the detector (at frequency  $f_c$ ) produced by the chopper, divided by the d-c radiation falling on the chopper. The fractional modulation m is expected to be a small number; on the order of 1%, perhaps.

Now consider the situation which exists when the image on the chopper is blurred, as it is in the ranging system under consideration. This blur is due to two things, the blur due to the optical system, and the blur due to the chopper being out of the plane of sharpest focus. These two effects are independent, and it is characteristic of optical systems that such effects tend to add in the square:

$$(\text{Total blur})^2 = (\text{Optical blur})^2 + (\text{Out-of-focus blur})^2.$$

Now from the geometry of the system, the out-of-focus blur diameter is  $\Delta D/f$  when  $\Delta$  is the distance away from the plane of sharpest focus, and D and f are the diameter and focal length of the optical system, respectively. Hence the angular diameter of the out-of-focus blur for small values of  $\Delta$  is

$$(\text{Out-of-focus blur}) = \frac{\Delta D}{f^2}.$$

Then if the angular diameter of the optical blur is  $\theta$ ,

$$(\text{Total blur}) = \sqrt{\theta^2 + \frac{(\Delta D)^2}{f^4}}$$

Now the affect of this blur on the pattern on the chopper must be considered. Assuming that the energy falling on a point in the image plane of a perfect optical system is spread uniformly over a circle having the above diameter, the effect on the amplitude of spatial frequencies  $k$  is to reduce them by a factor:

$$\frac{2}{y} \left| J_1(y) \right|,$$

$$\text{where } y = \pi k \sqrt{\theta^2 + \frac{(\Delta D)^2}{f^4}},$$

and  $J_1$  is the first order Bessel function.\*

Hence if the amplitude of the fluctuations in radiation falling on the detector was  $\sqrt{2} m E$  in the case of the ideal optical system,\*\* in the system under discussion,

$$Q(\Delta) = 2 \sqrt{2} m E \left| \frac{J_1(y)}{y} \right|$$

\* Very similar functions result from other assumptions about the energy distribution within the blur circle.

\*\* Note that  $mE$  is the r.m.s. value of the fluctuations.

$$\text{where } y = \pi k \sqrt{\theta^2 + \frac{(\Delta D)^2}{f^2}}.$$

This is the required function  $Q(\Delta)$ .

We now wish to design a system; this requires picking parameters so that  $(\Delta x)_{\min}$  is as small as possible.

In doing this it will be assumed for the time being that  $\theta$ ,  $D$ , and  $f$  are fixed; they will then appear in the final equation for system performance. Assuming for the moment that these are fixed,  $k$  and  $\Delta$  will be chosen to maximize  $|dQ(\Delta)/d\Delta|$ ; the resulting value of  $\Delta$  is  $\Delta_1$ , and the resulting value of  $|dQ(\Delta_1)/d\Delta|$  is to be substituted in the expression for  $(\Delta x)_{\min}$ . We have immediately

$$\frac{\partial Q(\Delta)}{\partial \Delta} = 2\sqrt{2} m E \left[ J_0(y) - \frac{2}{y} J_1(y) \right] \frac{\Delta}{\left[ \theta^2 + \frac{(\Delta D)^2}{f^2} \right]} \frac{D^2}{f^2}.$$

Now for any choice of the the other parameters, an optimum value of  $k$  can be found:  $k$  must satisfy

$$\frac{\partial \left( \frac{\partial Q}{\partial \Delta} \right)}{\partial k} = 0$$

But

$$\frac{\partial \left( \frac{\partial Q}{\partial \Delta} \right)}{\partial k} = \left( \frac{\partial \left( \frac{\partial Q}{\partial \Delta} \right)}{\partial y} \right) \left( \frac{\partial y}{\partial k} \right).$$

Since  $\frac{\partial y}{\partial k}$  is constant, the best k results when

$$\frac{\partial \left( \frac{\partial Q}{\partial \Delta} \right)}{\partial y} = 0,$$

or when y is such that

$$\frac{d}{dy} \left[ J_0(y) - \frac{2}{y} J_1(y) \right] = 0.$$

Differentiation yields the expression

$$\frac{4-y^2}{2y} J_1(y) = J_0(y);$$

this has a solution for  $y = 3.06$ , and for this value of y,

$$J_0(y) - \frac{2}{y} J_1(y) = -0.486.$$

Thus for this best choice of k

$$\left| \frac{\partial Q}{\partial \Delta} \right| = 2\sqrt{2} (0.486) m E \frac{\Delta}{\theta^2 + \frac{(\Delta D)^2}{f^4}} \frac{D^2}{f^4}.$$

A value of  $\Delta_1$  can now be chosen to maximize this expression. It will easily be seen that it is necessary that

$$\frac{\Delta_1 D}{f^2} = \theta.$$

So finally

$$\left| \frac{\partial Q(\Delta_1)}{\partial \Delta} \right| = \frac{0.687 m E D}{f^2 \theta}$$

The design requirements that have resulted from this process are

$$y = \pi k \sqrt{\theta^2 + \frac{(\Delta D)^2}{f^4}} = 3.06$$

and

$$\Delta_1 = \frac{f^2 \theta}{\Delta}$$

From these we may deduce that

$$k \theta = 0.69.$$

The ranging accuracy of this optimized system can now be expressed as

$$(\Delta x)_{min} = 2.29 \lambda^2 \frac{\theta}{D} \frac{P(\Delta f)^{1/2}}{m E}$$

The only remaining chore before numerical calculations can be made is to evaluate P and E. The necessary information appears in Appendix B. There it is shown that

$$E = 1.15 \times 10^{-6} L \rho \omega A_c \text{ watts, where}$$

L is the radiation incident on the terrain in foot-candles  
 $\rho$  is the average reflectivity of the terrain  
 $\omega$  is the angular field of view of the optical system, and  
 $A_c$  is the area of the entrance pupil of the optical system.

It is also shown for practical purposes,

$$P = (5.3 \times 10^{-18} \frac{E}{2})^{1/2}$$

Using these expressions, it is found that

$$(\Delta x)_{min} = 3.48 \cdot 10^{-6} \frac{x^2 \theta (\Delta f)^{1/2}}{D m (L \rho \omega A_c)^{1/2}}$$

Consider, for example, the following system:

$$x = 1340 \text{ cm (44 ft.)}$$

$$D = 7.5 \text{ cm (3 in.)}$$

$$A_c = 33 \text{ cm}^2$$

$$\theta = 10^{-4} \text{ radians}$$

$$\omega = 9.6 \times 10^{-5} \text{ steradians}$$

$$\Delta f = 16 \text{ cps}$$

$$m = 0.01$$

$$L = 1000 \text{ foot candles}$$

$$\rho = 0.2$$

For this system,

$$\begin{aligned} (\Delta x)_{\min} &= 4.19 \times 10^{-2} \text{ cm} \\ &= 0.016 \text{ inch} \end{aligned}$$

This represents the theoretical accuracy of this ranging process. An actual system will not be designed to have this accuracy, since achieving this performance would require unnecessary refinement in design and construction. This calculation does show that noise inherent in the ranging process does not limit system performance under the assumed conditions, and that therefore the precise values chosen for various parameters such as the percentage modulation are not critical.

### Image-Plane Rangefinder at Night

Night operation with the passive image-plane rangefinding system presents no problem; however, it does require the use of a searchlight to illuminate the terrain. Rather than performing a completely independent calculation to find the performance for this situation, it is possible by inspection of the previous calculations on both the active and passive systems, during daytime operation, to show the night-passive-system feasibility.

Calculations on the use of the arc light in the active c-w system yielded a value of  $E_t(S-20) = 4.2 \times 10^{-7}$  watt; and  $E_b(S-20) = 4.4 \times 10^{-5}$  watt, calculated for a terrain illumination of 11,000 foot candles. Thus, the return from the arc light would be equivalent to a terrain illumination of  $11,000 \times 4.2 \times 10^{-7} / 4.4 \times 10^{-5} = 105$  foot candles.

In the calculation performed in the previous section for the daytime-passive operation, I was assumed to be 1000 foot candles. Since

$$(\Delta x)_n \sim I^{-2},$$

night operation, using the passive system yields a value of

$$(\Delta x)_n = 0.016 \text{ inch} \times \left(\frac{1000}{105}\right)^{1/2} = 0.05 \text{ inch} .$$

The Effect of a Constantly Changing Target Area on the Determination of Best Focus

The preceding analysis of ranging by location of the position of best focus has assumed a fixed object field. Consideration must be given to the fact that normally the field is moving. The motion of the field has only a slight effect on the amplitude of the signal resulting from the chopping action of the reticle. If points enter or leave the field a phase shift and amplitude change may result, but this effect is small, since only points near the edge of the field can cause such effects. The rate at which these changes can occur is of course limited by the rate of motion of the field; if this motion is low compared with the chopping rate, only smooth amplitude changes will result from the moving field. Thus motion of the field has little effect on the chopping action.

Now consider the process of determining best focus. This is done by comparing the amplitudes of the interrupted signals produced alternately at two different points along the optical axis. Since the motion of the target area produces changes in these amplitudes, it is desirable to have the rate of alternation high enough so that a given point remains in the field for several complete cycles of this comparison. This constitutes a precaution to be observed in equipment design.

An estimate of this rate can be made if it is supposed that the vehicle is moving over level ground with a velocity  $V$ , that the vertical beamwidth of the sensor is  $\omega_2$ , and that the depression angle is  $\alpha$ . Then a point on

the terrain remains in the field of view for about

$$t_1 = \frac{\omega_2 R}{\alpha V} \text{ seconds.}$$

If it is desired to produce  $n_1$  alternations of the position of the chopper in this time, the rate at which these must be produced is

$$\frac{n_1 \alpha V}{\omega_2 R}$$

per second. For

$$\alpha = 0.114 \text{ radian}$$

$$V = 88 \text{ feet/second (60 mph)}$$

$$n_1 = 5$$

$$\omega_2 = 6.8 \times 10^{-3} \text{ radians}$$

$$R = 44 \text{ feet,}$$

the alternations of position should occur at a rate of 168 per second.

## TRIANGULATION TRACKING

The next ranging method to be considered is a method of triangulation. A narrow beam of light (which may be modulated for purposes of coding) is projected directly forward and slightly downward from a source on one side of the vehicle. The spot on the terrain illuminated by this beam is observed by a tracker mounted on the opposite side of the vehicle. This tracker is designed to measure the angle between a reference azimuth and the line of sight to the spot. When the range to the ground changes, this angle also changes, resulting in a different measured angle and a different output from the tracker.

The questions to be answered about such a system are 1) What angular accuracy must the tracker have? 2) Is it possible to obtain a signal-to-noise ratio great enough to achieve this accuracy? 3) What additional practical considerations are involved? 4) What is the equipment complexity?

The tracking accuracy required of such a system can be estimated from Figure 20, where S represents the source, T the tracker, R the range to the terrain,  $\theta$  the measured angle to the illuminated spot, and W the distance between the source and tracker. Then

$$\theta = \tan^{-1} \frac{W}{R}$$

$$d\theta = \frac{W}{R^2 + W^2} dR$$

( For  $W = 5$  feet,  $R = 44$  feet, and  $dR = 2$  inches (the required range accuracy),

$$|d\theta| = .42 \times 10^{-3} \text{ radian.}$$

This constitutes the required tracking accuracy; it is within the state-of-the-art of conventional optical trackers.

The signal-to-noise ratio required to achieve this accuracy depends on the total field of view the tracker must possess. This can be estimated by placing limits on the range to the terrain with which the system must cope. For example, if  $R$  varies between 100 feet and 25 feet, the change in  $\theta$  is

$$\begin{aligned} \Delta\theta &= \theta_{25} - \theta_{100} = \tan^{-1} \frac{5}{25} - \tan^{-1} \frac{5}{100} \\ &= 147 \times 10^{-3} \text{ radian.} \end{aligned}$$

Thus, over the total field, the tracker must detect a change of one part in  $\frac{147}{.42} = 350$  if the tracking head is fixed with respect to the vehicle.

(If the head is allowed to move, this may be reduced at the cost of increased complexity.) This value represents the approximate signal-to-noise ratio necessary for tracking over the required field to the required degree of accuracy.

The signal-to-noise ratio which may be attained by such a system can be calculated directly from data given previously. Let

$E_t$  = Power returned from the target area as a result of illumination by the transmitter.

$E_b$  = Power collected as a result of ambient illumination of the terrain.

$P$  = Multiplier phototube noise-equivalent power.

It is shown in Appendix B that when  $E_b$  is large (this represents the worst case for such a system), typical multiplier phototubes have a noise-equivalent power given by

$$P = \left[ 5.3 \times 10^{-18} E_b \right]^{1/2} .$$

Also, it is clear that the signal-to-noise ratio is simply  $E_t/P \sqrt{2B}$ , where  $B$  is the required system bandwidth. In the discussion of the active c-w ranger, values of  $E_t$  and  $E_b$  were computed for the field of view required by the sensor (22.7 milliradians horizontal beamwidth and 6.8 milliradians vertical beamwidth) and for a source and collector (tracker) aperture of  $125 \text{ cm}^2$ , and a multiplier phototube with an S-20 cathode:

$$E_t = 1.49 \times 10^{-7} \text{ watt}^*$$

$$E_b = 4.43 \times 10^{-5} \text{ watt}$$

---

\* A factor of  $2 \sqrt{2}$  has been introduced to convert peak-to-peak radiation fluctuations to rms, since the transmitted beam must be modulated for background discrimination.

Hence  $P = 1.53 \times 10^{-11}$  watt. For a system bandwidth  $B = 25$  cps, the signal-to-noise ratio is

$$S/N = \frac{1.49 \times 10^{-7}}{1.53 \times 10^{-11} \sqrt{50}} = 1.38 \times 10^3$$

This signal-to-noise ratio is adequate for achieving the required tracking accuracy.

It is now necessary to consider the nature of the target which is to be tracked. This target is a portion of the terrain which lies about 44 feet ahead of the vehicle and is illuminated by a beam 22.7 milliradians wide and 6.8 milliradian high. Figure 21 illustrates the geometry when the vehicle is located on a perfectly level surface. In this figure the illuminating source is located on one side of the vehicle and projects a beam directly ahead; the tracker is located on the other side and measures the angular location to the illuminated patch. In order to describe the appearance of this patch of terrain as seen from the tracker, we may imagine it to be projected on a plane located at the target and perpendicular to the line-of-sight from the tracker. It then appears to be approximately a parallelogram, as suggested in Figure 21, having a length of about 1 foot and a height of 0.3 foot. The short sides make angles of about  $45^\circ$  with the base.

A 2-inch change in the range to the terrain shifts this target laterally by 0.02 foot. (This shift is calculated from the range to the target and the angle of  $0.42 \times 10^{-3}$  radian previously shown to correspond to the

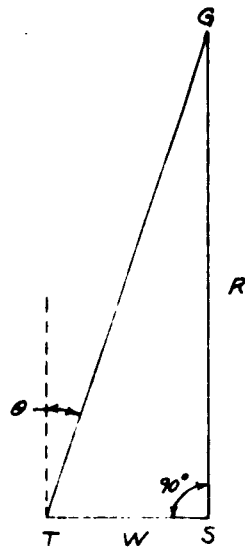


Figure 20 Tracker Geometry



Figure 21 Illuminated Portion of Terrain as Seen by Tracker.

( 2-inch range change.) This motion of the target is shown in dotted lines in Figure 21. It is immediately obvious that in practice a great deal of difficulty will be experienced in detecting this shift, because variations in the reflectivity of the terrain will cause much greater shifts in the apparent center of the target patch than the range shift. Thus the system does not appear attractive from this standpoint.

A final consideration is that of equipment complexity. It should be observed that this technique requires four optical systems (two sources and two trackers) to cover both tracks of the vehicle, and that the source and corresponding tracker must be mounted in separate locations on the vehicle, thus contributing to the installation problem.

#### TRIANGULATION TRACKING USING CORRELATION

A different form of triangular tracking has been considered which gives promise of eliminating the principal defect of the previous technique. This defect is the difficulty with conventional trackers in measuring a small shift in a large object (in this case the field of view of the system) when the received intensity distribution over the target may not be uniform. In the system to be considered now, the range to the terrain is determined by automatic triangulation which is accomplished by looking at the terrain ahead of the vehicle with two separated sensors. The system is passive rather than active, i.e., no source of energy is required for normal daylight operation. One sensor is fixed with respect to the vehicle (ignoring stabilization for the moment). The second functions as a tracker and directs itself until its field of view coincides with that of the first.

The angle between the two lines of sight then gives the distance to the terrain.

The principal problem to be solved in the design of such a ranging device is the determination of the coincidence of the fields of view of the two sensors. Obviously if the field contained only one small bright point, this would be rather easy, but the actual fields of view will be patches of terrain filled with various amounts of small detail.

A possible approach to this problem of recognizing the coincidence of the two fields of view is provided by some experiments recently performed at Emerson Electric. In these experiments, an object plane having some detail was imaged on a rotating chopper which bore a random pattern of spots. The waveforms resulting from rotating the chopper were examined as the object plane was moved. It was found that the correlation between the waveforms resulting from different positions of the object plane was a smooth function of displacement, being largest for small displacements and approaching zero for large displacements. This provides a way for comparing the field of view of the two sensors: identical synchronized choppers can be used, and the waveforms produced compared. When the correspondence between the waveforms is a maximum, the two sensors have nearly the same field of view.

The signal levels available in such a system are large compared to those which were obtained in the system discussed earlier, because the level of natural illumination is greater than can be obtained with the source used in the active system. To show this, we may use information developed in

the study of the active c-w rangefinder. In the present case, the signal-to-noise ratio, S/N is given by

$$S/N = \frac{m E_0}{P \sqrt{2B}}$$

where m is the fractional modulation of the field produced by the chopper. For the values previously quoted (which correspond to the field of view of the system and for an aperture of 125 cm<sup>2</sup>, and for a terrain illumination of 11,000 foot candles) we find that if m = 0.01, and B = 25 cps, the signal-to-noise ratio is about 4000.

Under lower levels of illumination, the signal-to-noise ratio falls as the square root of the illumination; for 100 foot candles, the signal-to-noise ratio is approximately 380.

This system has the advantages of being passive and of having large signal levels available. It has the disadvantages of requiring a baseline to be established, thus increasing the installation problem, and of possibly needing four sensors (two for each track) although these might be combined in pairs to reduce the number. In addition, the technique is new and untried, and so might require a somewhat longer development time.

#### LASER RANGEFINDING

The fifth optical method which has been considered for the terrain sensor application is the use of a laser.

In some respects calling this a separate ranging technique is not correct, since the laser may be thought of as an energy source which may be used with any of the ranging techniques which have been examined during the course of this study. However, the laser does permit pulsed operation, and represents the only known source of optical-wavelength energy which is effective in this form of operation. Therefore, aside from its possible use to replace a conventional source, the laser has been considered for use as a pulse-type of rangefinder.

Since a number of laser rangefinders have already been developed, the study of the laser ranging technique has been restricted to an examination of practical considerations involved in their use. Only the present state-of-the-art has been considered, since it seems desirable to consider a device which is feasible at the present time. Future improvements in the laser may be expected to remove most of the practical difficulties in their use.

The following factors may be considered: reliability, available bandwidth, beamwidth, accuracy, security, bulk, and power requirements.

Reliability - at the present time, the laser has not been tested under a variety of environmental conditions, and so its durability under prolonged and rapid pulsing is not known. It may compare favorably with other optical components.

Bandwidth - as shown previously, the terrain sensor requires a bandwidth of at least 11 cps if this is the only source of range error. This bandwidth requires a minimum pulse repetition rate of 22 pulses per second

from the laser. At the present time the highest rate we have found for a commercially available laser is 10 pulses per second. It is likely that this rate will be increased, of course.

Beamwidth - laser beamwidths are at present between  $10^{-3}$  and  $5 \times 10^{-3}$  radian wide. Optical techniques would allow the required tracker beamwidth to be obtained.

Accuracy - the accuracy of a pulsed laser rangefinder depends on the time resolution of the system, and is independent of the absolute range. The required range resolution of 2 inches represents a round-trip time increment of  $0.33 \times 10^{-9}$  second. This time resolution is rather difficult to achieve.

Security - pulsed laser systems, being active, are inherently less secure than passive systems, but the narrow spectral bandwidth involved makes them more secure than other active systems.

Bulk - the commercial laser producing 10 pulses per second requires a desk-type console. This volume can certainly be reduced; however, present laser equipments are rather bulky.

Power requirements - the power required for a laser rangefinder is somewhat greater than that required for more conventional devices, but does appear to be within the capability of military vehicles.

It is concluded that the use of a pulsed laser rangefinder for the terrain sensor requires advancing the present state-of-the-art in several directions.

## STABILIZATION AND COMPUTATION REQUIREMENTS

### ASSUMPTIONS

The stabilization and computation requirements for the terrain sensor have been studied within the framework established by the following assumptions:

- 1) Two optical terrain sensors measure the range to points on the terrain ahead of the vehicle along the paths to be followed by the wheels or tracks. Whether the sensors operate by active or passive means is not important in establishing stabilization and computation requirements.
- 2) The desired performance characteristics of the sensor in terms of the terrain information which is needed are as follows:
  - a) The terrain height is to be measured to an accuracy of plus or minus 2 inches.
  - b) The nominal distance from the sensor to the measuring point on the terrain ahead of the vehicle is 44 feet.
  - c) The maximum velocity of the vehicle is 50 miles per hour.

### STABILIZATION PROBLEMS

#### Errors in Terrain Coordinates due to Error in Depression Angle, Range Measurement, and Sensor Elevation Above the Terrain

Figure 22 shows the various parameters used in the measurement of the range to the terrain. As will be shown later in this section, a more complicated representation is necessary in order to describe continuous terrain measurements, but the geometry of figure 22 is adequate to indicate the degree of stabilization required for the sensor.

The optical sensor is positioned at point A on the vehicle, at a distance  $a$  above the terrain. The range,  $R$ , to point B is measured by the sensor with an error of  $\Delta R$ , resulting in a knowledge of the terrain at B, with respect to the indicated reference level, to an accuracy of  $\Delta y$  and  $\Delta x$ .

It is important to determine to what accuracy the values of  $a$  and  $\alpha$  (the depression angle of the sensor) must be defined by the stabilization system. From Figure 22, assuming that  $\alpha$  is less than about  $10^\circ$ ,

$$y = a + b - R \alpha \quad (12)$$

$$x = R \quad (13)$$

and it follows that

$$\Delta y = \Delta a + \Delta b - R \Delta \alpha - \alpha \Delta R \quad (14)$$

where the deltas refer to small changes or errors in the various parameters.



Assuming the following values, based on the model adopted previously,

$$R = 44 \text{ ft} \approx 528 \text{ inches}$$

$$\alpha = 0.114 \text{ radian}$$

$$\Delta y = 2 \text{ inches (maximum error)}$$

$$\Delta x = 2 \text{ inches (maximum error)}$$

we have

$$\Delta a + \Delta b - 528 \Delta \alpha = -0.114 \Delta R = 2 \text{ inches.} \quad (15)$$

Now from equation 13,  $\Delta R = -2 \text{ inches}^*$ , as the error in  $x$  is equal directly to the error in  $R$ , and

$$\Delta a + \Delta b - 528 \Delta \alpha = 1.77 \text{ inches.} \quad (16)$$

It is possible to arrive at some estimate of the three quantities  $\Delta a$ ,  $\Delta b$ , and  $\Delta \alpha$ , by assuming that the three contribute equally to the total error and that the errors have a Gaussian distribution such that

$$\Delta a = \Delta b = 528 \Delta \alpha = \frac{\sqrt{3}}{3} 1.77 \text{ inches} = 1.02 \text{ inches rms.}$$

Thus  $\Delta \alpha = .0019 \text{ radian} \approx 0.11 \text{ degree, rms.}$

#### Errors in Terrain Coordinates due to Cant

Figure 23 indicates a terrain measurement when the optical sensor has been canted through an angle  $\beta$  from the vertical. If the line of sight is stabilized in space, and if the terrain is level, the errors in the terrain

\* The minus sign is used, since these errors are considered to be independent and it is necessary to consider the worst possible case.

determination,  $\Delta y$  and  $\Delta x$ , are identical to the errors in the sensor position. No error in  $x$  results from the presence of  $\beta$  degrees of cant:

Therefore

$$\Delta y = 2 a \sin (\beta/2) \sin \beta \quad (17)$$

$$\Delta x = 2 a \sin (\beta/2) \cos \beta \quad (18)$$

For  $\beta$  small,  $2a$  equal to 120 inches, and  $\Delta y$  equal to 2 inches, equation (17) becomes

$$\frac{\beta^2}{2} = \frac{2}{120}$$

and  $\beta = 0.182 \text{ rad} = 10.4 \text{ deg.}$

Using the above result in equation 18 gives

$$\Delta z = 120 \times .091 \times .984 = 10.7 \text{ inches}$$

The above error in the  $z$  direction is somewhat large, considering the width of the track. For a 2-inch error in  $z$ ,  $\beta$  is approximately 2 degrees.

If the sensor is pitch-stabilized, rather than space stabilized, the allowable cant error can be greater than this under same conditions. For example, if the sensor is mounted directly over the wheel or track, the cant axis of each sensor tends to be at ground level, and in this case on relatively level terrain the error produced by cant is negligible.

#### Summary of Stabilization Problem

In summary, the following is a list of the allowable stabilization errors:

- 1) The r.m.s. error in the elevation of the optical sensor above the terrain,  $\Delta a = 1.0$  inch.
- 2) The r.m.s. error in the vertical reference level,  $\Delta b = 1.0$  inch.
- 3) The r.m.s. error in the terrain sensor depression angle,

$$\Delta \alpha = 0.11 \text{ deg.}$$

- 4) The maximum allowable angle of cant of the terrain sensor,

$$\beta = 2 \text{ deg.}$$

#### COMPUTATION REQUIREMENTS

The process of computing the terrain profile from range-to-the-terrain measurements made by the optical sensor is not complicated, but it is not completely straightforward, either. This computation process should be distinguished from the computation required before the active suspension system can make use of the terrain profile data. In practice, of course, it may be desirable to combine the two processes.

The computation of terrain profile from range-to-terrain measurements depends to some extent on the desired output, of course. Here it is supposed that the active suspension system has a certain short reaction time,  $t_p$ , and that the output of the sensing and computation process is to be the difference between the elevation of the terrain where the vehicle presently is, and the elevation where the vehicle will be the short time  $t_p$  seconds later. This continuously generated difference tells the active suspension system how much and in what direction to act.

Systems for deriving other outputs are not considered in this section, but, if necessary, other quantities can be obtained by modifications of

the technique described. For example, a frequency analysis of the profile generated can be used to measure "roughness" according to a predetermined standard, and the output can be used to adjust the vehicle speed or the stiffness of the suspension system.

The computation process which is described here proceeds as follows: The range-to-the terrain is measured, and the vertical and horizontal coordinates of the terrain with respect to the vehicle are determined from this measurement. As the vehicle travels over the terrain, it moves up and down, and this motion must be subtracted from the measured vertical terrain coordinates computed from range-to-terrain measurements. This is accomplished by determining the actual vertical motion of the vehicle with an (integrating) accelerometer mounted on the vehicle; the accelerometer is part of the data reduction process rather than the terrain sensor, and only short-term accuracy is required of its output. This computation process is considered in detail below.

#### Definition of Parameters

The many symbols required in the discussion of the computation method are listed in the following table. Many of these quantities are called out in Figure 24. Note that most of these quantities are functions of time.

- a - The height above the terrain of the terrain sensor, along the direction of gravity. The position of the sensor is assumed to be above the front point of contact of the vehicle track or wheels and the terrain.
- b - The difference between the actual terrain elevation\* and the elevation as measured by the accelerometer and attendant circuitry.

\* Above some Absolute reference level.

The value of  $b$  is a slowly varying function of time, but may become large for large changes in terrain elevation.

- $\alpha$  - The depression angle of the optical sensor. It is measured in the vertical plane and is the angle between horizontal and the direction through which the sensor is pointing.
- $x$  - The coordinate of the terrain along the horizontal measured from the present position of the vehicle, positive in the direction of motion of the vehicle.
- $y$  - The measured vertical coordinate of the terrain, positive upward. Values of  $y$  are primed when referring to those obtained from the optical sensor measurement. They are unprimed when obtained from the accelerometer.
- $R$  - The range to the terrain ahead of the vehicle measured along the direction that the optical sensor is pointing.
- $t_c$  - The time to contact. This is the time between the measurement of a point on the terrain and the arrival of the vehicle at that point. It is equal to the distance,  $x$ , to this point divided by the average velocity,  $\bar{v}$ , of the vehicle between the measurement and the time of contact.
- $t_r$  - Reaction time - the time required by the suspension system to react to the terrain change being fed to it. This, in general, is a fixed period.
- $y'$  - The change in terrain elevation experienced during a time  $t_r$ .

#### Computing Equations

Figure 24 shows the geometrical relationships for making continuous



terrain measurements. This information is stored and presented to the suspension system at the proper time. In figure 24, the vehicle is assumed to be at a position on the terrain corresponding to the time  $t_2$ . At this time, the optical sensor is measuring the range  $R(t_2)$ . Other quantities that are being measured at time  $t_2$  are the values  $\alpha(t_2)$  and  $a(t_2)$ . The velocity,  $v(t_2)$ , of the vehicle is also being monitored.

The remaining measured quantity is the value  $\ddot{y}$ , the vertical acceleration of the front part of the vehicle as it passes over the terrain. The value of acceleration may be measured by an accelerometer mounted near the axle of the front wheel of the vehicle. The necessity for the use of this method, independent of the optical sensor, to sense the present instantaneous terrain profile, will be apparent later.

Also shown in figure 24 is a measurement of range to the terrain made at an earlier time,  $t_1$ . This time has been chosen in such a way that at time  $t_1$  the value of  $\Delta y_1'$  is just being fed to the suspension system. This value,  $\Delta y_1'$ , is the difference between the terrain elevation computed at time  $t_1$  and designated as  $y'(t_1 + t_{c1})$  and the value of the terrain which had been measured at a somewhat earlier time  $t_0$  and which is designated as  $y'(t_0 + t_{c0})$ , where  $(t_0 + t_{c0} + t_r) = (t_1 + t_{c1})$ .

The equations necessary for the calculations are obtained as follows, (referring to figure 24):

$$z(t) = R(t) \cos \alpha(t) \approx R(t) \quad (19)$$

for  $\alpha$  less than about 10 degrees.

Now,

$$y'(t+t_0) + b(t+t_0) + R(t) \quad \propto(t) = y(t) + b(t) + a(t). \quad (20)$$

(In figure 24, when  $t = t_2$  the value of  $y(t_2)$  is negative.)

If

$$b(t+t_0) \approx b(t), \quad (21)$$

the computing equation for  $y'$  becomes

$$y'(t+t_0) = y(t) + a(t) + R(t) \quad \propto(t). \quad (22)$$

Note that the slowly changing function of time  $b(t)$  does not affect the accuracy of the computation.

The factor  $y(t)$  is the terrain elevation as measured by the accelerometer and essentially integrated twice, at time  $t$ . Since it is necessary to measure the terrain profile ahead of the vehicle, to store this information, and to use it at the proper time, it might be thought that the value of  $y(t)$  could be obtained from this stored data, thus eliminating the use of the accelerometer. This would be feasible if all the measurements and computations were error-free. However, analysis shows that errors, although small for any particular range measurement and profile calculation, would accumulate after a period of time and the system would not work. Thus, it is necessary to have an independent measure of the past terrain profile. A rate measuring device could also perform the required function. It would yield the value  $\dot{y}$  from which the value  $y(t)$  could be obtained.

#### Method of Computation

Figure 25 shows schematically the method of computing continuously the terrain profile which is fed to the suspension system. The computation

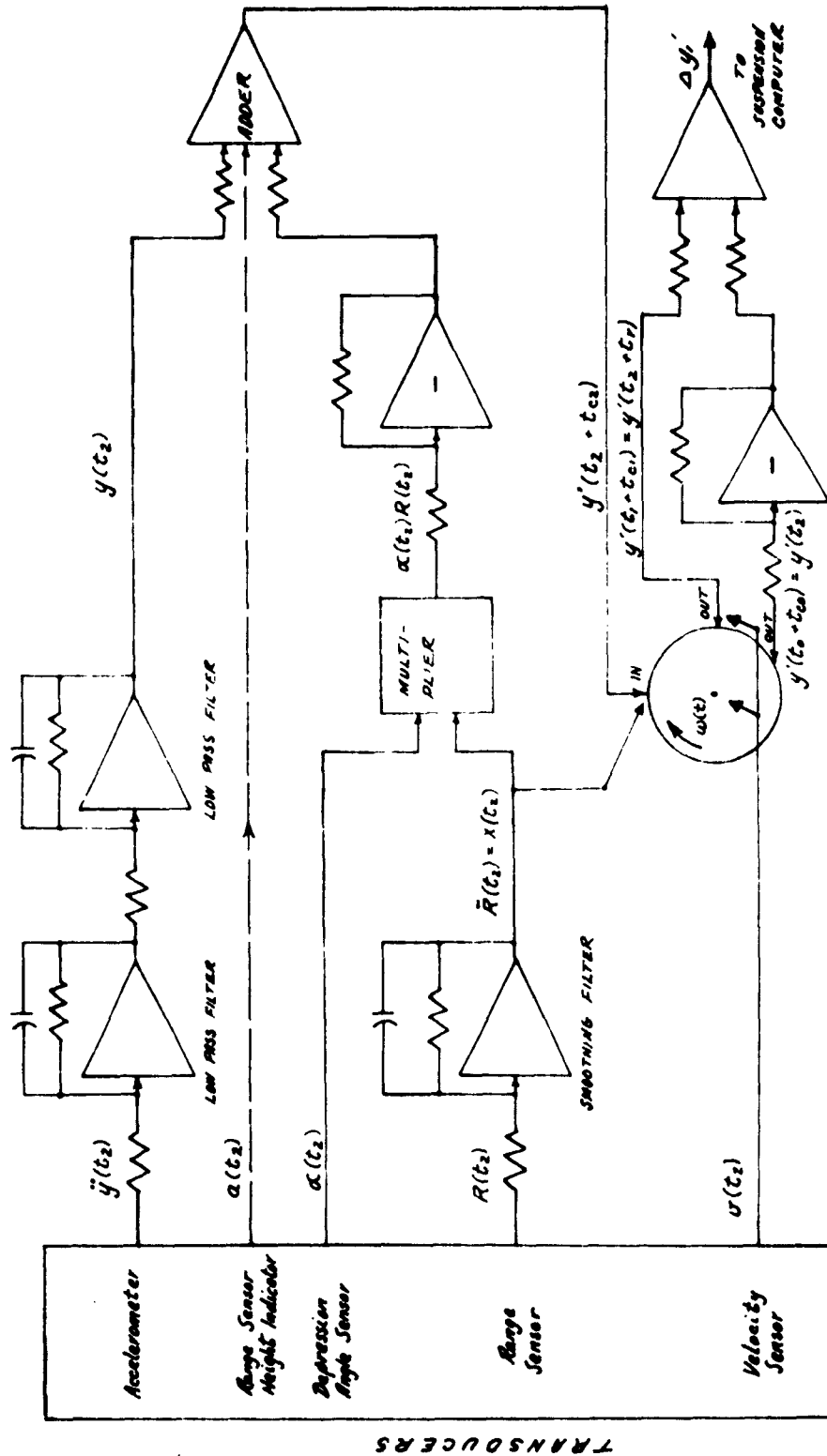


Figure 25. Functional Block Diagram of Computation Process.

that is represented corresponds to the time,  $t_2$ , as shown in the geometry of figure 24.

The output of the range sensor  $R(t_2)$  is smoothed through a low-pass filter to produce a smoothed or average value, as designated by  $\bar{R}(t_2)$ . The actual output of the optical range sensor will give such a smoothed value because of the finite electrical bandwidth of the sensor electronics as well as the optical beamwidth of the sensor.

The values of  $\alpha$  and  $a$  are shown as outputs from transducers. Stabilization will tend to hold these to constant values.

The output of the accelerometer,  $\ddot{y}(t_2)$ , is passed through two low-pass filters, yielding the result  $y(t_2)$ . Passing the accelerometer output through two integrators and two high-pass filters is equivalent to this use of two low-pass filters. This can be shown very simply by using Laplace transform notation, as follows:

integrator x integrator x high-pass filter x high-pass filter =

$$\frac{1}{s} \times \frac{1}{s} \times \frac{s}{\omega + s} \times \frac{s}{\omega + s} = \frac{1}{(\omega + s)^2}$$

and

$$\text{low-pass filter} \times \text{low-pass filter} = \frac{1}{\omega + s} \times \frac{1}{\omega + s} = \frac{1}{(\omega + s)^2}$$

The value of  $y(t_2)$  obtained from the integrator followed by two low-pass filters thus corresponds to the double integration of  $\ddot{y}(t_2)$  and the use of two high-pass filters, so that the resultant,  $y(t_2)$ , follows the rapid fluctuations of the terrain but not the slow fluctuations.

Solution of the computing equations, 19 and 22, results in the value of  $y'(t_2 + t_{c2})$  for the measurement made at time  $t_2$ . This is read into a storage element, which may be digital or analog. It is shown in figure 25 as a rotating drum. The terrain elevations  $y'(t_1 + t_{c1})$  and  $y'(t_0 + t_{c0})$ , where  $t_2 + t_r = t_0 + t_{c0} + t_r = t_1 + t_{c1}$  (from which  $\Delta y_1$  is computed for the suspension system), must at the same time be read from storage. This is accomplished as follows:

Suppose that  $\gamma_{in}(t)$  is the angular position of the input head,  $\gamma_{out}(t)$  is the angular position of the readout head which gives the stored value of  $y'(t_2)$  corresponding to the present position of the vehicle, and  $\omega(t)$  is the rotational speed of the drum. If  $y'(t_2)$  was entered at time  $t_0 = t_2 - t_{c0}$ ,

$$\int_{t_0}^{t_2} \omega(t) dt = \gamma_{out}(t_2) - \gamma_{in}(t_0).$$

Also, if the vehicle itself is considered,  $t_0$  and  $t_2$  must be related by

$$\int_{t_0}^{t_2} v(t) dt = x(t_0).$$

These two equations can be satisfied if

$$\omega(t) \approx v(t),$$

$$\gamma_{\text{out}}(t) = 0$$

$$\gamma_{\text{in}}(t) \approx -x(t).$$

Now let  $\delta(t)$  be the angular position of a second readout head which gives the value of  $y'(t + t_r)$  which corresponds to the vertical coordinate of the terrain which will be encountered  $t_r$  seconds from the present time. ( $y'(t_2 + t_r)$  was read in at time  $t_1$ .) It is necessary that

$$\frac{\gamma_{\text{out}}(t) - \delta(t)}{\omega(t)} = t_r,$$

since it must be assumed that the vehicle will move with constant velocity during time  $t_r$ . Thus  $\gamma_{\text{out}}(t) - \delta(t) = t_r \omega(t)$ , or from the previous expressions

$$\delta(t) \approx -t_r v(t).$$

Thus the storage drum which has been used as a model to discuss the storage requirements has the following characteristics:

1. The drum turns with angular velocity proportional to vehicle velocity.
2. The readout head giving present terrain elevation is fixed.
3. The angular displacement between this readout head and the readout head giving terrain elevation  $t_r$  seconds in the future is proportional to the horizontal velocity of the vehicle.

4. The angular displacement between the first readout head and the readin head at any instant is proportional to the computed horizontal coordinates of the terrain being viewed at that instant.

#### System Simplification

In the preceding discussion it has been assumed that the accelerometer has been mounted on the axle to measure  $y(t)$ , and that the distance between this point and the sensor,  $a(t)$ , is also measured continuously. Inspection of the computing equations, 19 and 22, shows that only the sum  $y(t) + a(t)$  is used, and that these quantities are not separately required. Thus the system can be somewhat simplified by mounting the accelerometer at the sensor and integrating its output to obtain the sum  $y(t) + a(t)$ . This has the following effects on the system. First, one measurement,  $a(t)$ , is eliminated. Second, the sensor-plus-accelerometer becomes a self-contained package, which simplifies installation. Third, since the suspension system prevents some variations in the terrain from being transmitted to the vehicle hull, the accelerometer has smaller variations to measure, and so a given percentage error yields a lesser total error. This system is considered to be the simplest and most effective, and is recommended. However, for completeness the system including measurement of  $a(t)$  is analyzed below.

#### Computing Errors and Circuit Parameters

For equation 21 to hold, the dashed line in figure 24, which is the terrain profile as measured by the system, must follow the actual terrain, but this is only essential for rapid changes in the terrain. Thus the following requirements are placed on the values of  $y$ , as measured by the accelerometer:

1. It must not respond to slow changes in the terrain. This is made evident by referring to figure 24. At some initial time,  $t_0$ , the vehicle was at a much lower elevation. If the value of  $\ddot{y}$ , obtained from the accelerometer were truly integrated twice, the value of  $y$  would be increased to a large magnitude resulting in too great a dynamic range of  $y$  for the equipment to handle.
2. The measured value of  $y$  must respond to rapid changes in the terrain, to give the required accuracy for the calculation of  $y'$ .

The above requirements may be adequately handled by passing the output of the accelerometer through two low pass filters. This section discusses the feasibility of the use of an accelerometer and attendant circuitry to provide the necessary system inputs within the required accuracy of the terrain profile.

Ramp Function Terrain. Figure 24 shows the terrain increasing up a long slope from time  $t_0$ . Assume that the terrain input to the accelerometer is a ramp function, ( $y = mx$ ), whose Laplace transform is  $\frac{m}{s^2}$ . The output  $y$  through the accelerometer and double-time-constant low-pass filter is

$$y = \mathcal{L}^{-1} \left[ \frac{m}{s^2} \times \frac{1}{s + \omega_0} \times \frac{1}{s + \omega_0} \right] = \mathcal{L}^{-1} \left[ \frac{m}{(\omega_0 + s)^2} \right]$$

and

$$y = m \times c^{-\omega_0 x} \quad (23)$$

Let  $y_{pk}$  (see figure 24) be the maximum value of  $y$  for a response to slow changes in the terrain. Differentiating equation 23, and solving for the maximum value yields

$$y_{pk} = \frac{A}{e \omega_b} \quad (24)$$

Thus by proper choice of the time constant of the low-pass filter, the value of  $y_{pk}$  can be controlled.

Sinewave Terrain. Next assume that the terrain is in the shape of a sinewave, such that

$$y = y_1 \sin \beta x \text{ where } \beta = \frac{2\pi}{x_1}, \text{ for } x > 0$$

$$y = 0 \text{ for } x \leq 0$$

so that  $x_1$  is the wavelength and  $y_1$  is the peak amplitude. The output through the accelerometer and double-time-constant filter is

$$\begin{aligned} y &= \mathcal{L}^{-1} \left[ \frac{4\beta}{\beta^2 + \Delta^2} \times \Delta^2 \times \frac{1}{\omega_0 + \Delta} \times \frac{1}{\omega_0 + \Delta} \right] \\ &= \mathcal{L}^{-1} \left[ \frac{\Delta^2 y_1 / \beta \omega_0^2}{(1 + \frac{\Delta}{\omega_b})^2 (1 + \frac{\Delta^2}{\beta^2})} \right] \end{aligned}$$

and

$$\frac{y}{y_1} = \frac{1}{1 + \frac{\omega_b^2}{\beta^2}} \sin(\beta x + \pi - \psi) - \left( \frac{\omega_b / \beta}{1 + \omega_b^2 / \beta^2} \right) \left( \frac{2}{1 + \omega_b^2 / \beta^2} - \omega_b x \right) e^{-\omega_b x}$$

$$\text{where } \psi = 2 \tan^{-1} \left( \beta / \omega_0 \right). \quad (25)$$

Consider only the first term of equation 25 which is the steady-state case\*. The error in the value of  $y$  is

$$\Delta y = y_1 \sin ( \beta x + \pi - \psi ) - y_1 \sin \beta x$$

if  $\omega_0^2 / \beta^2 \ll 1$  . (It will be seen later that this assumption is valid.) Hence for  $\pi - \psi$  small,

$$\frac{\Delta y}{y_1} = ( \pi - \psi ) \cos \beta x.$$

The above error is a maximum at that point in the terrain where  $\cos \beta x$  equals unity, and we have:

$$\frac{\Delta y}{y_1} = [ \pi - 2 \tan^{-1} \beta / \omega_0 ] . \quad (26)$$

Error Tradeoff. Consider equations 24 and 26. The former specifies the maximum allowable value of  $y$  for slowly increasing (or decreasing) terrain elevation: the later relationship determines the maximum error in  $y$  for a sinewave terrain, or a rapidly changing terrain. They are both dependent on the value of  $\omega_0$ . Too large a value of  $\omega_0$  will keep  $y_{pk}$  small, but will result in too large a value of  $\Delta y$ . If  $\omega_0$  is decreased to minimize  $\Delta y$ , then  $y_{pk}$  will increase. The two equations yield

\* The second term of equation 25 is the transient term. Its value is neglected for the purposes of these calculations. It is reported here for completeness.

$$\frac{\Delta y}{y_1} = \pi - 2 \tan^{-1} \left( 2 \frac{\pi e y_{pk}}{x_1 m} \right) \quad (27)$$

This equation can be further simplified by using the series expansion for  $\tan^{-1} x$ :

$$\tan^{-1}(x) = \frac{\pi}{2} - \frac{1}{x} + \frac{1}{3x^3} - \dots$$

Only the first two terms are important in this application as  $x \gg 1$  and equation 27 becomes

$$\frac{\Delta y}{y_1} = \frac{x_1 m}{\pi e y_{pk}} \quad (28)$$

Assuming a maximum ramp function slope equal to  $45^\circ$ ,  $m$  is unity. The above equation is plotted in figure 26 for various values of  $x_1$  and  $y_{pk}$ . For example, from the graph, if  $y_{pk}$  is set at  $10^3$  inches, and the wavelength of the sine wave representing the terrain is 20 ft., a maximum of 3% error results in the computation of  $y$ . If the allowable error is 2 inches, the value of  $y_1$  (the height of the hills) is 5.6 ft. - certainly a large value. Actually a value of  $y_{pk}$  equal to  $10^3$  inches may be a little extreme. Consider the adder in figure 24. It should compute a value of  $y(t + t_c)$  to an accuracy of about 2 inches. Therefore the error in one of its inputs,  $y(t)$  must be less than 2 inches, and a 2-inch error in a maximum of  $10^3$  inches requires circuitry accurate to 0.2% of its maximum value. However, figure 26 indicates that an adequate tradeoff can be made and the computing method presently visualized can be instrumented.

LOGARITHMIC  
SCALE & PAPER  
359-110

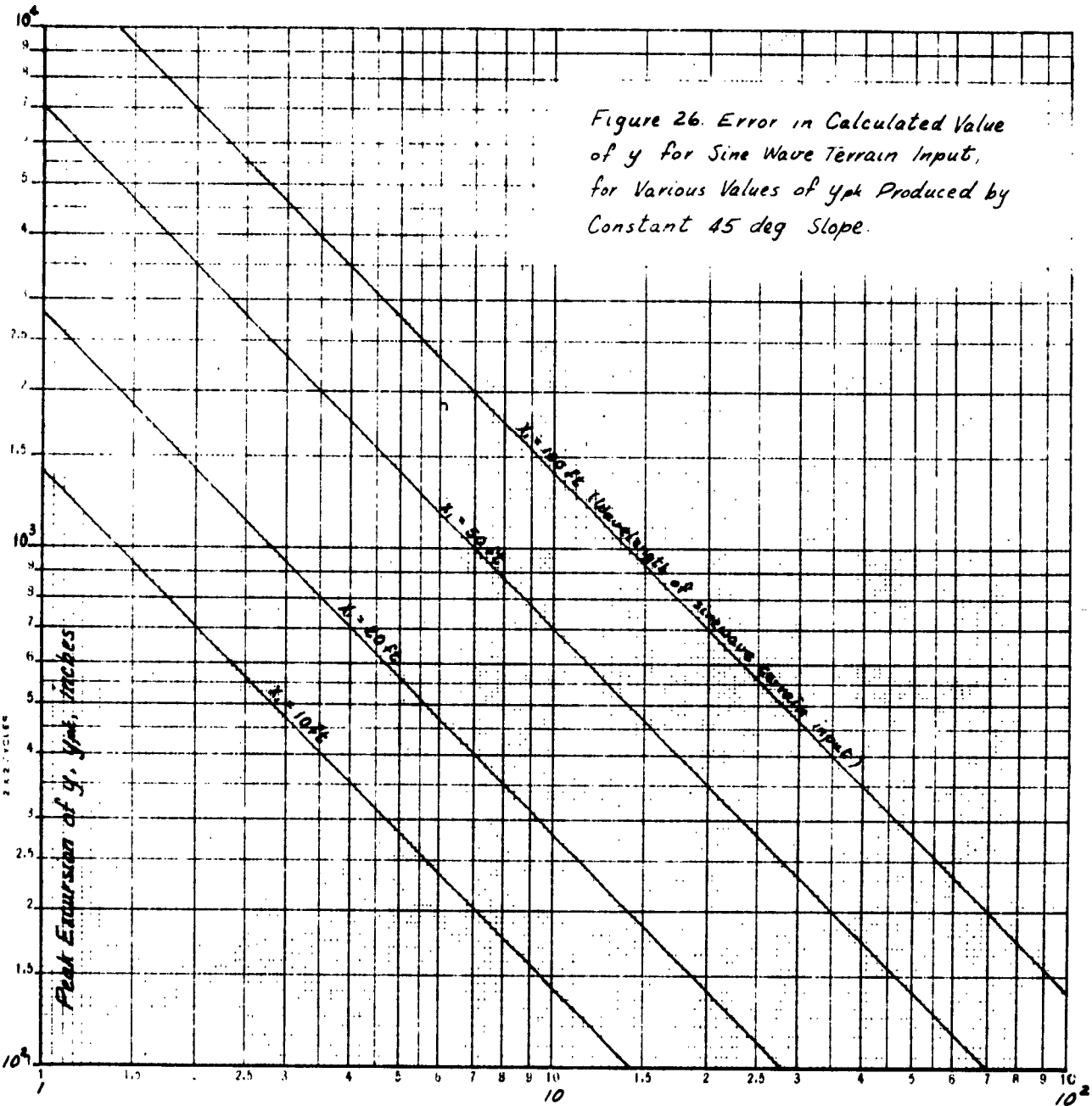


Figure 26. Error in Calculated Value of  $y$  for Sine Wave Terrain Input, for Various Values of  $y_{pk}$  Produced by Constant 45 deg Slope.

Maximum Percentage Error in  $y$ ,  $\frac{\Delta y}{y} \cdot 100$

### Alternate Computation Techniques

The preceding discussion has indicated that one of the basic problems in profile computation is due to the fact that measurements of the terrain are not made at a uniform distance ahead of the vehicle, and therefore profile information is read into storage at a variable rate that is different from the readout rate. This section discusses alternate methods of solving this problem.

The first solution is based on the use of a digital storage which contains terrain elevation data on a sequence of discrete points ahead of the vehicle. If these points are closely spaced they contain adequate information for operation of the active suspension system. If in addition the points are uniformly spaced, the information can be read out at a rate corresponding to vehicle velocity and the computation process is considerably simplified. Therefore it is desirable to consider the process of deriving profile information at a set of points spaced uniformly and closely along the path of the vehicle.

As shown above, a particular range measurement  $R(t)$  yields a value of terrain elevation  $y(t)$  given by

$$y(t + t_c) = y(t) + a(t) - R(t)\alpha \quad .$$

Let  $X(t)$  represent the horizontal coordinate of the terrain point being measured, taken from an origin such that  $X(0) = x(0)$ . Then

$$X(t) = \int_0^t v(t) dt - R(t) \cos \alpha \quad .$$

Here  $\alpha$ , the depression angle, is assumed to be fixed, but the horizontal velocity  $v(t)$  may be a function of time.

Consider the problem of determining the value of  $y$  at a set of points  $\{X_i\}$  such that  $X_{i+1} = X_i + \Delta X$  where  $\Delta X$  is a small fixed separation. Suppose that one value  $y, y_i$ , has just been determined at time  $t_i$ . At later times the difference between  $X$  and  $X_i$  is

$$\begin{aligned} X(t) - X(t_i) &= \int_0^t v(t) dt + R(t) - \int_0^{t_i} v(t) dt - R(t_i) \\ &= \int_{t_i}^t [v(t) + R(t)] dt. \end{aligned}$$

Thus  $t_{i+1}$ , the time at which  $y_{i+1}$  is to be found by sampling  $y(t)$ , can be determined from the equation

$$\Delta X = \int_{t_i}^{t_{i+1}} [v(t) + R(t)] dt.$$

This leads to the mechanization of the process shown in figure 27.  $R(t)$  and  $v(t)$  are added and integrated. The integrated output is compared with a  $\Delta X$  reference; when it reaches  $\Delta X$  the value of  $y(t)$  is sampled and entered into storage, and the integrator output is zeroed. In this way values of  $y$  are entered into storage corresponding to values of  $X$  separated by fixed increments  $\Delta X$ .

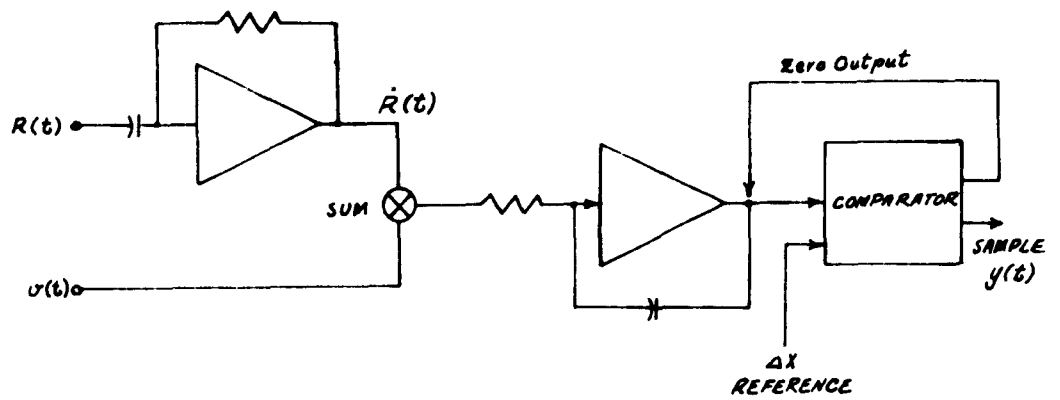


Figure 27. Functional Block Diagram of Alternate Computation Process.

As a second alternative, consider the equations

$$X(t) = \int_0^t v(t) dt + R(t) \cos[\alpha(t)]$$

$$y(t+t_c) = y(t) + a(t) - R(t) \sin[\alpha(t)]$$

where  $\alpha$ , the depression angle, has been written as a function of time. We may imagine a system so designed that as the vehicle moves over the terrain  $\alpha$  is varied in such a way as to hold  $R(t) \cos[\alpha(t)]$  constant. This corresponds to tilting the sensor head automatically in such a way as to keep the measured range to the terrain constant. Then

$$X(t) = \int_0^t v(t) dt + X_c$$

where  $X_c = R(t) \cos[\alpha(t)]$  is constant.

$$y(t+t_c) = y(t) + a(t) - X_c \tan[\alpha(t)]$$

The waveform  $y(t+t_c)$  now represents the terrain contour a fixed distance ahead of the vehicle, and only current velocity knowledge is needed to gain access to stored information at the right time. In particular, in the constant velocity case a simple fixed delay can be used to yield access to terrain information a given distance ahead of the vehicle.

## CONSISTENCY DETERMINATION

Optimum operation of the terrain sensor system requires that means be provided for determining the consistency of the terrain to be traversed and of the obstacles to be encountered. It is clear, for example, that the suspension system must react differently if the vehicle encounters, say, a hard rock or a bush of approximately the same size and shape.

Although a number of possible approaches may be postulated to this problem, including both sonic and electromagnetic methods, the one that appears to hold the greatest promise of both successful operation and equipment practicality is based on optical techniques.

That this is a reasonable approach can be seen by a simple experiment. If various types of terrain and obstacles are viewed through a small hole in a sheet of cardboard held at arm's length, objects are seen in a restricted field, are unrelated to their surroundings, and cannot necessarily be distinguished by shape or outline. The human observer is nevertheless able to make a highly reliable estimate of their consistency, based on the colors of the objects and their textural patterns. From the studies conducted to date, it is reasonable to believe that an automatic consistency analyzer can be based on the same approach.

The light reflected from an object does not give a direct indication of the consistency of that object, because the reflection of light is a surface phenomenon, while the consistency is, so to speak, a volume phenomenon.

Hence, in order to determine consistency of the use of reflected optical radiation it is necessary to classify objects which may be encountered according to their consistency, and then attempt to discover properties of the reflected optical energy which correlate with the assigned consistencies.

It may be concluded then, that the determination of consistency by means of reflected optical radiation is in theory feasible. On the other hand, the mechanization of an optical energy consistency analyzer may present serious practical problems unless suitable simple means of categorizing obstacles by optical means can be discovered.

The first step in investigating this requires deciding on a consistency terrain model, and attempting to find criteria for distinguishing between hard and soft model obstacles. The procedure will consist of describing typical terrain objects and surfaces, and of using available data to describe how energy received from different objects differs.

A second part of the consistency study is the determination of the characteristics of terrain from available reports. Among the information that would be desirable is:

1. The amount of energy received from the terrain in the visible region.
2. The spectral reflectivity of different types of terrain.
3. The changes in these with changes in the angle of view.
4. The amount of energy from the sun falling on surfaces under various weather conditions and times of day.

5. A comparison of the above with the energy available from a searchlight.

#### CONSISTENCY MODEL OF TERRAIN

For the study of consistency determination it is desirable to specify a few types of terrain and terrain obstacles to serve as a model for investigation.

For the initial investigation, the terrain surface has taken to be level or undulating and composed of grass or clay. The obstacles considered are:

<u>Obstacle</u>	<u>Consistency</u>
1. Isolated rock	Hard
2. Isolated bush	Soft
3. Log on ground	Hard
4. Hedge	Soft
5. Stone wall	Hard
6. Ditch with dirt sides and bottom	- -
7. Ditch partly filled with water	- -

Each obstacle has been put into one of two consistency classes - hard or soft. It will be assumed that the terrain and obstacles may be either dry (except for the water in the ditch) or wet as they would be immediately after a rain. In addition, it will be considered that the terrain may be covered with snow.

It has not been possible to consider several important types of terrain within the limited scope of the study; among these are tall vegetation such as high grass, corn, grain; cultivated fields in which high vegetation may occur in regular rows; and badly broken paving. It appears likely that some of these do not present unique problems and can be handled if the first set of obstacles can be distinguished.

One other soft obstacle might be considered - a mound of earth or mud. This has been discarded as an obstacle for the initial study because it is felt that if the vehicle is traveling over hard ground the mound will be hard and constitute part of the undulating terrain. It is also supposed that a mound of loose earth, which would be a soft (or perhaps more properly, a semi-soft) obstacle does not naturally occur very often.

#### CONSISTENCY MEASUREMENTS

We now turn to the ways in which the chosen obstacles differ. It will be noted that the listed obstacles fall into three fairly definite classes: 1, 3, and 5 are hard, homogeneous, rocky, brown or grey to the eye. Obstacles 2 and 4 are soft; they consist of vegetation, change with the season, have leaves and branches (much small detail), and are green to the eye, or orange-brown. The remaining obstacles are ditches or simple depressions in the terrain which may be filled with water.

The differences between the listed hard and soft objects suggest that two ways may be investigated for discriminating between them optically. One of these is by texture, roughness, or the degree of detail in the object. The second is by the difference in spectral reflectivity which is revealed by the differences in color between earth and vegetation.

### SPATIAL DETAIL ANALYSIS

In considering the use of detail as a means of discrimination it is necessary at the present time to discuss the subject without experimental supporting data. A simple experiment which will yield information on the utility of detail for discrimination is described later in this section.

Vegetation has many small variations in shape and color, and so the energy received from vegetation varies widely from point to point. Thus the image of vegetation is generally full of high-contrast detail.

Clay and other bare ground surfaces are relatively uniform in color and the amount of fine detail tends to be less. Grassy surfaces have the general character of vegetation, although the detail is very fine-grained.

Rocks vary; some such as limestone are rather uniform, while others (e.g., granite) may have very fine detail. In general, rocks appear to be more uniform than trees and bushes when viewed at medium resolution.

Hedges have the general character of vegetation, but brick and stone walls may also be expected to contain much detail.

It appears from these considerations that the amount of roughness in an object may be useful in identification, but will probably provide only partial consistency determination. Measurements are necessary for further conclusions, and no source for this data is known.

## SPECTRAL REFLECTANCE ANALYSIS

Spectral analysis of consistency depends on the accuracy with which terrain types - rock, mud, grassland, etc. - can be identified by examination of their spectral reflectance in the visible and infrared regions. The spectral reflectance,  $r_{\lambda}$ , of an object is ideally the fraction of monochromatic incident energy of wavelength  $\lambda$  that is reflected by the object; in practice, of course,  $\lambda$  refers to a finite narrow band. To be practical, a consistency sensor will necessarily divide the total spectrum into a few bands of finite width, both to reduce equipment complexity and to insure that a workable energy level is obtained with a sensor aperture of reasonable size.

As a starting point, it has been assumed that three spectral regions will be used, and that only the relative values of average spectral reflectance in these three regions are determined. This approach circumvents the problem of making an absolute determination of spectral reflectance and thus, if successful, can lead to simpler equipment. The questions of necessary aperture sizes, required dynamic range, etc., have also been deferred so that attention can be concentrated on the basic problem: can terrain types, and thus consistency, be determined by relative spectral reflectance measurements in three spectral regions?

### Spectral Reflectance Data

The most complete collection of spectral reflectance data available for this initial study is that of Krinov,<sup>1</sup> as given in the Air Force Handbook of Geophysics.<sup>2</sup> Krinov's data provides values of spectral

1. Krinov, E. L., "Spektral'naya otrazhatel'naya sposobnost' prirodnykh obrazovaniy," (Spectral Reflectance Properties of Natural Formations), Laboratoriya Aerometodov, Akad.Nauk SSSR, Moscow, 1947.
2. Handbook of Geophysics, Revised Edition, The Macmillan Co., New York, 1961.

reflectance for eleven types of natural terrain, given in 0.01 micron intervals over the spectral range from 0.400 to 0.840 micron. The data fall into eleven types as follows:

**Class A, Water Surfaces**

**Class B, Bare Areas and Soil**

Curve 1a - Fresh fallen snow

Curve 1b - Snow covered with a thin film of ice

Curve 2 - Characteristic of limestone, clay and similar bright objects

Curve 5 - Characteristic of sands, bare areas in the desert, and some mountain outcrops

Curve 7b - Typical of podzol, clay loam and other soils, paved roads, and some buildings

Curve 8c - Characteristic of black earth, sand loam, and earth roads

**Class C, Vegetation**

Curve 1a - Characteristic of coniferous forests in winter

Curve 1b - Typical examples are coniferous forests in summer, dry meadows, and grass in general, excluding lush grass

Curve 1c - Typical examples are deciduous forests in summer and all lush grass

Curve 1d - Typical examples are forests in the autumn and ripe field crops

The spectral reflectance data for these terrain features are shown plotted in figure 28. Although these do not represent all the varieties of terrain that might be of interest (including such important ones as marshland and mud), they do provide a good representative sample for judging whether spectral measurements will permit consistency determination.

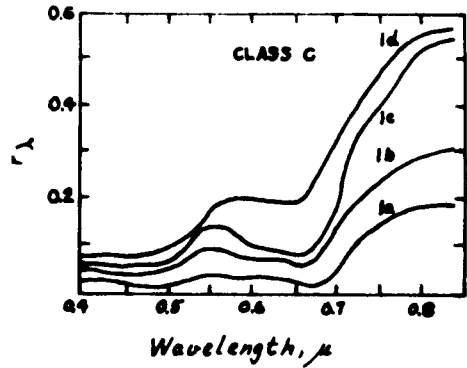
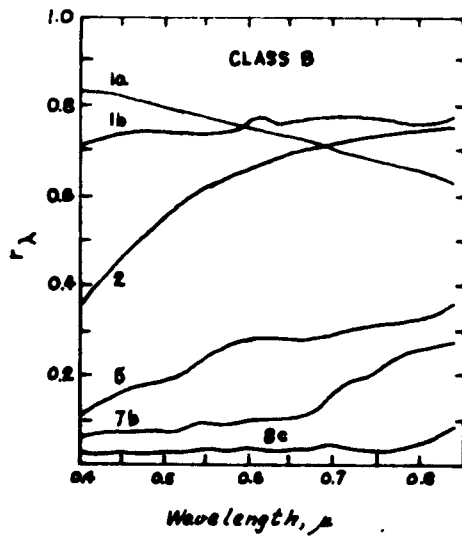
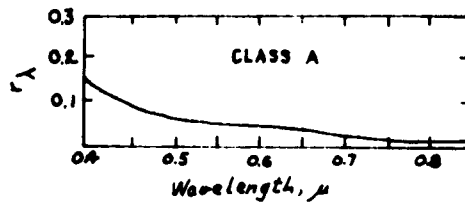


Figure 28. Spectral Reflectance for Eleven Types of Natural Objects as Measured by Krinov.

### Spectral Calculations

Examination of figure 28, and particularly of the "Class C" data, leads to an initial selection of the three spectral regions of greatest promise as  $0.40 - 0.52 \mu$ ,  $0.52 - 0.66 \mu$ , and  $0.66 - 0.84 \mu$ . The intermediate values of  $0.52 \mu$  and  $0.66 \mu$  are the approximate positions of natural break points in many of the curves, leading to a good probability that the three regions considered will be well suited for spectral discrimination.

For the purposes of the calculations, it has been assumed that these three regions can be separated by ideal bandpass filters with 100% transmission in the pass band, and no transmission elsewhere, and that the detector has uniform response over the complete spectral region. These conditions cannot be attained in practice, but they do represent factors over which the equipment designer has some control. The calculations have been carried out for two types of illumination: sea-level sunlight with the sun 30 degrees above the horizon, and artificial light with a tungsten-filament source operating at  $3000^{\circ}\text{K}$ . These are taken to represent day and night conditions.

To determine the relative energy in each band, the product of spectral irradiance and spectral reflectance for each terrain type was taken for 0.02 micron intervals, and the resulting curves were integrated over the spectral bands of interest. This data was then used to calculate the fraction of total energy in each spectral band.

The results are shown plotted in Figure 29 for sunlight and Figure 30 for artificial illumination. In these triangular-coordinate plots, A represents the fraction of the total energy in the 0.40 - 0.52  $\mu$  region, B represents the 0.52 - 0.66  $\mu$  region; and C represents the 0.66 - 0.84  $\mu$  region.

The data for artificial illumination was then "corrected" by applying factors based on the relative energy between natural and artificial light for the three spectral regions.

The data for natural sunlight and the corrected data for tungsten are shown plotted in Figure 31. The results show excellent agreement, indicating that the effects of variation in illumination over the spectral regions can be compensated for in a straightforward way.

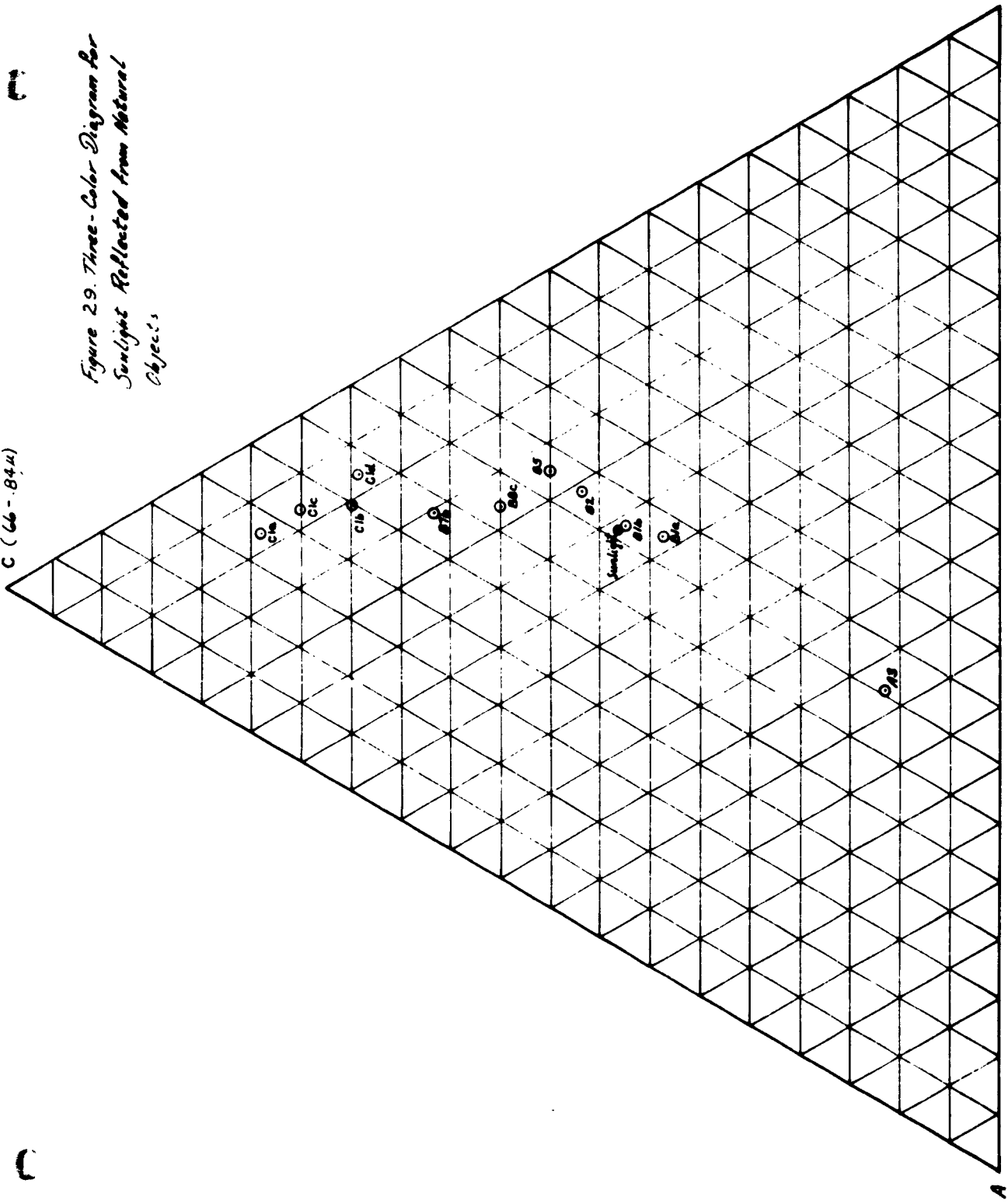
#### Discussion

The results of the calculations show that there is definite promise in using spectral analysis as a means for consistency determination. Based on the available data, spectral measurements can give reasonably clean-cut discriminations between various types of terrain features. No information is available on the probable variability in the data, however, so these results can only be considered as suggestive rather than conclusive.

In particular, additional information is needed on the spectral reflectance of wet soils, mud, marsh, and the like that form typical soft terrains. It might be expected that the data points shown in the figures

C (66-84u)

Figure 29. Three-Color Diagram for  
Sunlight Reflected from Natural  
Objects

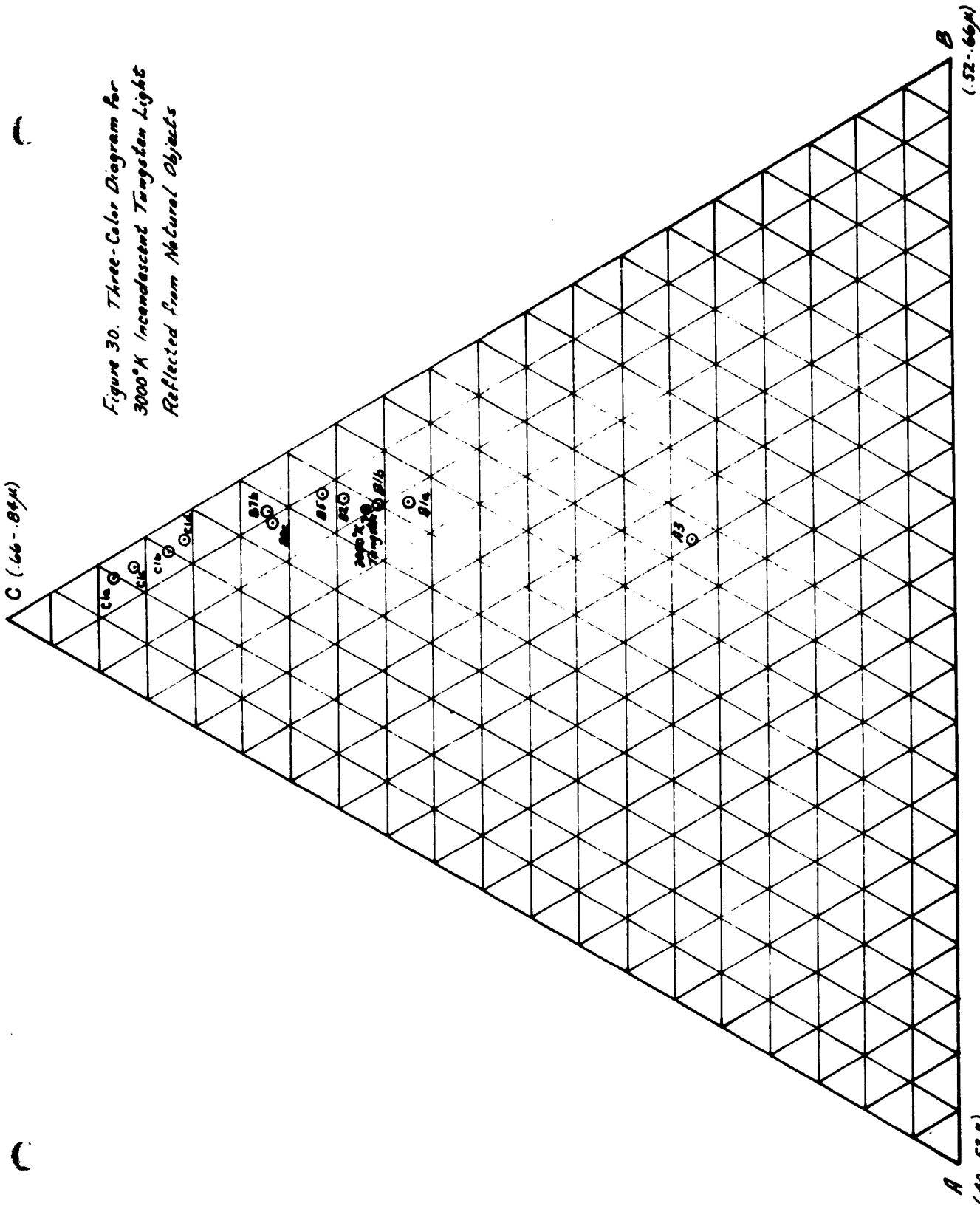


A (40-52u)

B (52-66u)

C (66-89μ)

Figure 30. Three-Color Diagram for  
3000°K Incandescent Targeted Light  
Reflected from Natural Objects



A (40-59μ)

B (52-66μ)

C (.66 - 84μ)

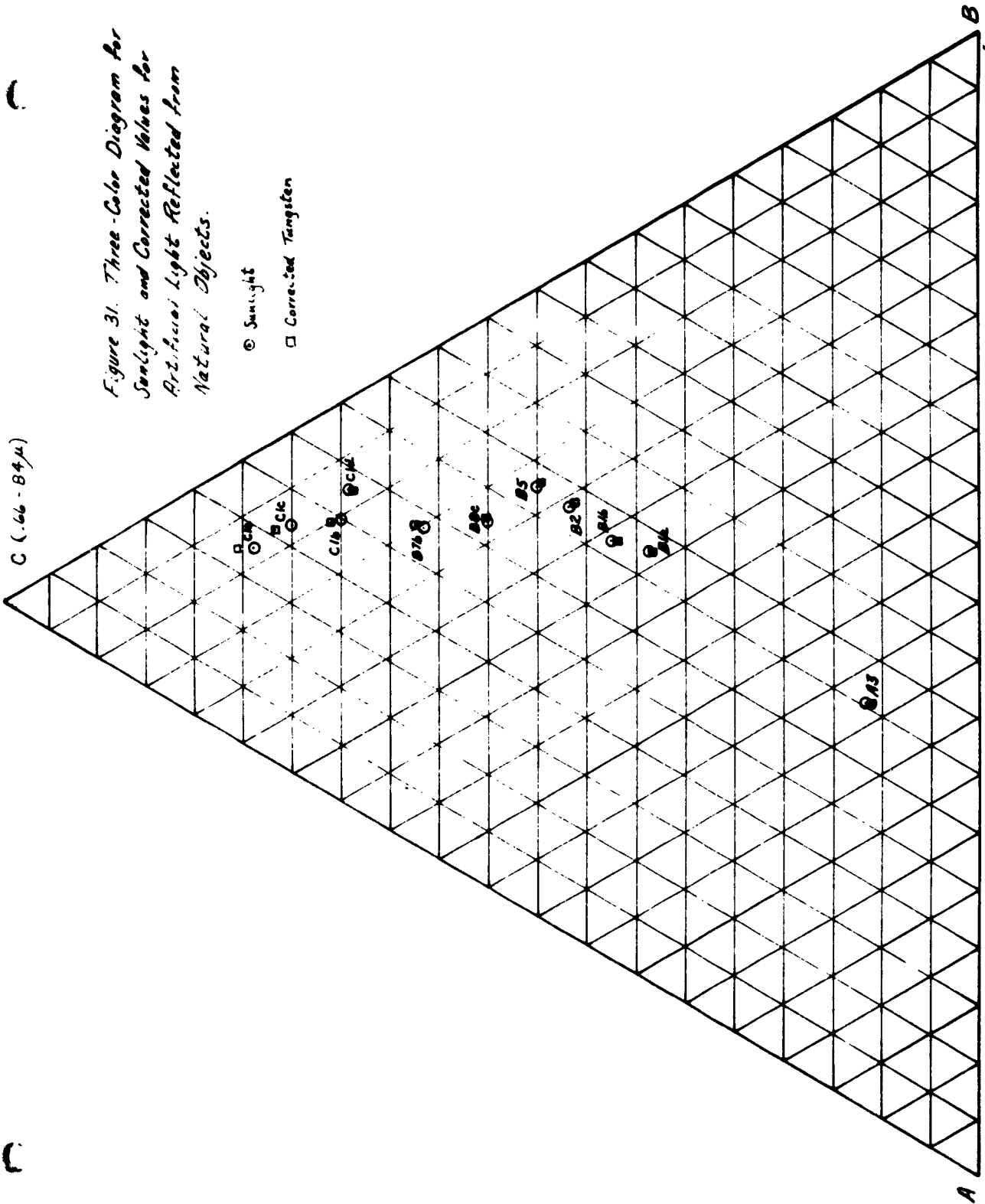


Figure 31. Three-Color Diagram for Sunlight and Corrected Values for Artificial Light Reflected from Natural Objects.

- Sunlight
- Corrected Tungsten

A (.40 - 52μ)

B (.52 - 66μ)

would move toward point A3 (water), but this can only be considered conjectural in the absence of valid data. It is, in fact, not unlikely that the measurements from which the data for curve A3 were derived were influenced by the mirroring of blue skylight into the measuring instrument. The extent to which this would be a problem in an actual instrument for terrain consistency measurement will require further investigation, regardless of the validity of the data point for water. The effects of wetness in general are discussed in more detail later in this section.

The data strongly suggests that reasonable discrimination between important terrain categories would be possible with only two spectral regions (B and C), thus simplifying the equipment and very likely reducing the problem of reflected skylight. If the blue (A) region is used, trouble might also be expected during operation in regions of patchy shade, as there is a much higher proportion of blue light in the shade than in the open sun.

#### Infrared Spectral Analyses

Since ultimately it may be desirable to operate the terrain sensor system in such a way that little or no visible energy is required at night, a brief study was made to investigate the possibility of using only the near infrared region for discrimination. The spectral range from 0.70 to 0.84 micron was divided into two bands: 0.70 to 0.77 micron, and 0.77 to 0.84 micron. The average reflectivities for each band, and the ratios of reflectivities in the two bands were then computed for the same terrain types, and using the same basic data as for the three-color analysis above.

The results of the calculations are given in the following table:

FACTOR	TERRAIN TYPE										
	A3	B1a	B1b	B2	B5	B7b	B8c	C1a	C1b	C1c	C1d
Reflectivity, .70-.77 $\mu$	.013	.672	.760	.728	.300	.191	.044	.118	.212	.328	.416
Reflectivity, .77-.84 $\mu$	.009	.652	.760	.746	.325	.245	.060	.175	.286	.513	.539
Reflectivity Ratio	1.5	1.06	1.00	.976	.926	.777	.75	.694	.738	.640	.772

In order of decreasing ratio of reflectivity in the 0.70 - 0.77 $\mu$  region to that in the 0.77 - 0.84 $\mu$  region, the data show the following sequences:

A3	1.5	Water
B1a	1.06	Fresh snow
B1b	1.00	Icy snow
B2	.976	Limestone, clay
B5	.926	Sand, bare desert, etc.
B7b	.777	Clay loam, pavement, etc.
C1d	.772	Autumn forests, ripe field crops
B8c	.748	Black earth, sand loam, earth roads
C1b	.738	Coniferous forests in summer, dry meadows, grass
C1a	.674	Coniferous forests in winter
C1c	.640	Deciduous forests in summer, lush grass

Clearly, water is readily distinguishable from other terrain features. Smooth bare materials such as limestone, clay, and snow-covered terrain form another natural grouping. The distinction between vegetation and other terrain types is not as prominent as when the visible region is used, but it can be seen that lush vegetation gives the lowest reflectivity ratio, and it is not unlikely that very lush soft terrain, such as marshes, would be easily distinguished.

Further detailed analysis must await the availability of additional data. It is tentatively concluded that a three-color system including the visible region would be more reliable in discrimination than the two-color infrared system, but that the infrared system need not be ruled out if other factors (such as visual security) strongly favor its use. In the three-color analysis in particular, a strong distinction exists between the spectral characteristics of the hard and soft obstacles previously described, but more detailed data is required than is presently available in the literature.

#### WET OBJECTS

We may now consider the determination of the consistency of elements of the model when they are wet as during and immediately after a rain. The principal effect of this wetting to be considered will be the resulting film of water on the surface of the objects. A second effect of wetting, of course, is to turn dirt or clay to mud. This appears to be important principally when the vehicle is traveling on a hard surface (paving) and it is desired to run from the paving onto hard ground. The determination of the muddiness of this bare ground appears to be a more difficult problem than those discussed below, since the optical reflectivity will be the same for a thin layer of mud and for one deep enough to form a serious obstacle.

Turning to the effects of a film of moisture on the surface of objects, it may be noted first that spectral data for wet objects comparable to that given above for dry objects has not been discovered. However, the following comments can be made.

First, visual observation shows that a film of moisture on objects has little effect on the observable texture of vegetation compared with rock and earth. Likewise, the color of objects is not grossly affected by their being wet. Thus it appears likely that color and texture criteria suitable for dry objects will be applicable to wet objects.

A second effect to be considered, as mentioned earlier, is that the film of moisture tends to act as a reflector and reflects the sky, the sun, and nearby objects. Since the sensor responds to this reflected light, it may give a different indication in the presence of wet objects. (This effect will have to be taken into account when evaluating the specific ranging process.) An estimate of the magnitude of this effect can be obtained by considering what natural objects in the open look like when wet. Vegetation looks rough and green. Clay, rock, and so on, look shiny, but are perceived as brown. Thus it may be concluded that probably the reflections from the water film do not completely change the spectral content of terrain reflections. However, since the received energy is probably due to a mixture of energy reflected by the object itself and energy reflected by the surface film, the spectral reflectivity curves may all be tilted in the direction of the water curve (Figure 28, curve A.)

Another effect that should show promise in determining texture (particularly in case of water) is the polarization of the reflected radiation. It is reasonable to assume that the degree of polarization is related to the wetness of the surface. Future study of this aspect could be fruitful.

It may be concluded that although insufficient data has been discovered, it appears that spectral and texture analysis can be used against wet terrain objects.

#### DITCHES

The remaining obstacles which have not yet been considered are ditches. Dry ditches are sensed in the normal manner, and should yield no misleading signal, although the shadow problem has not been completely solved.

Water-filled ditches, on the other hand, require more examination. We may consider the signals which may be expected to be returned from such obstacles; for convenience the effect on passive systems will be considered first, followed by active systems. Because different effects are anticipated depending on the condition of the water in the ditch, the discussion will include still water, rough water (ripples), and muddy water.

In a passive ranging system the return from still water is due to a large extent to specular return of light falling on the surface, and hence the reflections of nearby objects or the sky are sensed. Because of the uniformity of the sky, little energy will be available for passive range measurement. If nearby objects are reflected, long and erroneous ranges will be calculated. The spectral characteristics of this reflected energy will approximate the object reflected, but will probably be mixed with a class A (typical of water) spectral distribution of energy. The long measured range will indicate a steep terrain drop which would act as an alarm.

Usually the surface of the water might be expected to be slightly rough or covered with ripples. Here the range to the surface is sensed by a passive system, and (because of the large brightness of the sky) spectral characteristics typical of class A would be expected. Hence the location of the surface is measured and it is determined to be water. No information is obtained about the depth of the water.

The water may contain various amounts of suspended dirt. Muddy water reflects the sky; it also has the color of the suspended clay or dirt. Hence it would be expected that the received energy would have a spectral content somewhere between those typical of class A and class B objects. Thus the water surface would not be mistaken for vegetation, but it might be mistaken for a level stretch of earth; smooth moist clay, for example, might have very similar characteristics. The exact characteristics require measurement, since the possible degree of discrimination cannot be determined from available data.

So far, attention has been restricted to passive systems. Active systems may be discussed based on the three types of water surfaces described.

In the case of still water, if the sky is reflected, no return is received by an active system, and since no energy is available the system hunts. This lack of a positive return might be used to indicate water; care must be taken that very smooth road surfaces do not give the same indication. If reflections of other nearby objects can be seen by an observer from the sensor location, and the reflectivity of the surface

is sufficiently high, the range to these reflected objects might be measured. As with the passive system the large resulting range indication would suggest a steep drop and serve as an alarm.

If the surface of the water is covered with ripples, it still may not be possible to make a range measurement unless the surface scatters or reflects part of the transmitted energy toward the receiver. If this is the case, a valid range estimate can be made, and the reflectance characteristics will agree with those described above as class A.

If a portion of the energy from the active source is reflected specularly by the wavelets (this would ordinarily require quite steep waves) the return would be large and have the spectral characteristics of the source.

If the water is muddy, and looks brown, the energy reflected will be due to a large extent to reflection from the surface, but the energy would be colored to a considerable extent by the suspended material. Hence the above remarks apply to this case, but the spectral characteristics are somewhat more characteristic of earth.

#### SNOW

Finally, the process of consistency determination when the ground is covered with snow will be considered briefly. Assume the vehicle is traveling on or near the surface of the snow. The terrain appears to be a surface of high uniform reflectance with obstacles such as posts, bush tops, hedges, fences, and walls standing out. Any obstacle which

is covered with snow will yield the same consistency determination: such obstacles may be considered solid with fair accuracy, since they will probably be rocks or frozen ground. Other obstacles differ in color from the snow-covered terrain, and those which are not hard will, in general, be "perforated"; they will have large amounts of high contrast detail - for example, the branches of a bush. This latter is the principal distinguishing characteristic in winter, and may provide a useful consistency criterion.

## MEASUREMENTS PROGRAM

Although spatial and spectral analysis hold distinct promise in providing terrain consistency measurements, the available published literature is insufficient to permit either a detailed theoretical analysis or optimum equipment design. For completeness, therefore, a program has been evolved for deriving the required measurements in a form specifically applicable to terrain consistency sensing. The basic features of this program are reported here for future reference. Conduct of such a program is not within the scope of the present contract.

The objectives of such a program would be as follows:

1. To make measurements of the optically observable textures of various terrain objects in various spectral regions. These measurements would be made in such a way that they apply directly to the design of a consistency measurement device for incorporation into the terrain sensor.
2. To correlate the results of the measurements with the consistencies of various terrain objects.

The resulting data could then be incorporated into the design of a consistency sensor, by guiding the choice or design of choppers or other spatial-spectral analysis devices, and the design of the necessary decision-making switching circuitry.

### Procedure

The general approach that appears most practical is measurement of

the fractional modulation of energy in different electrical frequency bands produced by chopping the images of various terrain features with different spatial filters in various spectral regions.

In order to do this as simply as possible and under controlled conditions, it would be desirable to make the first measurements in the laboratory. These measurements would be made using both photographic techniques and samples of natural objects, as follows:

1. Color photographic transparencies of the terrain would be made, incorporating a variety of natural and man-made objects. The consistencies of these objects would be recorded in the field at the time the photographs were taken.

A simple projection system would be set up in the laboratory which would allow desired small portions of the color transparencies to be imaged on a rotating chopper disk placed in front of a photomultiplier. Various chopper patterns and spectral filters would be used, and for each combination of target type, spatial filter (chopper), and spectral filter, the fractional modulation of energy in various electrical frequency bands would be measured.

(Although the spectral region which can be examined using color transparencies is somewhat narrower than may be used in the ultimate equipment, it is nevertheless wide enough to be of considerable value, and the restrictions imposed by this technique, which would be made up for in the measurements on samples and

in the later field tests, are compensated for by the simplicity and flexibility of the photographic technique.)

2. Samples of natural materials would be brought into the laboratory. These samples would be illuminated and imaged in the proper scale on the rotating chopper disk, using the same projection lens and additional folding mirrors to properly direct the line of sight. The measurement would be similar to those made using photographic transparencies.

The sample materials examined in the laboratory would be principally such things as rocks, sand, and earth, which can be kept for long periods of time without changing. However, vegetation could also be examined to the extent that it can be brought into the laboratory and kept from wilting during measurements.

The results of these two sets of measurements would then be correlated with the consistencies of the terrain objects, and a preliminary determination would be made of the best combination of spatial chopper patterns and spectral regions.

3. Then in order to verify these preliminary conclusions under more realistic conditions (such as the inclusion of a larger variety of materials studied in the wider spectral region and under various lighting conditions) the combinations adjudged best during the laboratory program would be incorporated into

simple field test equipment having characteristics (such as field-of-view) as required by the terrain sensor. Field measurements would then be made with this equipment under a variety of conditions and the results compared with the results of the laboratory measurements. Any changes found desirable in the filtering or decision techniques could then be made and performance rechecked in the field.

#### Laboratory Setup

A possible laboratory setup is shown in Figure 32. The necessary optical equipment is shown mounted on an optical bench, which would give convenience and flexibility. The projection portion of this equipment consists of the following: a projection bulb used as a light source, a condensing system, a slide carrier, and a projection lens. The detection portion consists of an aperture, referred to as a field stop, behind which is a rotating chopper driven by an electric motor, and a photomultiplier which measures the interrupted energy passing through the field stop and chopper. Not shown is a simple folding mirror system which would allow terrain samples to be imaged on the field stop and chopper.

Except for the slide carrier, the projection portion of the equipment is conventional; its purpose is to form an enlarged image of a portion of the transparency or the terrain sample on the field stop. The slide carrier is unusual in that it has two degrees of freedom to allow any selected portion of the slide to be imaged on the field stop. This field stop simulates the field stop in an actual equipment; in both cases it

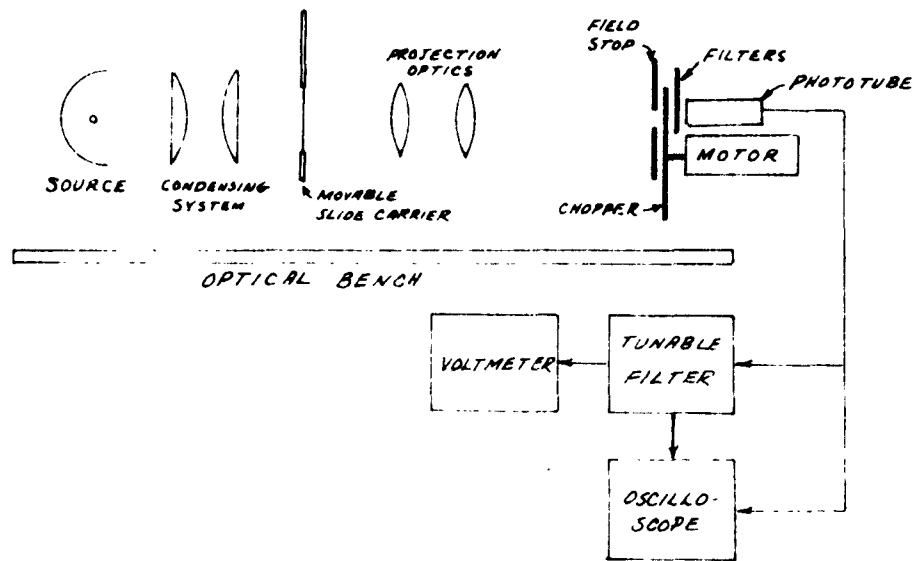


Figure 32 Suggested Laboratory Setup for Spectral-Spatial Analysis.

erves to limit the field of view of the detector. The experimental field stop, chopper, and the degree of enlargement produced by imaging the photographic transparency or terrain sample on the field stop, are selected together to simulate the proper field of view.

The chopper disk could be made conveniently from a double disk of plastic or glass, with a piece of photographic film placed between the two layers to form a sandwich. This film would bear the desired chopper pattern. This technique makes it easy to change choppers, and also easy to fabricate new ones, since it is only required that the desired pattern be drawn up and photographed on high-contrast film.

The photomultiplier produces an electrical output proportional to the energy which passes through the field stop and is interrupted by the chopper. A photomultiplier with S-20 response would cover the entire visible spectrum. Filters could be placed in the optical path to do two things: first, to balance the light from the tungsten source to give a spectral content equivalent to that of sunlight at different times of day, and, second, to select specific spectral regions for investigation.

The electrical output of the photomultiplier is amplified as necessary and the nature of the electrical output is examined using bandpass filters, and measured with an a-c voltmeter.

A typical experiment would proceed as follows: A photographic transparency or an actual terrain sample is selected and the desired

portion is imaged on the field stop with the proper degree of enlargement. Then a chopper disk composed of opaque and transparent sectors which are large with respect to the field stop is rotated in the light path. The amplitude of the low-frequency detector output measures the average energy level, to serve as a reference level. Then various choppers having fine detail are substituted and the modulation produced in various spectral regions with different choppers is analyzed. Data from a series of similar experiments is used to determine the best chopper configurations and spectral regions for consistency determination. This process is discussed in more detail below.

#### Field Test Equipment

A field test equipment that could be designed on the basis of the laboratory experimental findings is shown in schematic form in Figure 33. In this equipment the terrain is imaged by the optical system on a fixed field stop. A 1-inch-diameter objective lens would be adequate for the purpose. The choppers used would be interchangeable, but because the less effective ones would have been weeded out during the laboratory experiments, only a few would be needed. These choppers combine the spectral and spatial filters and so resemble as closely as possible the consistency measuring device that would be used in an actual terrain sensor. The detector output and rotational reference signals as necessary are recorded and measured as before. The equipment is mounted on a tripod, and an optical sight is used to aim the equipment at desired portions of the terrain. The data gathered during this phase would verify the conclusions reached during the laboratory program, and would allow final equipment design parameters to be established.

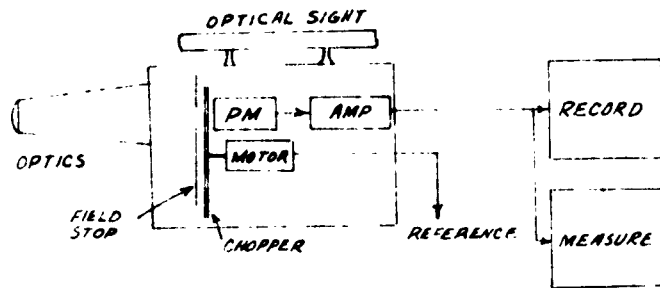


Figure 33. Field Test Equipment

### Design of Logic Circuits

Now the question of the design of the logic circuits for terrain identification and consistency determination will be considered. In a way, calling this part of the equipment "logic circuits" is somewhat misleading since the required functions are performed by simple diode networks rather than complicated computer circuits. The design of this part of the consistency sensor would proceed as follows:

It is assumed that as a result of the measurement program, the electrical detector outputs obtained when different types of terrain are imaged on a particular chopping disk can be predicted. In the simplest case the detector output may then be thought of as indicating "rough," "smooth," or "medium" texture, and the spectral filters may indicate "blue," "red," or "medium" color.

Now a table may be drawn up. Each type of terrain or obstacle is listed, and put into one of several consistency categories. Then the texture and spectral characteristics of each terrain type are listed. Examination of the correspondences between texture-spectral categories and consistency categories indicates the necessary logic processes. For example, it may be found that "medium" color and "smooth" texture always correspond to objects of "hard" consistency. In this case, whenever the consistency sensor determines that the field of view is "smooth" in texture and "medium" in color it indicates "hard" consistency. In this way various combinations of spectral filtering and texture analysis (using different chopper reticles) are examined until the best patterns and filter choices for reliable consistency determination are discovered.

## CONCLUSIONS

On the basis of the limited data available it cannot be asserted that this optical technique for consistency determination will be infallible. However, it does appear reasonable to estimate that 80% to 90% of the terrain obstacles encountered will be correctly identified. The improved vehicle performance which will result from this degree of terrain identification is well worth the small additional terrain sensor complexity involved.

Both texture and spectral analysis can be carried out during night operations. Night operation of the terrain sensor involves illuminating the terrain ahead of the vehicle with a light in the vehicle. For security this may be a very narrow beam, or perhaps an infrared source. During the course of the present study both the use of a tungsten and an infrared source have been examined for spectral analysis and found to be satisfactory. Since the detail seen in an object is affected only to a small extent by the spectral characteristics of the incident radiation, texture analysis can also be used under artificial illumination.

## PRELIMINARY DESIGN

On the basis of the results presented in the preceding sections, it is possible to proceed with a preliminary design for a terrain sensor. This involves at the start the following steps: the choice of a ranging technique, the choice of a computation method, the choice of a consistency measurement technique, preliminary optical design and preliminary system design. These are discussed in various paragraphs of this section.

### CHOICE OF RANGING TECHNIQUE

While the final choice of a ranging technique for the terrain sensor is based on the facts and calculations available on the different methods, the actual choice remains somewhat subjective, since the weights given to the various factors depend on judgement and intuition. Also, not all of the possible techniques have been analyzed completely, so the discussion must be based on data which is to some extent incomplete.

With this in mind, it appears that the best choice is passive ranging by image-plane location, described previously. The reasons for this choice are as follows:

1. The system meets the basic requirements on range and accuracy.
2. The system is passive under usual operating conditions, leading to simplicity and security.
3. Only one station is required for each track (two per vehicle) rather than two per track (four per vehicle) as required by

active systems and those based on triangulation. This leads to simplicity of installation and alignment.

4. If a source of illumination on the vehicle is required for night operation, considerable freedom of choice is allowed; the source may be either a very narrow beam boresighted with the sensor, which leads to good security, or may cover a broad area as do conventional headlamps.
5. This ranging method is based on well-known optical principles and does not require the development of a technique.
6. Certain of the parameters have already been investigated experimentally to verify calculations. (See Appendix C.)
7. The equipment configuration is relatively simple -- apparently as simple as the equipment for any other method. This leads to low cost and high reliability.

For these reasons we have recommended the use of optical rangefinding by image plane determination, and have chosen this method as a basis for a preliminary equipment design.

#### CHOICE OF COMPUTATION METHOD

The next step in the preliminary design of the terrain sensor is the choice of the computation process from among the three techniques discussed in a previous section. The first and second consist, in

simplest terms, of looking out at the terrain with a fixed depression angle\*, and measuring the range to the terrain. Values of the terrain elevation are computed from this measured range. Data processing continues by reading these values into a buffer storage unit as they are computed, and reading them out at a variable rate so that the values of terrain elevation at the output correspond to the terrain a fixed distance ahead of the vehicle, or a fixed time ahead, by taking velocity into account.

The third computation process requires varying the depression angle in such a way that the horizontal distance to the point measured is always constant. If this is done, values of  $y$  computed from the measured depression angle represent immediately the terrain elevation a fixed distance ahead of the vehicle, without the need for an auxiliary buffer storage.

In either case an integrating accelerometer is mounted in the sensor;

---

\* The variation in this depression angle as the vehicle tilts is actually taken into account in the computation process.

C

the output of this is subtracted from the measured values of terrain elevation so that the final terrain elevation output is given relative to a fixed reference level and does not depend on the momentary position of the vehicle.

As far as they have been studied, any of these computation methods is feasible, and therefore the choice is to some extent arbitrary, as in the choice of a ranging technique. We have chosen the third method, in which the sensor is caused to look a fixed distance ahead of the vehicle, on the basis of the following considerations:

1. Buffer storage or extensive computation is not required. This significantly simplifies the equipment.
2. The selected method of ranging requires some physical motion of optical elements in order to locate the image plane at different ranges. This motion can be replaced by the change in the depression angle if a fixed range is used, as in the selected computation method. Thus, the need for one other major motion is eliminated.
3. This method eliminates the need for measuring ranges greater than the nominal horizontal distance, thus contributing to range accuracy (which falls as the square of range).
4. Since the sensor operates at a nearly constant range, the determination of consistency by texture analysis may be simplified.

## PRELIMINARY OPTICAL DESIGN

As has been seen, the system to be investigated during the preliminary design stage consists of an optical rangefinder functioning by image plane location, which keeps itself aimed at the terrain a fixed distance ahead of the vehicle. A number of optical configurations have been considered for this sensor; one which seems suitable for analysis is described in this section.

The optical layout for this system is shown in Figure 34. This figure is drawn to approximately half scale. Radiation enters the system from the right and strikes the large flat pierced mirror. This mirror is an ellipse, about 3 inches by 4-1/2 inches, and can be rocked about an axis perpendicular to the plane of the drawing to change the depression angle. Energy is reflected via a fixed folding mirror to the 3-in. parabolic primary mirror of 12-inch focal length which is fixed with respect to the sensor frame. The converging cone is again folded and then passes through the elliptical hole in the large flat rocking mirror, is folded by a fixed mirror, and an image is formed near the fixed field stop and dual-thickness rotating chopper. The interrupted energy then falls on a multiplier phototube, generating an a-c waveform. Details such as the required light baffles have been omitted from this sketch.

The chopper is shown (not to scale) in Figure 35. A reticle on the flat surface interrupts the incident radiation to generate the a-c output. This is a maximum when the field object is focused on the pattern.

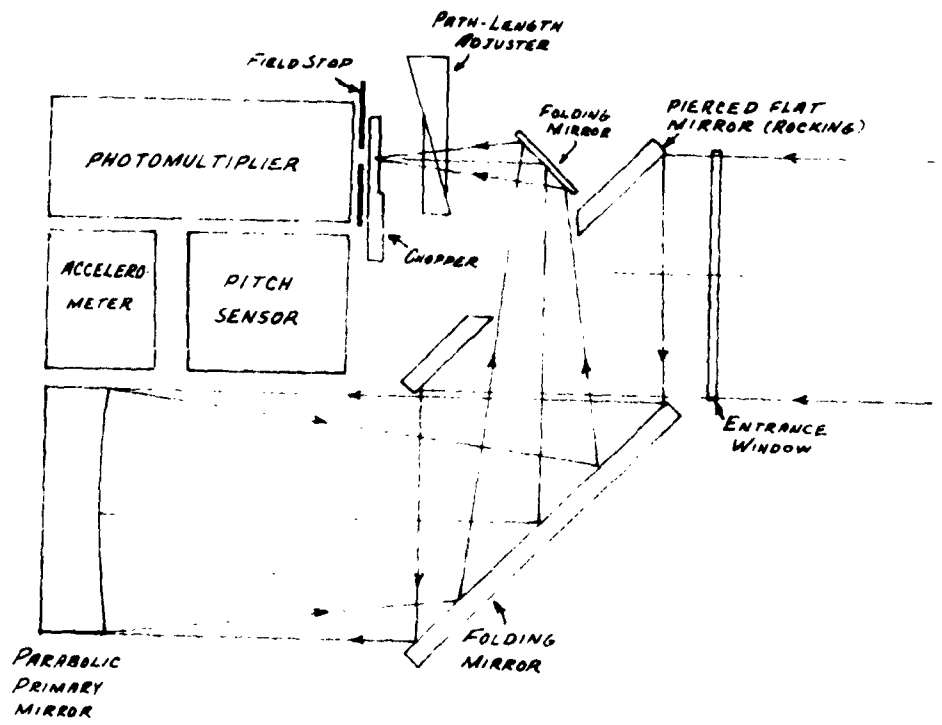
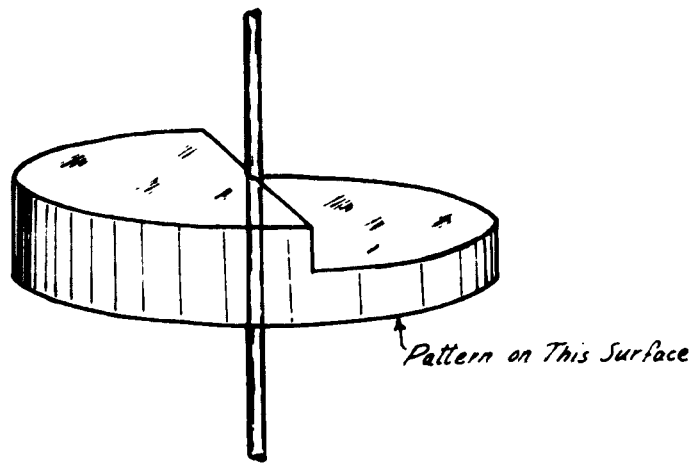


Figure 34. Preliminary Optical Design



*Figure 35. Dual-Thickness Chopper*

Because of the dual-thickness chopper, the optical path is longer for one half a revolution than it is for the other half. Thus the focal position shifts back and forth with respect to the reticle. This results in amplitude modulation of the a-c waveform out of the multiplier phototube. Phase detection of this waveform permits the determination of whether the object field is too far away or too near; this information is used to rock the large flat mirror in such a way as to reduce the amplitude modulation of the a-c waveform to zero.

One other optical element, the optical path length adjuster, is shown in the figure. This consists of a pair of glass wedges, one sliding and one fixed. As the movable wedge slides, the pair has the same effect on radiation passing through them as would a plate of glass having a varying thickness. Thus, sliding one of the wedges changes the optical path length by an amount proportional to the motion.

This optical element serves two purposes. It adjusts the optical system for pitch of the vehicle, making stabilization of the entire optical unit unnecessary, and it improves the accuracy of the values of terrain elevation which appear as the output of the system. This will be shown in the discussion in the next section.

#### COMPUTATION EQUATIONS FOR PRELIMINARY DESIGN

Figure 36 is a simplified version of Figure 24. The following definitions of the symbols are the same as those used in the section on Stabilization and Computation Requirements.

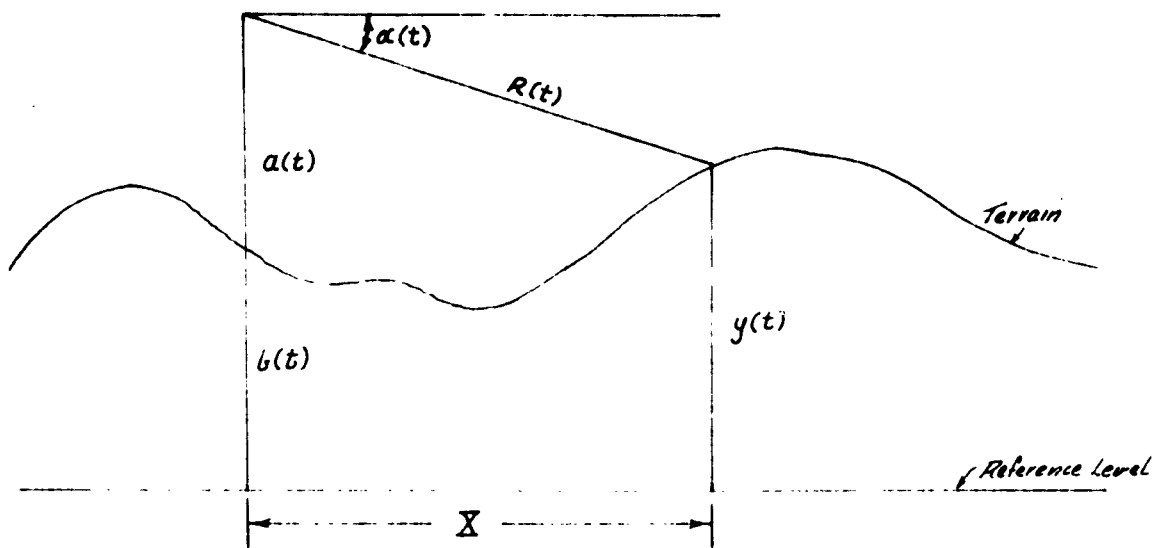


Figure 36. Terrain Sensor Geometry

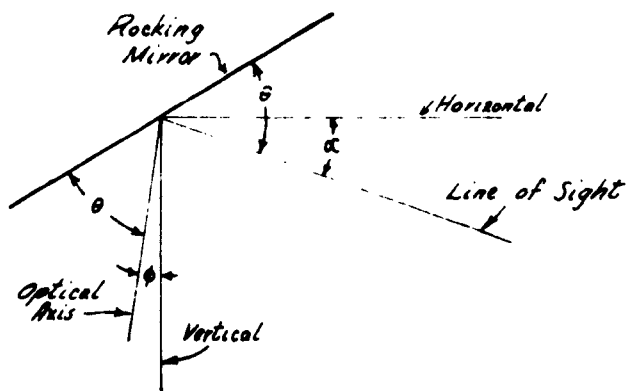


Figure 37. Pitch-Axis Geometry

- a -- The height above the terrain of the terrain sensor, along the direction of gravity. The position of the sensor is assumed to be above the front point of contact of the vehicle track or wheels and the terrain.
- b -- The difference between the actual terrain elevation\* and the elevation as measured by the accelerometer and attendant circuitry. The value of b is a slowly varying function of time, but may become large for large changes in terrain elevation.
- $\alpha$  -- The depression angle of the optical sensor. It is measured in the vertical plane, and is the angle between the horizontal and the direction through which the sensor is pointing.
- x -- The coordinate of the terrain along the horizontal, measured from the present position of the vehicle, positive in the direction of motion of the vehicle.
- y -- The measured vertical coordinate of the terrain, positive upward.
- R -- The range to the terrain ahead of the vehicle measured along the direction that the optical sensor is pointing.
- $X_c$  -- The fixed horizontal distance ahead of the vehicle at which terrain measurements are to be made.

We will define a quantity  $A(t)$ :

$$A(t) = a(t) + b(t)$$

---

\* Above some absolute reference level.

(  $A(t)$  thus represents the terrain height as obtained from the integrated accelerometer output. It accurately represents short-term fluctuations in the terrain.

It can be seen from Figure 36 that

$$\begin{aligned} y(t) &= a(t) + b(t) - R(t) \sin \alpha(t) \\ &= A(t) - R(t) \sin \alpha(t). \end{aligned}$$

This ranging process consists in adjusting the rocking mirror until

$$X_c = R(t) \cos \alpha(t).$$

When this holds, we have

$$y(t) = A(t) - X_c \tan \alpha(t).$$

( Now the effects of vehicle pitch on  $\alpha$  will be considered. The allowable stabilization errors in cant (motion about an axis parallel to the motion of the vehicle) and pitch (motion about an axis perpendicular to the cant axis and parallel to the ground) were discussed in a previous section. The allowable rms error in pitch (or the equivalent error in terrain sensor depression angle) was found to be 0.11 degree. The allowable error in cant was found to depend on the criterion used, but was at least 18 times greater than the allowable pitch error, and under certain conditions is negligible.

Because the effects of pitch on the terrain sensor accuracy are so much greater than those of cant, they have been taken into account in the preliminary design stage. This is done as follows: In Figure 37, let  $\phi$  be the pitch angle between a nominally vertical reference axis in the vehicle\* and true vertical, and let  $\theta$  be the measured angle of the rocking mirror with respect to this axis. Then it can be seen from the figure that

$$\alpha = 2\theta + \phi - \frac{\pi}{2},$$

and that therefore (using the cotangent to eliminate  $\frac{\pi}{2}$ )

$$y(t) = A(t) + X_c \cot(2\theta + \phi).$$

This is the final computation equation.

This does not complete the analysis, however. In order to insure that the depression angle arrived at as a result of rocking the flat mirror actually represents the depression angle to a point on the terrain a fixed distance  $X_c$  ahead of the vehicle, the equation

$$X_c = R(t) \cos \alpha(t)$$

must always be satisfied. This requires that the range measured by the optical ranging system must be a function of  $\alpha$ .

\* For example the optical axis of the primary optical system.

It will be seen that what is required is that as the angle of the mirror,  $\theta$ , and the vehicle pitch,  $\phi$ , vary, the point in the focal system where best focus is found must be varied.

Letting  $\delta$  be the location of best focus, measured from the back focal point of the optical system, and measuring  $R$  from the front focal position of the optical system, if the focal length of the system is  $f$  we have the requirement that

$$\delta = \frac{f^2}{R} = \frac{f^2}{X_0} \sin (2 \theta + \phi).$$

In the optical system described above, the optical path length is varied to accomplish this, by sliding one of the glass wedges with respect to the other one. This method makes it unnecessary to move either the chopper assembly or the primary mirror, and thus simplifies the maintenance of optical alignment.

#### PRELIMINARY SYSTEM BLOCK DIAGRAM

A functional block diagram of the system described is presented in Figure 38. In order to make the diagram easier to follow, the system has been broken down into three main subsystems, the blocks corresponding to each one being marked with a different symbol. The blocks marked with a double circle constitute the main optical loop of the system. Those having a square comprise the readout and terrain elevation computation subsystem. Those marked with a black disk perform the necessary adjustment of optical path length described above.

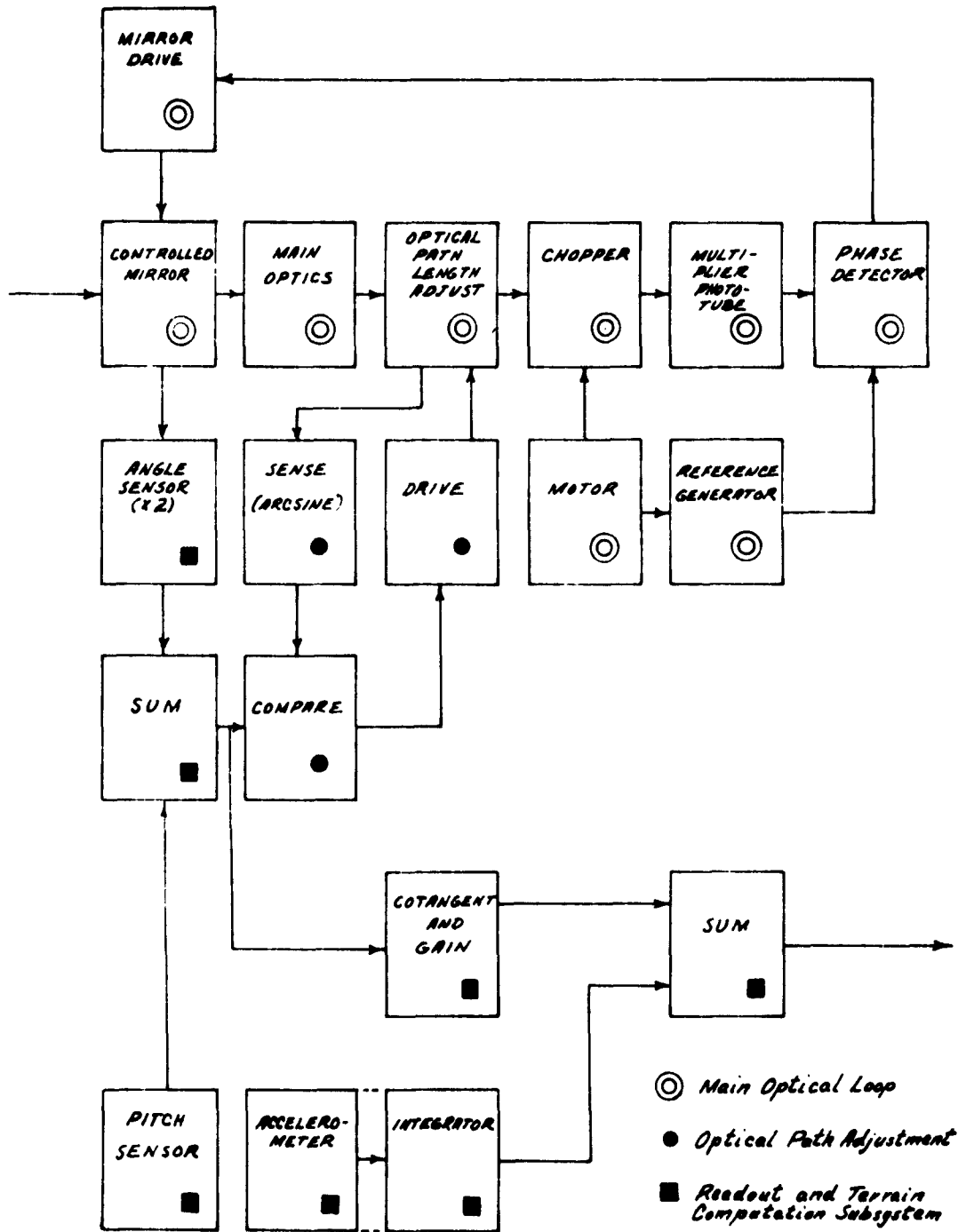


Figure 38 System Functional Block Diagram.

The main loop contains first the controlled rocking mirror, which directs incident radiation onto the main optics, consisting of the parabolic primary and necessary folding mirrors. The energy passes through the optical path length adjuster (the prisms previously described) and then the dual-thickness chopper. The chopped energy falls on the multiplier phototube, which produces an electrical output. The chopper is driven by a motor which also drives a reference generator, the output of which is used in the phase sensitive detector to determine which way to drive the rocking mirror.

The readout and terrain computation subsystem can be followed through, starting with the angle sensor. This sensor has an output  $2\theta$ , twice the angle of the mirror with respect to a fixed axis in the vehicle. To this quantity is added  $\phi$ , the pitch angle, obtained from the pitch sensor. The cotangent of this angle is then introduced into the output summer.

The integrated accelerometer output provides the other input to the summer; the output is  $y$ , the desired terrain elevation.

The blocks marked with black disks constitute a small loop for adjusting the optical path length. The path length, which is a linear function of the position of the movable prism, is sensed, and the arcsine of this quantity is compared with the sum  $2\theta + \phi$  computed in the previously considered subsystem. This comparison generates an error signal which drives the optical path length adjuster to reduce the error to zero.

## CONSISTENCY SENSOR DESIGN

In this section a preliminary design for that portion of the terrain sensor which determines consistency is discussed. An outline of the principles of operation and a block diagram of the necessary processing electronics is given. However, as pointed out earlier, it is not possible to describe in detail the spatial and spectral filtering and the data processing circuits to be employed, because of the lack of adequate terrain data.

### Principle of Operation

The consistency sensor is designed to use differences in texture and spectral content for determining the nature of terrain obstacles. It contains an optical system smaller than the one required for the automatic ranging portion of the terrain sensor, because the energy required for simple spectral or terrain analysis is much less than that required for accurate ranging. This optical system is boresighted with that of the primary optics of the automatic rangefinder; because of the small size required (a one-inch diameter aperture should be sufficient) it can be a separate system looking out through the same tilting mirror. The field of view of the consistency sensor is identical with that of the rangefinder.

The image of the terrain formed by the consistency sensor is analyzed for texture and spectral content. The spectral analysis is accomplished by rotating a wheel containing various wide-band spectral filters in the incoming radiation. (See Figure 39.) This modulates the

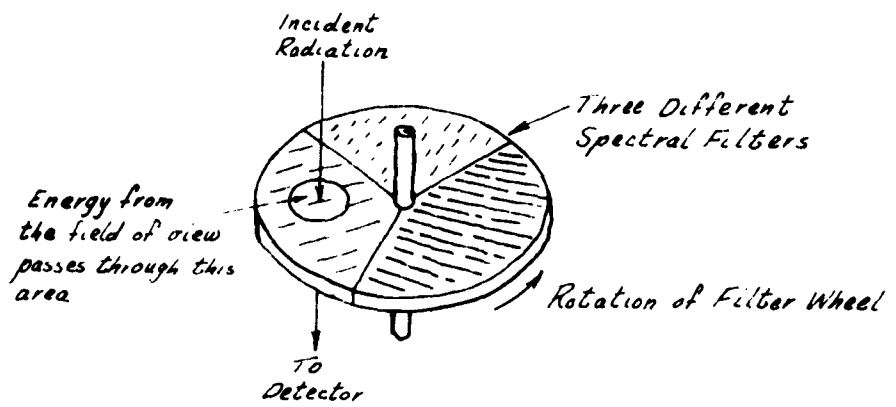


Figure 39. Rotating Filter Wheel for Spectral Analysis.

received radiation and produces an electrical waveform at the output of the detector; the shape of this waveform is a function of the spectral content of the radiation. Simple analysis of this waveform by synchronous rectification allows the relative amounts of energy in the various spectral regions to be determined. The relative levels so generated can be used to operate switching circuitry. This may be very simple (for example the output may consist of any one of three signals indicating "red," "blue," or "medium" color), or more complex (including the relative amounts of energy in various spectral regions) if more information is found to be useful.

Now a similar process is performed to determine the amount of detail in the image; this corresponds to the optically observable texture or surface roughness in the terrain being viewed. Figure 40 is a sketch of a second chopper wheel, bearing various transmission patterns, which might be rotated in the image plane of the consistency sensor optical system. As different portions of the rotating reticle pass through the image of the field of view, e c waves of different amplitude appear at the output of the detector. The relative amplitudes of these waves indicate the amount and nature of the fine detail in the image, just as the similar signals generated by the rotating spectral filter wheel indicate the spectral content of the radiation from the field of view. Again, simple circuits allow the classification of the return into "rough," "smooth," or "medium" or into more highly differentiated categories.

In practice the two operations of spectral and texture analysis are

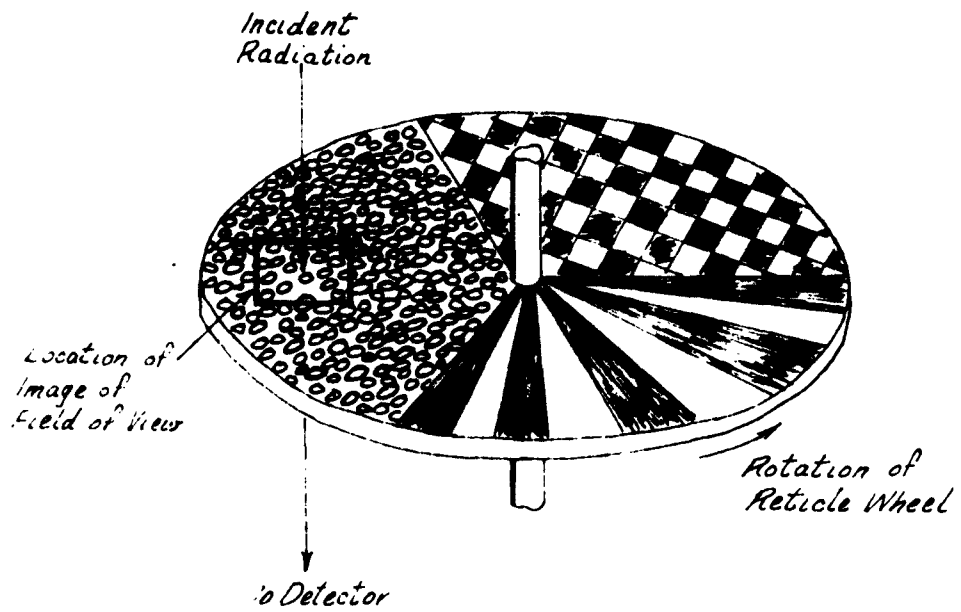


Figure 40. Rotating Chopper Wheel for Texture Analysis.

combined; as will be seen in the next paragraph, the reticle for texture analysis may be laid down directly on the spectral filter wheel.

#### Preliminary Design of Consistency Sensor

The consistency determination portion of the terrain sensor is sketched in Figure 41. It consists of an objective lens which images the field of view on a field stop; as described previously this optical system is boresighted with the automatic rangefinder portion of the terrain sensor. Behind this field stop is the rotating reticle or chopper and a photomultiplier tube. The chopper is rotated by a small motor which also drives a commutator from which reference signals for synchronous detection are derived.

A hypothetical chopper disk is shown in Figure 42. This disk contains five sections, each embodying different combinations of spectral and spatial filters. As various portions of the disk pass by the field stop, a-c signals of various amplitudes are generated.

The data processing system is shown in block diagram form in Figure 43. As shown, the reference signals from the synchronous pick-off are used to sort out the particular portions of the detector output which correspond to each sector of the chopper disk, so that at the output of each of the five synchronous detectors a signal appears which represents the result of chopping the image with one particular sector

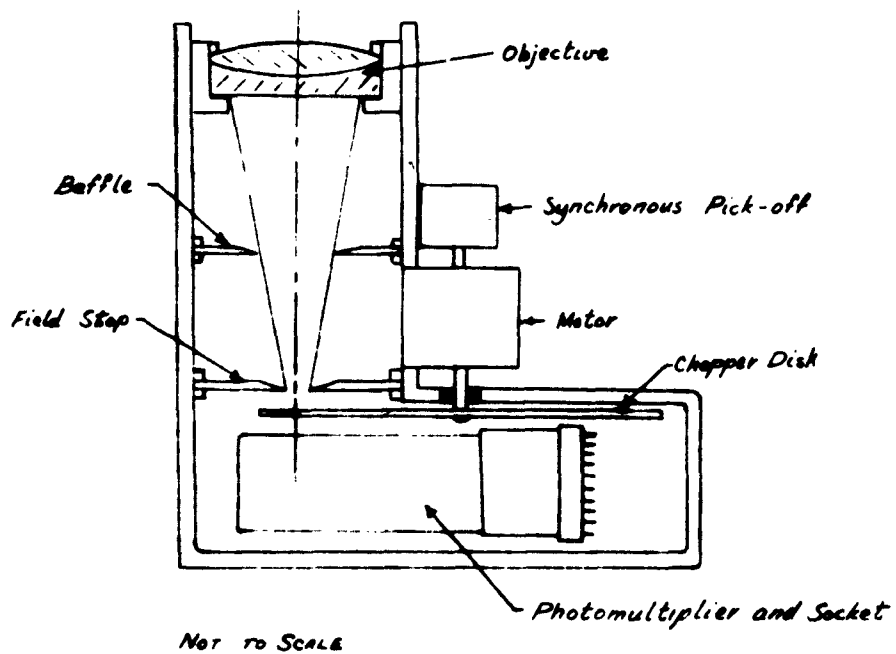


Figure 41. Consistency Sensor Optics and Detector.

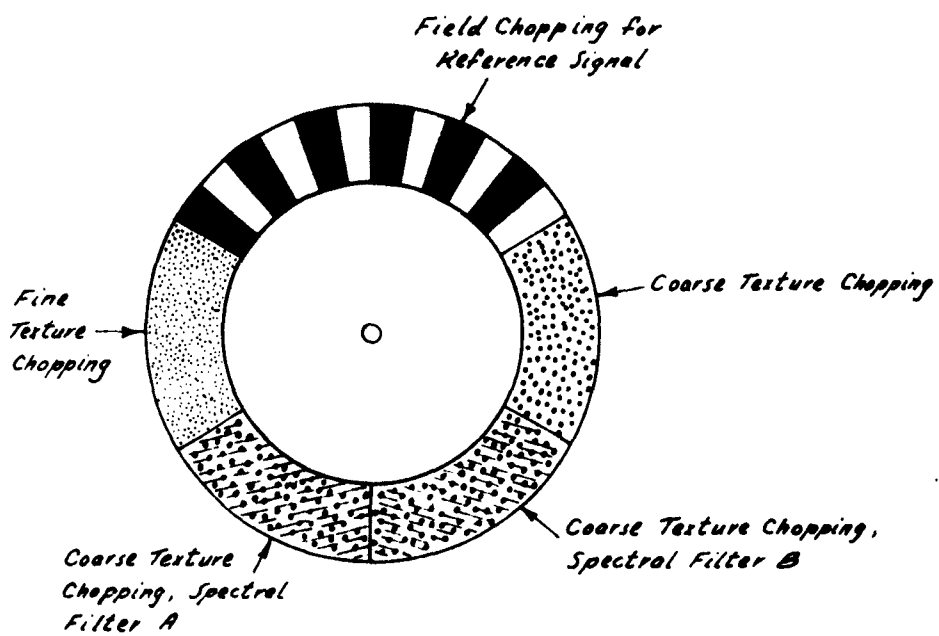


Figure 42. Hypothetical Chopping Disk.

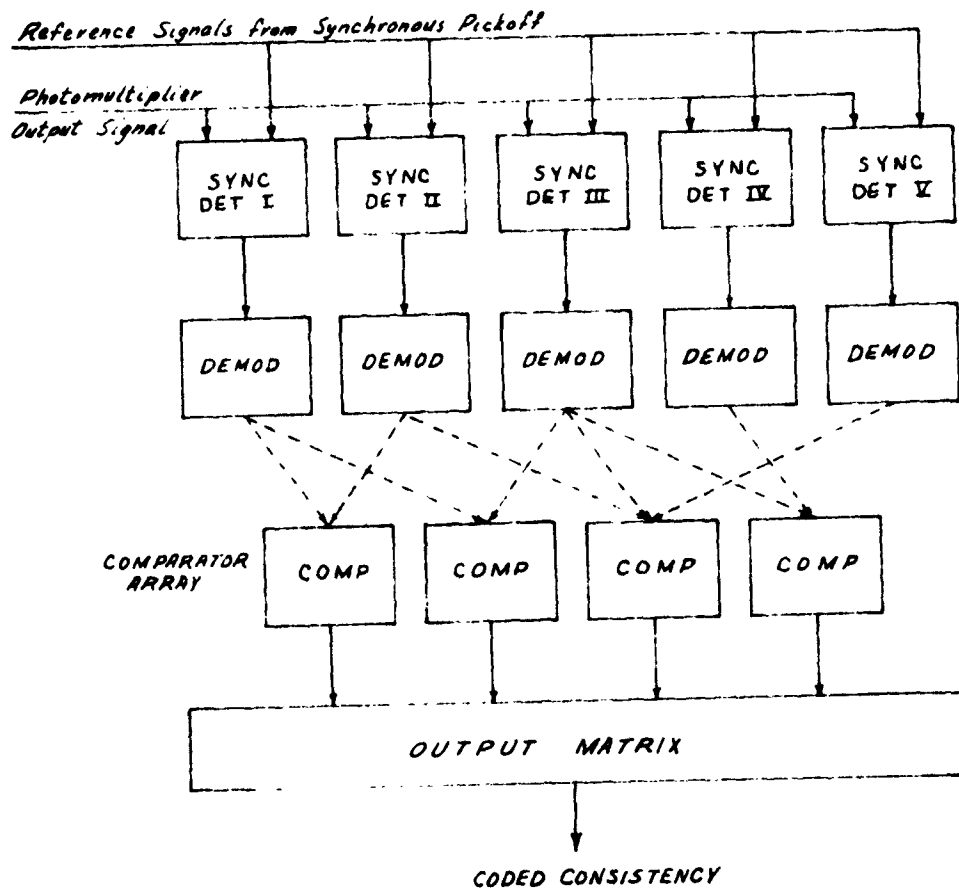


Figure 43. Block Diagram of Data Processing System.

of the disk. These outputs are further demodulated to yield amplitude information. The resulting amplitudes are compared in a set of comparators in accordance with the chosen logic for consistency determination. The outputs of the comparators activate an output switching matrix which yields an indication of consistency properly coded for use in the suspension system.

#### OPTICAL CONSIDERATIONS

The general optical system for the passive rangefinder is composed of the flat pierced mirror which directs the energy to the primary mirror, the primary mirror of parabolic shape, and two constant-thickness elements. These are 1) the path-length adjuster consisting of two wedges whose combined thickness adjusts the focal position, and 2) the dual thickness chopper. Thus the aberrations in the image will be a function of these three elements.

##### 1. Parabolic Reflector

The parabolic reflector is ideal for this system because of its "perfect" image quality on axis, where the angular blur size is theoretically limited only by diffraction. The effective angular

size of the on-axis blur spot, at the diffraction limit, is  $2.44 \lambda / D$ , where  $\lambda$  is the wavelength and  $D$  is the mirror diameter. At a wavelength of 0.6 micron and a 3 inch diameter, the blur is 0.005 milliradians. In practice, the diffraction limit is not realized and the actual image size required over the whole field will be a function of the off-axis characteristics of the paraboloid.

There are three aberrations inherent in the off-axis image of a paraboloid. They are coma, astigmatism, and field curvature. The sagittal coma patch, identified here as  $\beta_c$ , is the width of the triangular shape containing most of the energy. The total height of the coma patch is three times this value. The sagittal coma blur is

$$\beta_c = 0.0625 \theta (f/\#)^{-2} \text{ radians}$$

where  $\theta$  is the off-axis angle, and  $f/\#$  is the focal ratio.

The astigmatic angular blur of the paraboloid is given by

$$\beta_a = 0.5 \theta^2 (f/\#)^{-1} \text{ radians}$$

The field curvature of this type of system is not strictly an aberration, but if the chopping motion occurs in a plane, the result is that when the best on-axis image is chopped, the chopping will occur in a region progressively further from the best image as the field angle increases.

( Assuming that the best image plane lies on a circle whose radius is the focal length, then the off-axis chopping (at  $\theta$ ) will occur a distance  $x$  along the optical axis from the best on-axis image where, to a good approximation,

$$x = f(1 - \sqrt{1 - \theta^2})$$

and the angular blur due to field curvature is

$$\beta_{fc} = x(f/\#)^{-1} \text{ radians}$$

Another factor affecting these aberrations is the position of the limiting or entrance aperture. Coma ( $\beta_c$ ) does not vary with stop position. The above relationship for the astigmatic blur holds for the limiting aperture at the reflector or primary objective. It is zero when this aperture is located one focal length in front of the reflector, and varies as the square of this separation. Thus for the stop positioned a distance one-half the focal length in front of the reflector,  $\beta_a$  is one-fourth the value obtained from the above equation.

Assume the following design parameter:

$D = 3$  inches

$f/\# = 4$  ( $f = 12$  inches)

$\theta = 0.010$  radian (total horizontal field equals 0.020 radian;

total vertical field equals 0.005 radian.)

Therefore

$$\begin{array}{l} \text{Coma:} \quad \beta_c = (0.0625)(0.010)(4)^{-2} = 0.039 \text{ milliradian} \\ \text{Astigmatism:} \quad \beta_a = (0.5)(0.010)^2 (4)^{-1} = 0.013 \text{ milliradian} \\ \text{Field} \quad \left. \vphantom{\begin{array}{l} \text{Coma:} \\ \text{Astigmatism:} \end{array}} \right\} x = 0.006 \text{ inch} \\ \text{Curvature} \quad \left. \vphantom{\begin{array}{l} \text{Coma:} \\ \text{Astigmatism:} \end{array}} \right\} \beta_{fc} = 0.015 \text{ milliradian} \end{array}$$

The contribution from coma is the largest and determines the resultant resolution over the whole field. Since coma is not a function of the position of the entrance aperture, this stop position may be put at any convenient place. The comatic blur is 8 times the diffraction limit. At a range of 44 feet, this blur size corresponds to a resolution of 0.02 inch in the object plane.

## 2. Path-Length Adjuster

The path-length adjuster is composed of one sliding and one fixed wedge mounted together to form a parallel plate of variable thickness. As the sliding wedge moves, the focal position for a particular range changes. This serves to adjust for vehicle pitch, and to keep the optical system pointed a fixed horizontal distance ahead of the vehicle.

Two factors must be considered in regard to the optical effects of the parallel plate. These are 1) the relationship between the combination of the effects of the thickness of the plate,  $T$ , the optical index of refraction,  $n$ , and the focal position displacement, and 2) the amount of aberration introduced by the plate. The image shift,  $S$ , can be stated to a good approximation by

$$S = T \left( 1 - \frac{1}{n} \right).$$

The above shift can also be related to the change in object distance from the relationship

$$\Delta x' = \frac{f^2}{x^2} \Delta x$$

where  $\Delta x'$  is equal to  $S$ ,  $\Delta x$  is the equivalent object distance shift, and  $f$  is the focal length. So

$$\Delta x = \frac{x^2}{f^2} T \left( 1 - \frac{1}{n} \right).$$

The maximum change in the object distance that may occur is on the order of one foot. This value is determined by assuming that the optical system views first the level terrain a distance of 44 feet ahead of the vehicle and then the terrain slopes downward an equivalent of 5 feet during the next 44 feet. Thus if  $f = 12$  inches, and  $\Delta x = 12$  inches,

$$T \left( 1 - \frac{1}{n} \right) = .0062 \text{ inch}$$

and  $\Delta T$  is the maximum change in thickness required. If  $n = 1.5$ ,

$$\Delta T = .019 \text{ inch}$$

If the wedge angle is  $10^\circ$ , the movable wedge must shift a total of 0.11 inch to produce the above value of  $\Delta T$ .

The other consideration is the amount of spherical aberration caused by the path-length adjuster. The angular blur introduced by the spherical aberration of a parallel plate of thickness  $T$  and index  $n$  is\*

$$\beta_s = \frac{T}{4(F/\#)f} \left[ \left( \frac{4(F/\#)^2 - 1}{n^2 4(F/\#)^2 - 1} \right)^{1/2} - \frac{1}{n} \right] \text{ radians.}$$

For a focal length of 12 inches, a focal ratio,  $(F/\#)$ , equal to 4 and  $n = 1.5$ , the above relationship reduces to

$$\beta_s = 0.15 \text{ milliradians (T in inches).}$$

Thus a thickness of 0.26 inch would give a blur size equal to the maximum comatic blur  $\beta_c$  of 0.039 milliradian, as computed above.

If the value of maximum blur is assumed to be equal to 0.10 milliradian (as taken in the previous section) an equivalent

\* This rather cumbersome expression can be readily obtained from some simple geometrical considerations using the paraxial and marginal rays and Snell's Law.

spherical aberration blur  $\beta_s$  would be introduced by a parallel plate thickness of 0.67 inch. The wedge may easily be kept to much less than this value and thus spherical aberration presents no problem.

In case greater resolution is required, it would be possible to manufacture the paraboloid to allow for the thickness. Since the final polishing of a parabola is performed using a method like the "knife-edge" test it should be easy to perform this operation to allow for the parallel plate.

### 3. Dual-Thickness Chopper

The same considerations apply to the optical effects of the dual-thickness chopper as were discussed for the path-length adjuster. The chopper acts as a parallel plate with either of two thicknesses which will introduce both image position shift and spherical aberration.

In the previous section a derivation is given for the value of sensitivity  $(\Delta x)_{\min}$  using the proposed system design parameters. The contrast difference,  $2 \Delta I$ , between the two image positions as determined by the dual-thickness chopper was found to equal  $2\theta f^2/D$ .

Using the same system parameters as before where  $\theta$ , the angular diameter of the optical blur equals  $10^{-4}$  radians, D, the diameter of the optics was 3 inches, and a focal length, f, of 12 inches, results in

$$2 \Delta_1 = 0.0096 \text{ inch}$$

In order to effect this shift in focal position, the change in thickness required ( $n = 1.5$ ) is

$$T = \frac{0.0096}{1 - \frac{1}{1.5}} = .029 \text{ inch.}$$

Now spherical aberration is a function of the actual thickness of the element. This could easily be kept to around a value of 0.1 inch, and the total contribution to spherical aberration is again not of importance ( $\beta_s = 0.015 \text{ nr}$ ).

Another method of producing this image shift besides a dual thickness design is the use of two cemented half disks, each of different indices of refraction. The following relationship,

$$\Delta n = \frac{R^2}{T} \Delta S$$

C  
represents the index change necessary to produce a focal shift of  $\Delta S$ . For  $n$ , the value of index for one of the materials, equal to 1.5,  $T$  equal to 0.1 inch, and  $\Delta S$  equal to 0.0096 inch,

$$\Delta n = 0.22 \text{ .}$$

Combination of the various optical glasses of crown and flint may be readily found to exhibit this value of difference in index of refraction.

Another aberration that must be considered in the use of the chopper and the path-length adjuster, is longitudinal chromatic aberration. It is proposed to use an S-20 wavelength region which is responsive between about 0.32 to 0.62 microns. The variation in index of refraction over this wavelength region for the optical material or materials used in the wedges and chopper will introduce chromatic aberration.

Assume that the total thickness of the optical elements is 0.2 inch. A typical low dispersion crown glass exhibits a change in index of about .035 over this wavelength region, at a nominal index value of 1.52. The equivalent change in focus is

$$\Delta S = \frac{0.2}{1.52} \times 0.035 = .0025 \text{ inch.}$$

This is only a factor of four less than the required shift in focus caused by the dual-thickness chopper. Thus some achromatism is required in the optical design. The wedges and chopper disc may be color-corrected by constructing them of different materials. This is entirely feasible. The detailed calculations demonstrating these achromatic elements are not considered important at the present state of design

#### Conclusion

The following table summarizes the various optical design parameters discussed. In general, there are no serious optical design problems. The optical elements are well within the state of the art. The parabolic primary mirror should only be of moderate cost. For production quantities; replica mirrors can be made at low cost.

TABLE 1  
SUMMARY OF CHARACTERISTICS  
OF OPTICAL ELEMENTS

ITEMS	PARABOLIC PRIMARY $D=3'$ $f=12'$	PATH LENGTH ADJUSTER (Double Wedge) $T=0.1''$ ( $10^\circ$ )	DUAL-THICKNESS CHOPPER $T=0.1''$
DIFFRACTION LIMIT ( $0.6\mu$ )	0.005 <i>mr</i>	—	—
COMA ( $\theta/2 = 10$ <i>mr</i> )	0.039 <i>mr</i>	—	—
ASTIGMATISM	0.013 <i>mr</i>	—	—
FIELD CURVATURE	0.015 <i>mr</i>	—	—
SPHERICAL ABERRATION	—	0.015 <i>mr</i>	0.015 <i>mr</i>
CHROMATIC ABERRATION	—	REQUIRES	ACHROMATIZATION
OTHER PARAMETERS		$\Delta T = 0.019''$ Total Lateral Movement: 0.11	$\Delta T = 0.020''$ or $\Delta n = 0.22$ ( $n = 1.5$ )
DESIGN OBJECTIVE IMAGE SIZE	0.10 <i>mr</i>	0.10 <i>mr</i>	0.10 <i>mr</i>

## MODULATION IN THE TERRAIN SENSOR

When a chopper is moved in the image space of an optical system, the resulting modulation of the transmitted radiation may be due to either of two separate effects. One of these effects may be called detail chopping. It results from the detail in the image: point-to-point variations in the intensity of the target result in fluctuations at the detector as the chopper alternately transmits energy first from one small portion of the field of view and then another. This is the effect which is exploited in image-plane location

The other of the effects may be called field chopping. The chopper and field stop (which may be the detector area itself) together may cause the energy falling on the detector to fluctuate even if the object field is uniformly illuminated, because when the chopper is in certain positions with respect to the field stop more radiation is transmitted than when the relative positions of chopper and field stop are slightly different.

It is important to reduce or eliminate field chopping in a ranging system, because field chopping generates a large signal which is independent of the relative positions of the image plane and chopper; this dilutes the signal which results from detail chopping and thus makes it more difficult to determine the location of the plane of best focus .

This can be seen from a rather general discussion. Suppose the signal due to detail chopping is

$$S(t) = S_0(1 + \epsilon \cos 2\pi pt) \cos 2\pi f_c t,$$

as before, where  $\epsilon$  can be approximated as a linear function of the object displacement. Then the minimum detectable value of  $\epsilon$  can be translated directly into range accuracy, as was done before. If no field chopping occurs, this minimum detectable fractional modulation  $\epsilon_{\min}$  is

$$\epsilon_{\min} = \frac{2\sigma}{S_0} (\Delta f)^{1/2},$$

where  $\sigma$  is the input noise power per unit bandwidth, and  $\Delta f$  is the system bandwidth.

Now if field chopping is present, it results in adding to the above signal another unmodulated signal of the same frequency but possibly different phase, and the result,  $S_1(t)$ , is

$$S_1(t) = S_0(1 + \epsilon \cos 2\pi pt) \cos 2\pi f_c t + S_f \cos(2\pi f_c t + \alpha)$$

where the amplitude of the signal due to field chopping is  $S_f$  and  $\alpha$  represents an arbitrary phase angle.

This can be written as

O

$$S_i(t) = [S_0(1 + \epsilon \cos 2\pi pt) + S_f \cos \alpha] \cos 2\pi f_c t - [S_f \sin \alpha] \sin 2\pi f_c t$$

and hence if

$$\beta(t) = \tan^{-1} \frac{S_f \sin \alpha}{S_0(1 + \epsilon \cos 2\pi pt) + S_f \cos \alpha}$$

$$\begin{aligned} S_i(t) &= \sqrt{[S_0(1 + \epsilon \cos 2\pi pt) + S_f \cos \alpha]^2 + [S_f \sin \alpha]^2} \cdot \cos [2\pi f_c t + \beta(t)] \\ &= \sqrt{(S_0^2 + 2S_0 S_f \cos \alpha + S_f^2) + 2(S_0^2 + S_0 S_f \cos \alpha) \epsilon \cos 2\pi pt + (S_0 \epsilon \cos 2\pi pt)^2} \times \\ &\quad \times \cos [2\pi f_c t + \beta(t)] \end{aligned}$$

When  $\epsilon$  is small, this can be approximated as

$$\begin{aligned} S_i(t) &\approx \sqrt{S_0^2 + 2S_0 S_f \cos \alpha + S_f^2} \left( 1 + \frac{S_0^2 + S_0 S_f \cos \alpha}{S_0^2 + 2S_0 S_f \cos \alpha + S_f^2} \epsilon \cos 2\pi pt \right) \times \\ &\quad \times \cos [2\pi f_c t + \beta(t)] . \end{aligned}$$

This expression again represents a modulated carrier, but now the amplitude of the carrier is given by the radical, and the fractional modulation is the coefficient of  $\cos 2\pi pt$ . Hence the minimum detectable modulation,

$C_{1\mu}$  satisfies

O

$$\frac{S_o^2 + S_o S_f \cos \alpha}{S_o^2 + 2 S_o S_f \cos \alpha + S_f^2} (\epsilon_1)_{\min} = \frac{2 \sigma (\Delta f)^{1/2}}{\sqrt{S_o^2 + 2 S_o S_f \cos \alpha + S_f^2}}$$

$$(\epsilon_1)_{\min} = 2 \sigma (\Delta f)^{1/2} \frac{\sqrt{S_o^2 + 2 S_o S_f \cos \alpha + S_f^2}}{S_o^2 + S_o S_f \cos \alpha}$$

Thus in the presence of the disturbing signal due to field chopping,  $(\epsilon_1)_{\min}$  depends on  $\alpha$ , which represents the phase difference between the average signal due to detail chopping and the signal due to field chopping.

$$\text{When } \alpha = 0, (\epsilon_1)_{\min} = \epsilon_{\min}$$

where  $\epsilon_{\min}$  is the minimum detectable modulation with no field chopping.

If on the other hand,  $\alpha = \pi/2$ ,

$$(\epsilon_1)_{\min} = \epsilon_{\min} \frac{\sqrt{S_o^2 + S_f^2}}{S_o}$$

and if in this case  $S_f$  is large

$$(\epsilon_1)_{\min} \approx \epsilon_{\min} \frac{S_f}{S_o}$$

Thus in the worst case, the minimum detectable modulation is increased by the ratio  $\frac{S_f}{S_o}$ , and hence the range accuracy is decreased by the same

factor. This is especially bad, since, in any case range accuracy is least when there is little detail in the image, making  $S_0$  small; and it is under just such conditions that the effect of a large constant  $S_f$  will cause the maximum effect.

The effect would be reduced, of course, if  $\alpha$  could be chosen as zero; however  $\alpha$  depends on the nature of the object field and so cannot be controlled.

Another factor which must be considered in the design of the terrain sensor is the choice of the modulating frequencies. In order to achieve the previously calculated range accuracy, it is necessary that no disturbance appear in the system at the carrier modulating frequency  $p$ . Any such disturbing signal appears at the output as noise in the output pass-band of the system, and consequently reduced system accuracy.

In the employment of the terrain sensor a built-in mechanism exists for producing such undesirable disturbances. This mechanism is the motion of the terrain through the field of view of the device as the vehicle moves along. As various portions of the terrain having various degrees of brightness move through the field of view of the sensor, the carrier generated by detail chopping is modulated by a wide-band a-c signal. Most of the energy in this signal is concentrated at low frequencies, and so if the modulating frequency is chosen to be high enough, the modulation produced by the terrain motion will not interfere with the ranging process. However, the magnitude of the effect requires further study.

## LIMITS ON SENSOR OPERATION

### INTRODUCTION

In this section the effects of atmospheric conditions on the operation of the terrain sensor and the problems of increasing the operating range of the sensor are described. The discussion of atmospheric effects is separated into two parts. The first covers the effects of atmospheric turbulence ("shimmer," "boil") on the performance of the sensor; the second discusses the effects of climatic conditions. On the basis of the effort reported here, it is concluded that neither turbulence nor climatic conditions normally encountered will seriously reduce the effectiveness of the terrain sensor. Finally, it is shown that the operating range of the terrain sensor can be increased, but that many factors must be considered in doing this.

### EFFECT OF ATMOSPHERIC TURBULENCE

If the air between the terrain and the terrain sensor is still and clear, it has no effect on the performance of the optical system, but commonly the atmosphere is a turbulent medium of varying refractive index as a result of non-uniform heating by the earth and non-uniform mixing by the wind. This lack of homogeneity of the atmosphere may affect the performance of optical instruments.

Three affects on the image formed by optical instruments may be distinguished. These are intensity fluctuations, generally called scintillation, image motion, and image blurring. These will be discussed separately below.

There is quite an extensive literature on these atmospheric effects. One of the best bibliographies is given by Wimbush.\* However, most of this literature applies to the affects of the atmosphere on stellar observations and on long range terrestrial observations, and little investigation has been directed to the effects of the turbulent atmosphere made at the range the terrain sensor is to operate, (about 44 feet). One reason for this is that atmospheric effects increase with the length of the optical path, and therefore, the effects generally constitute a problem only when precision observations (as with an astronomical telescope) are to be made over long paths through the atmosphere. Thus it can be said at the start that the terrain sensor would be expected to be relatively unaffected by atmospheric effects, because of the short path length involved.

In discussing atmospheric effects, the effect of intensity fluctuations, or scintillation, may be considered first. Scintillation is commonly observed in the twinkling of the stars at night. If the energy received from the target area fluctuated in the same way, it would produce amplitude modulation of the detector output, and this would interfere with the determination of best focus, since the latter is measured by reducing the envelope modulation to zero (at one frequency).

\* Wimbush, Mark H. Optical Astronomical Seeing: A Review. Hawaii Institute of Geophysics, University of Hawaii, Honolulu, Hawaii. Contract AF19(604)-2292. May 1961.

Intensity fluctuations are generally measured by observing a point source of energy. Under these conditions the percentage modulation increases linearly with range.\* Under the worst conditions measured in the program at the University of Michigan, the extrapolated value for modulation would be about 1% at a range of 44 feet.

On the other hand, when looking at an extended source, such as the terrain, these effects are much smaller; in the case of stellar observations, for example, the planets appear to twinkle less than the stars. Also, the greater part of the fluctuations occur at frequencies below 100 cps. Hence if the modulation produced by the relative shift of the chopper and optical system is considerably above this, the effect of such intensity fluctuations is still further reduced.

The second atmospheric effect to be considered is image motion, or variations in the line of sight to a fixed target. The principal data available on this subject comes from astronomical measurements. Under conditions of very poor seeing it is observed that the motion of the image of a star is on the order of 10 seconds of arc (about 0.05 milliradian). This particular effect is due primarily to the lower layers of the atmosphere in which the telescope is immersed, and so possibly gives a good indication of the amount of image motion

\* Bellaire, F. R. and Ryznar, E. Scintillation and Visual Resolution Over the Ground. Institute of Science and Technology, The University of Michigan. Contract DA-36-039-SC-78801. September 1961.

experienced when looking horizontally; with the reservation, however, that the effects observed through a horizontal path near the surface of the terrain might be somewhat greater due to greater turbulence at the surface.

It does not appear that image motion will be a problem in the operation of the terrain sensor, for the following reasons. The path length in the lower atmosphere is very short compared with those for astronomical observations; this is expected to more than compensate for the effect of greater turbulence near the surface of the terrain. Image motion of 0.05 milliradian is less than the optical resolution of the system, and very much smaller than the field of view (which is about 5 milliradians by 20 milliradians) so motion of the image is expected to have no observable effect.

The third effect is that of image blur. Image blur is the enlargement of the image of a point target and can be distinguished from the relative motion of different parts of an image with respect to another; the latter does not affect the performance of an image plane location system.

Less applicable information is available on the amount of image blur to be expected than on image motion and scintillation, because most measurements and observations represent the time averaged effects of atmospheric turbulence on point targets, rather than the deterioration of

extended images when they are observed for a very short time.

The image blur might be taken to be due to the independent motion of various neighboring points of the image. Since as reported above image motion is expected to be less than 0.05 milliradian, blurring due to this effect would not apparently reduce the observable detail in the image.

Image blurring may be a low frequency phenomenon which is not observed when integration times are short. Atmospheric turbulence is not generally considered to degrade the resolution of photographs made with relatively short exposures. The terrain sensor has a resolution of about photographic quality and operates with chopping rates on the order of 1/1000 second or less and hence would be similarly unaffected.

Image blurring is commonly observed only with long optical paths. To gain a qualitative feeling for its effects at short ranges, objects were examined outdoors at ranges on the order of 50 feet with binoculars, which permitted fine detail in the objects to be studied. Lines of sight extended over asphalt, concrete and earth. At no time was any image blurring observed, and in particular, detail on the order of 1/16 inch (which corresponds to 0.1 milliradians at 50 feet) such as blades of grass, letters on boxes and so forth were clearly visible. Therefore it is felt that image blurring will not affect the performance of the terrain sensor system.

In summary, it may be said that because of the short ranges involved

and the resolution requirements on the optical system, no significant degradation in performance is anticipated as a result of atmospheric turbulence.

#### EFFECT OF CLIMATIC CONDITIONS

The effectiveness or accuracy of the terrain sensor will be reduced by various climatic conditions such as fog, haze, dust, rain, and snow. In general these factors have about as much effect on the terrain sensor as they do on human vision. That is, the terrain sensor makes use of the visible spectral region and is quite sensitive, and so it is not unduly affected by climatic conditions; on the other hand, the sensor is not able to see into or through such phenomena to any greater extent than can a human being. Incidentally, it may be assumed that the driver of the vehicle must see the terrain in order to operate the vehicle, and so it may be expected that the speed of the vehicle will have to be reduced anyway under conditions of reduced visibility, so the requirements on the terrain sensor may then be less severe.

Fog, haze, and dust have similar effects on optical instruments. Each of these consist of small particles of various sizes which scatter some of the light. Thus they reduce somewhat the amount of illumination falling on the object being observed, and they interrupt some of the light coming from the target to the observer. Such a scattering medium has no effect on the sharpness or resolution with which such an object is observed; it does, however, reduce the observed contrast of the object.

This effect increases with range, and at long ranges objects cannot be detected not because they have become blurred, but because their contrast with the background drops below the human (or instrumental) threshold.

The contrast of objects observed at range  $x$  is given by\*

$$C_x = C_0 e^{-\beta x}$$

where  $C_x$  is the contrast at range  $x$ ,  $C_0$  is the contrast in the absence of the scattering medium, and  $\beta$ , the scattering coefficient, depends on the nature of the medium.

For a given medium the visual range  $V_n$  is defined as the value of  $x$  which makes  $C_x/C_0 = 0.02$ , since the contrast threshold for normal human vision is about 2%. Hence

$$\begin{aligned} \exp[-\beta V_n] &= 0.02, \\ \beta &= 3.912/V_n, \text{ and} \end{aligned}$$

$$C_x = C_0 \exp \left[ -\frac{3.912x}{V_n} \right]$$

This expression allows the contrast reduction to be calculated as a function of range  $x$ , if the visual range  $V_n$  is known.

---

\* Handbook of Geophysics p 14-14

In the calculation of the performance of the terrain sensor in the previous section, it was shown that the noise-equivalent range increment at 44 feet was 0.016 inch for the system described. An actual system will not be designed to have this accuracy, since achieving this performance would require unnecessary refinement in design. This range accuracy calculation shows that the inherent noise in the ranging process will not normally affect the accuracy of the system. It will, however, become a factor when the calculated range accuracy approaches the system requirements of 2 inches. This expression just calculated, permits the determination of the visual range which exists when the latter condition occurs.

Inspection of the range equation shows that the factors of interest here can be summarized in the proportionality

$$\Delta x \sim \frac{1}{m\sqrt{I}},$$

where  $\Delta x$  is the range accuracy,  $m$  is the fractional modulation produced by the chopper, and  $I$  is the intensity of light falling on the object. It is clear that  $m$  is a linear function of the contrast  $C$ . Hence

$$\begin{aligned} \Delta x &= (\Delta x)_0 \frac{C}{C_x} \sqrt{\frac{I_0}{I}} \\ &= (\Delta x)_0 \sqrt{\frac{I_0}{I}} \exp\left[\frac{172}{V_n}\right], \end{aligned}$$

where  $C$  is the contrast in the object field in the absence of scattering,  $C_x$  is the contrast in the presence of scattering,  $(\Delta x)_0$  and  $\Delta x$  are the noise equivalent range increments in the absence and presence of scattering, and  $I$  and  $I_0$  are the intensities of illumination of the object field with and without the scattering medium;  $172 = 3.912 \times 44$ .

Suppose that  $\Delta x$  is to be 2 inches. If  $(\Delta x)_0 = 0.016$  inch, and  $I_0/I = 10$  (corresponding to a 10-fold reduction in available energy due to the presence of the scattering medium), then

$$V_n = 46.8 \text{ feet.}$$

Thus for the assumed conditions terrain contour measurements can be made when the visual range is only about 50 feet.

This suggests that under some conditions of bad visibility the terrain sensor may permit operation of a cross country vehicle at higher speed than otherwise would be possible, since it would serve as an obstacle warning device which could see as far as the vehicle driver, but would have a much shorter reaction time. For simple obstacle warning, less range accuracy would probably be satisfactory; lowering the requirement for range accuracy increases the effectiveness of such an obstacle warning system still further.

The discussion so far applies to fog, haze, and dust. The analysis

of the effects of rain and snow is more difficult because the particle size is much larger and simple attenuation relations may not apply exactly. However, it is believed that the above calculations give a fairly good representation of operation in rain and snow, and so it appears that the terrain sensor will be effective under most conditions.

Other problems remain, of course. For example, the window through which the terrain sensor looks must be kept fairly free of rain, snow, dust, or condensation. This has not been considered at this stage of the study.

Another problem which has not been studied in detail is the effect of climatic conditions on the determination of consistency. However, the following observations may be made. First, because scattering media cause only loss of contrast, the amount of detail in an image is unaffected by scatter, and so texture analysis is relatively unaffected by fog, haze, and dust. Also, fog and dust consist of particles of various sizes, but the largest particles are most effective in causing scattering, and the larger particles are typically greater than 1.0 micron in diameter. For particles of this size, scattering in the visible region is independent of spectral wave length, and so spectral analysis is expected to be relatively unaffected by fog and dust. Haze, on the other hand, consists of very small particles and scattering is a function of spectral wave length. (This is observed in the bluish cast haze gives to distant mountains.) However, the effect of haze at ranges of 40 or 50 feet is usually not too pronounced, and so this may not interfere with spectral analysis, either.

#### DAY OR NIGHT OPERATION

If a light source is not available on the vehicle, operation of the passive terrain sensor is limited to daytime hours. However, if a light source, which may be either an ordinary headlamp or a special narrow beam lamp is provided for night use, the sensor will operate both day and night. The passive sensor makes use of all the energy reflected from the terrain in its spectral region, and so during twilight hours a mixture of natural and artificial light may be used with no adverse effect on the ranging process. (Such an adverse effect would be expected if the natural light constituted an undesirable background to operation by artificial light.)

The mixture of light at twilight may affect consistency determination by spectral analysis, if different techniques or filters are used in natural and artificial light. One solution would be to filter the transmitted light to match the spectral characteristics of sunlight, although this solution introduces several problems. It reduces the energy available; this effect is not too serious, since much of the energy removed by filtering lies outside the spectral region in which the photomultiplier responds. Filtering a light source constitutes a problem because the filter must absorb rather large amounts of energy. Finally, if ordinary headlamps rather than special sources are used, this solution is not satisfactory, because special lamps would be required.

The alternatives to filtering the transmitted radiation are to filter the received energy and adjust the amount of filtering, or to make the response of the consistency sensor relatively independent of the nature

of the light source. The extent to which either of these can be done cannot be determined without further analysis of the technique of consistency determination.

#### RANGE LIMITATIONS

The terrain sensor design has been based on the concept of determining the contour of the terrain with a vertical accuracy of  $\pm 2$  inches, and a distance of 44 feet ahead of the vehicle, as noted in Monthly Progress Report No. 1.

Under normal conditions, the sensor is capable of measuring the range to the terrain a greater distance ahead of the vehicle. If the actual field of view of the sensor is held constant, range accuracy is proportional to  $x^3$ , and the percent accuracy is proportional to  $x^2$ . Thus the system previously considered has a theoretical 2-inch range accuracy at a range of  $(2/0.016)^{1/3} (44) = 220$  feet, and the original percentage range accuracy (0.38%) at 490 feet. If these range accuracies are not required, as for obstacle warning, or if the sensor is made larger, these ranges can be extended even further.

However, in extending the range of the terrain sensor certain problems arise.

1. In order to make use of an accurate determination of contour, it is necessary to know at what instant the vehicle will reach a certain point on the terrain. This requires very accurate velocity information: for example, to use information about

the location of an obstacle to an accuracy of 2 inches at 44 feet, the average velocity over the distance must be known to 0.38 percent. This accuracy requirement increases as the range to the obstacle increases.

2. If information is collected about the terrain a longer distance in front of the vehicle, the vehicle travels a greater distance after maneuvers before complete information is again available. Hence greater ranges increase information drop-out due to maneuvers.
3. Measuring the terrain contour accurately at greater ranges requires equipment of greater precision; it is thus more costly and perhaps less reliable.
4. Measuring the terrain contour at greater ranges with a device restricted to an optical line-of-sight increases the "shadow problem" - the fact that portions of this terrain such as depressions are concealed by obstacles in front of them. Assuming that the elevation of the sensor above the terrain is held constant, increasing the sensing range makes the line of sight more and more parallel to the surface, and more and more of the terrain will be found to be shadowed.
5. Increasing the range of the terrain sensor requires that under normal conditions the equipment is operating closer to the theoretical limit, and hence climatic and similar environmental effects would produce greater degradation in performance.

On the other hand, if only general information such as average roughness, is required about the terrain ahead of the vehicle a larger

( actual field of view can be used, and range accuracy requirements relaxed. For example, if only one percent range accuracy is adequate, the system studied previously has a maximum range of 14,520 feet.

## HUMAN FACTORS ENGINEERING

Because of the theoretical nature of the study performed under this contract and because of the preliminary nature of the design, which includes only an optical layout and a functional block diagram, human factors engineering is not applicable to this research and development work.

APPENDIX A  
DERIVATION OF EQUATIONS  
FOR ACTIVE C-W RANGER

Details of the active c-w ranging system described in the body of this report are revealed in the following equations.

A-1 Synchronous Detection

Suppose the input to the synchronous detector is:

$$I = D \sin(\Omega t - \alpha) + N \sin(\Omega + \sigma)t,$$

where D is the amplitude of the signal, and N represents a spurious signal (noise) at a slightly different frequency. If this is multiplied by the signal reference  $\sin(\Omega t - \beta)$  where  $\beta$  is a controllable phase shift, the output is:

$$O = \frac{D}{2} [\cos(\alpha - \beta) - \cos(2\Omega t - \alpha - \beta)] + \frac{N}{2} [\cos(\sigma t + \beta) - \cos\{(2\Omega + \sigma)t - \beta\}]$$

After low-pass filtering, the output is:

$$O = \frac{1}{2} [D \cos(\alpha - \beta) + N \cos(\sigma t + \beta)]$$

If

$$Q(\alpha - \beta) = \left( \frac{\text{DC Level}}{\text{rms Noise}} \right)_{\text{output}}$$

$$Z = \left( \frac{\text{Peak-to-Peak Signal}}{\text{rms Noise}} \right)_{\text{input}}$$

then from the first and last expressions above it can be seen that for the special case described above,

$$Q(\alpha - \beta) = \frac{1}{2} Z \cos(\alpha - \beta)$$

and that if the noise is a random signal,

$$Q(\alpha - \beta) = \frac{1}{2\sqrt{2}} Z \cos(\alpha - \beta)$$

if  $Q$  and  $Z$  are measured in the same bandwidth. (The extra factor of  $1/\sqrt{2}$  appears because noise on both sides of the carrier frequency appears in the output.)

Since a signal-to-noise ratio change of 1 results from a signal change equal to noise, the noise equivalent change in  $\alpha$ ,  $\Delta\alpha$ , is given by

$$\Delta\alpha \left| \frac{dQ}{d\alpha} \right| = 1$$

or

$$\Delta\alpha = \left| \frac{2\sqrt{2}}{Z \sin(\alpha - \beta)} \right|$$

The value of  $\Delta\alpha$  has a minimum at  $(\alpha - \beta) = -\frac{\pi}{2}$ ; at this point  $\Delta\alpha = 2\sqrt{2}/Z$ , and the DC output level is zero. This is applied to the ranging system in the following way: let the transmitted signal be  $\sin(\Omega t)$  and the received signal from a target at range  $R$  be  $B \sin(\Omega t - \alpha)$ . It can be seen that  $\alpha = 2R/c$ , where  $c$  is the velocity of light. The received signal

is multiplied by  $\sin(\Omega t - \beta)$ , and  $\beta$  is increased from  $\pi/2$  until the measured DC output is zero. This value of  $\beta$  allows  $\alpha$  and therefore R to be determined. For an unambiguous indication,  $0 < \alpha < \pi$ , because zero output can also be obtained for  $\alpha - \beta = +\frac{\pi}{2}$ . Hence,  $R_{\max} = \frac{\pi c}{2\Omega}$ . Also  $R = \frac{\alpha}{\pi} R_{\max}$ , so  $\Delta R = \frac{\Delta\alpha}{\pi} R_{\max}$ , where  $\Delta R$  is the noise equivalent range change.

Therefore,

$$\Delta R = \frac{2\sqrt{2} R_{\max}}{\pi \epsilon}$$

This is the basic equation for calculating performance.

#### A-2 Maximum Possible Chopping Frequency

Since  $R_{\max} = \pi c / 2\Omega$ , where c is the velocity of light and  $\Omega$  is the radian chopping frequency, the maximum frequency (cycles/second) is

$$f_{\max} = \frac{c}{4R_{\max}}$$

#### A-3 Energy Returned From Target Area

Here and generally throughout these calculations, all measurements of power are made in the spectral region in which the multiplier phototube responds (about 0.35 to 0.55 microns for an S-11 response). These limits are approximate and in practice vary from tube to tube. If W watts/cm<sup>2</sup> - ster are radiated,  $WA_c \omega$  watts strike the target within the field of view of the receiver. Then  $\rho WA_c W / \pi$  watts/steradian are reflected (assuming that the target is normal to the line of sight and radiates according to the cosine law), and so

$$E_t = \frac{WA_t A_r \rho W \epsilon}{\pi R^2}$$

## APPENDIX B

### THE MULTIPLIER PHOTOTUBE

#### INTRODUCTION

The most sensitive detector that is available for use in measuring radiation in or near the visible region is the multiplier phototube. Its high sensitivity and fast response time make it ideal for the measurement of reflected sunlight in a passive ranging determination. For an active system using a lamp with a color temperature at about 3000°K, the multiplier phototube is an ideal detector. This discussion of the multiplier phototube for use in the range measuring device does not preclude the use of other detectors such as the silicon photovoltaic detector, which is sensitive out to about 1.0 micron, or the lead sulfide detector, sensitive out to about 2.5 microns. The examination of the measurement of consistency by spectral analysis discusses the use of the spectral region from about 0.4 to 0.8 microns. A multiplier phototube with S-20 spectral response is especially suitable for such a wide region.

#### MULTIPLIER PHOTOTUBE SENSITIVITY

The ordinary method of defining sensitivity of a radiation detector is the use of the spectral noise equivalent power. The noise equivalent power,  $P$ , is the power in watts required on the detector to produce a signal equivalent to the noise produced at the output of the detector. Since the signal from the multiplier phototube is also a function of the wavelength of the incident radiation, for exactness the value of  $P$  should be specified at each wavelength. Actually,  $P$  is usually determined at the peak wavelength response of the particular detector; this value in watts is assumed to apply over the

equivalent spectral bandwidth of the detector. For example, a bandwidth between 0.35 and 0.55 micron for the S-11 multiplier phototube is accepted.

Two difficulties arise in the specification of the value of  $P$  (or  $P_{\lambda}$ ) for a particular multiplier phototube. One is that the noise level at the output of the multiplier phototube is not constant, and is a function of the illumination striking the detector. Also, the multiplier phototube has an inherent "dark" noise; this contribution to the noise is negligible at high levels of illumination. The other difficulty is that most multiplier phototubes are specified in terms of their response to energy expressed in lumens. The energy specified in lumens refers only to that energy present in the visible region. (The visible portion of the spectrum is usually defined specifically in terms of the "Standard Observer" response, which peaks at 0.556 micron and extends from about 0.40 to 0.70 microns.) For a multiplier phototube whose spectral response differs from that of the Standard Observer and whose response to a certain number of lumens is given, it is also necessary to specify the color temperature of the radiation source used in defining this response.

Fluctuations in the output current of the multiplier phototube occur because the output current is due to the independent random ejection of electrons from the cathode. These events result from the input signal and from the spontaneous emission which exists even with no incident signal (dark current). If the total average incident energy is  $E$ , the resulting average anode current is  $i + SE$ , where  $i$  is the multiplier phototube dark current (amperes) and  $S$  is the multiplier phototube responsivity

(amp/watt). The above expression, divided by the multiplier phototube gain,  $G$ , is the cathode current in coulombs per sec. Dividing by the charge on the electron,  $e$ , in coulombs yields the number of events occurring per second at the cathode, which is

$$\frac{i + SE}{eG}$$

The rms variation in this number is

$$\left[ \frac{i + SE}{eG} \right]^{1/2} \text{sec}^{-1/2},$$

assuming that these events are randomly produced and independent.

If the fluctuations are measured in a one-cycle bandwidth, the number of watts incident on the cathode required to produce the above equivalent variation is

$$\begin{aligned} P &= \sqrt{2} \left[ \frac{Ge}{S} \right] \left[ \frac{i + SE}{eG} \right]^{1/2} \\ &= \left[ \frac{2Ge}{S} \left( \frac{i}{S} + E \right) \right]^{1/2} \end{aligned}$$

(B-1)

The quantity  $\sqrt{2}$  is the bandwidth in  $\text{sec}^{-1/2}$  required for a measurement over a period of one-half-cycle - the minimum measurement necessary to

determine the electrical waveform.  $G/S$  is the reciprocal of the responsivity or the number of watts necessary at the cathode to produce one ampere at the anode.

The quantity  $E$ , the total average incident energy, depends upon what is being measured and the environment. In an active system,  $E$  is equal to  $0.625 E_t + E_b$ . Here,  $E_t$  is the target energy, and the factor of 0.625 results because  $E_t$  is modulated.  $E_b$  is the power collected from the ambient unmodulated energy incident on the target, and may be appreciable in an active system during certain daytime conditions of illumination, but is negligible at night. In a passive system,  $E$  is equal to  $E_b$ .

This relationship is expressed in the above form since the quantities  $i$ ,  $G$ , and  $S$ , (or  $S/G$ ) are most usually given in specifications for multiplier phototubes.

Multiplier phototubes differ in their spectral response, and in their values of sensitivity and dark current. Two types are considered here for the purpose of calculation. These are the types using a photocathode material of cesium-antimony, which is usually designated as type S-11, and which covers the spectral region from 0.35 to 0.55 microns; the other type is the S-20, with a tri-alkali cathode such as Sb-K-Na-Cs, and includes the spectral region from about 0.32 to 0.62 microns; the response extends at a lower level to 0.8 microns. Either type would be almost ideal for measuring sun-reflected energy. In an active system, with the effective target source at about  $3000^{\circ}\text{K}$ , either of these two types would be quite suitable.

Values of  $i$ , the dark current, may vary from 0.1 to 0.0003 microampere, depending upon the application. A value equal to 0.001  $\mu$ a is considered here as being easily achievable for both the S-11 and S-20 types. This value corresponds to a cathode diameter between one and two inches. (It should be remembered that in the final design of a system, there is not complete freedom in choosing the size of the cathode. The focal length and field stop may have to be tailored somewhat to fit the standard photocathode supplied by the manufacturer. This will present no problem, however.)

The multiplier phototube gain,  $G$ , is a function of the anode-supply voltage, and may assume values between about  $10^5$  to  $10^7$  for most tubes. A value of  $10^6$  may be considered typical for both the S-11 and S-20 types.

The remaining quantity necessary to solve for the equivalent noise input in watts in the sensitivity  $S$  in amperes per watt. Most manufacturers quote data in terms of the quantity  $S/G$ , the photocathode sensitivity in units of amperes per lumen. Values of  $S/G$  for the S-20 type are approximately twice those of the S-11 type. A value of 70  $\mu$ a per lumen is considered typical for the S-11, and 140  $\mu$ a per lumen for the S-20. These values are referenced to a source with a color temperature of 2870°K.

In order to find the number of effective watts in the spectral region of either the S-11 or S-20, corresponding to the measured number of lumens from the 2870 K source, the following considerations are essential.

At the peak of the Standard Observer curve (0.556  $\mu$ ), 0.00147 watt

corresponds to one lumen. This is the mechanical equivalent of light\*. The total effective watts in the visible region from a source at a color temperature T corresponding to one lumen is .00147 watt. The total effective watts, from this source, in the spectral region of the multiplier phototube is .00147 multiplied by the ratio of the fractional energy in the spectral region of the phototube divided by the fractional energy in the visible or Standard Observer region, both from a blackbody at temperature T. This relationship is expressed as

$$0.00147 \left\{ \frac{\int_0^{\infty} W_{\lambda}(T) S_{\lambda} d\lambda}{\int_0^{\infty} W_{\lambda}(T) d\lambda} \right\} \left\{ \frac{\int_0^{\infty} W_{\lambda}(T) K_{\lambda} d\lambda}{\int_0^{\infty} W_{\lambda}(T) d\lambda} \right\}^{-1},$$

where  $S_{\lambda}$  and  $K_{\lambda}$  are the relative responses of the phototube and Standard Observer, respectively, normalized to unity at the peak.  $W_{\lambda}(T)$  is the ordinate of the Planck blackbody function at wavelength  $\lambda$ , corresponding to the temperature T.

Figure 44 gives the values of

$$\eta(R_{\lambda}, T) = \frac{\int_0^{\infty} W_{\lambda}(T) R_{\lambda} d\lambda}{\int_0^{\infty} W_{\lambda}(T) d\lambda}$$

\* Smithsonian Physical Tables, Ninth Revised Edition, Smithsonian Institution, 1954, Page 94, Table 73.

KOE SEMI-LOGARITHMIC 359-73  
 HELPFUL EDSER CO. MADE IN U.S.A.  
 3 CYCLES X 140 DIVISIONS

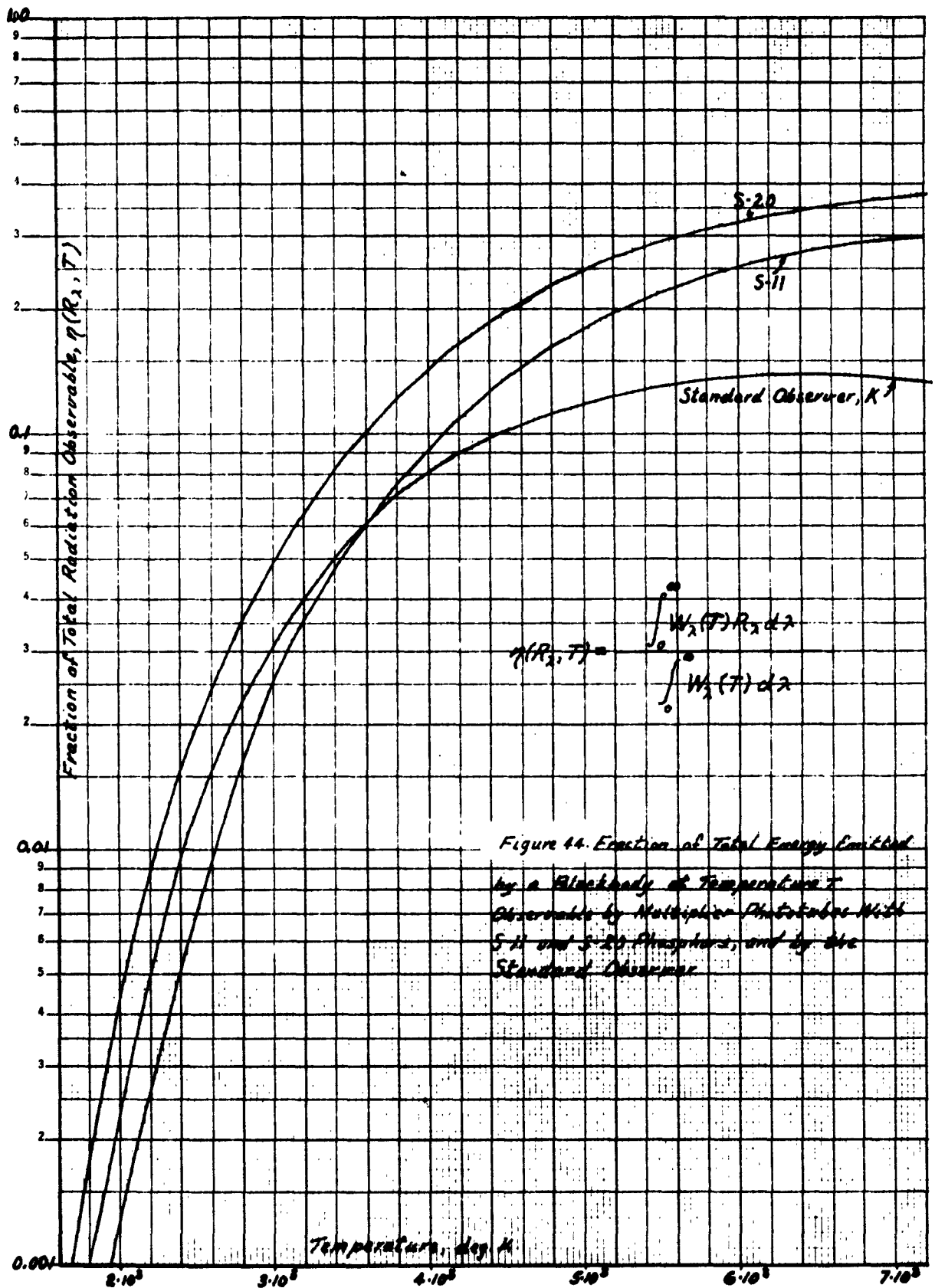


Figure 14. Fraction of Total Energy Emitted by a Blackbody at Temperature T Observable by Multiplier Phototubes With S-11 and S-20 Phosphors, and by the Standard Observer

versus the blackbody temperature, T, in degrees Kelvin, where  $R_{\lambda}$  represents the relative response. These curves were obtained using numerical integration and represent the multiplier phototubes with S-11 and S-20 responses, and the Standard Observer. Figure 45 shows their relative responses.

From figure 44, when T is 2870°K, the conversion factor from lumens to watts becomes

$$.00147 (.0400) (.0249)^{-1} = .00236 \text{ watts/lumens}$$

for the S-20; and

$$.00147 (.0193) (.0249)^{-1} = .00113 \text{ watts/lumens}$$

for the S-11.

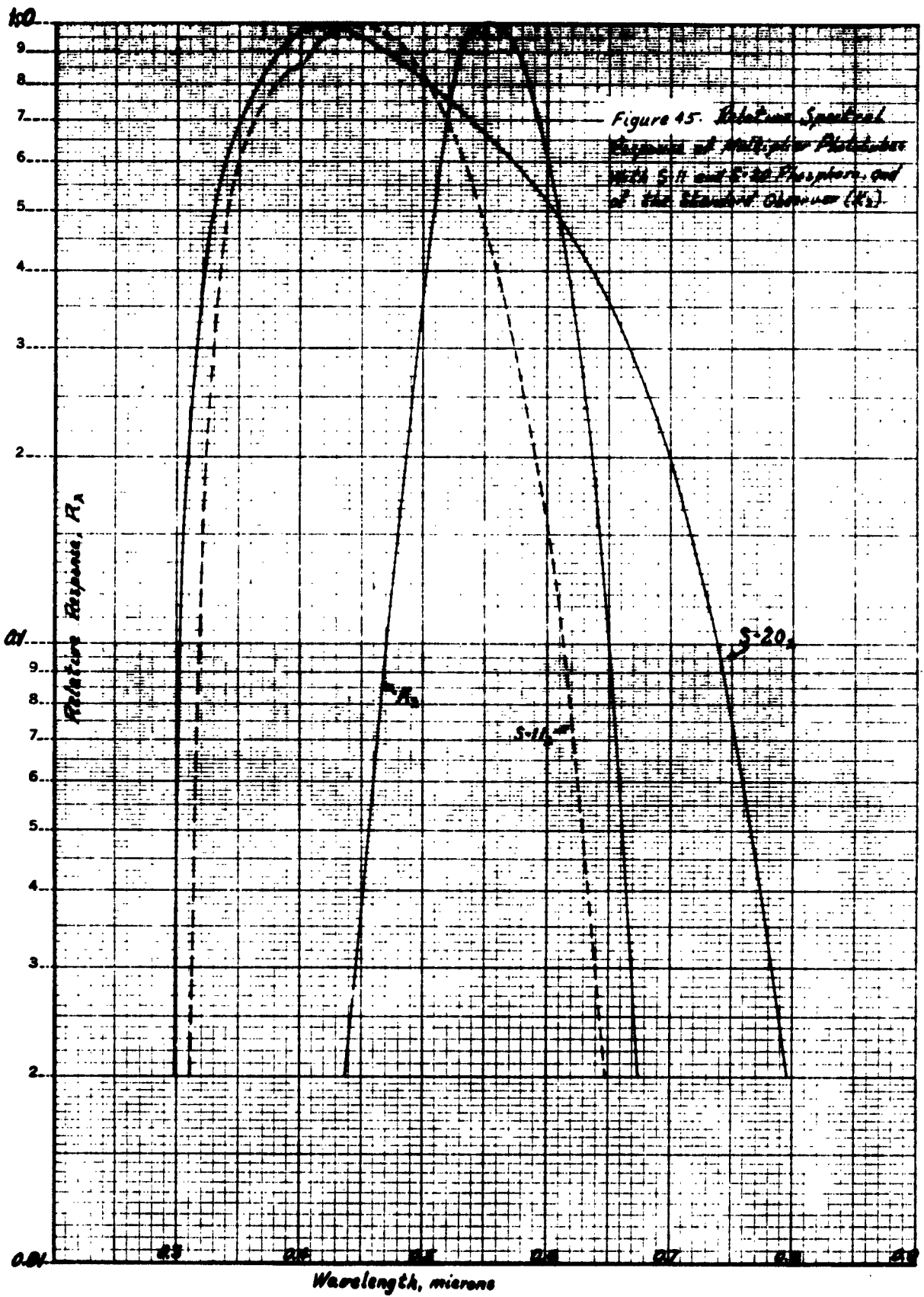
Using the above conversion factors and the values for i, G, and S given before for the S-20 and S-11, the following table results:

( $e = 1.6 \times 10^{-19}$  coulombs)

Type	i ( $\mu a$ )	G	S/G ( $\mu a/l$ )	S/G (s/w)	P(watts)(Eqn.B-1)
S-20	.001	$10^6$	140	.059	} $[5.3 \times 10^{-18} (1.6 \times 10^{-14+E})]^{\frac{1}{2}}$
S-11	.001	$10^6$	70	.062	

\* Since the values of S/G in  $\mu a$  per watt are essentially equivalent, the above value of P is taken for both types S-20 and S-11.

ALBARENE NO 1962 1-1-57  
1074



The determination of  $P$ , the noise equivalent power in watts, in the spectral region of the detector can now be made as a function of  $E$ , the average incident energy in this spectral band.

#### AN EXAMPLE

The following is an example of the usefulness of the equations and relationship depicted in figure 44. Consider a passive system receiving energy from the terrain illuminated by the sun and scattered sunlight from the sky. Figure 45<sup>(1)</sup> is a plot of the total illumination on the horizontal plane of the earth due to both direct sunlight and sky light versus solar altitude.

At a solar altitude of 45 degrees, the illumination is 7300 foot candles. This corresponds to  $7300/30.48^2 = 7.86$  lumens/cm<sup>2</sup>. If  $\rho Y$  represents the power in the reflected sunlight, and  $\rho$  is the reflectivity, the power on an S-20 detector using a collector of area,  $A_c$ , and an optical system with a solid angular field of view,  $\omega$  is

$$E = \rho Y \omega A_c (0.00147) [\eta(S-20, 5900^\circ K)] [\eta(K_2, 5900^\circ K)]^{-1}$$

The last two terms above are used to convert the reflected power from units of lumens to effective watts in the S-20 spectral bandwidth. These are

1. Handbook of Geophysics, pp.14-13, Revised Edition, The MacMillan Co. New York, 1961.

K&E SEMI-LOGARITHMIC 350-73  
ADAPTATION FOR THE U.S. NAVY  
1 INCHES BY 140 DIVISIONS

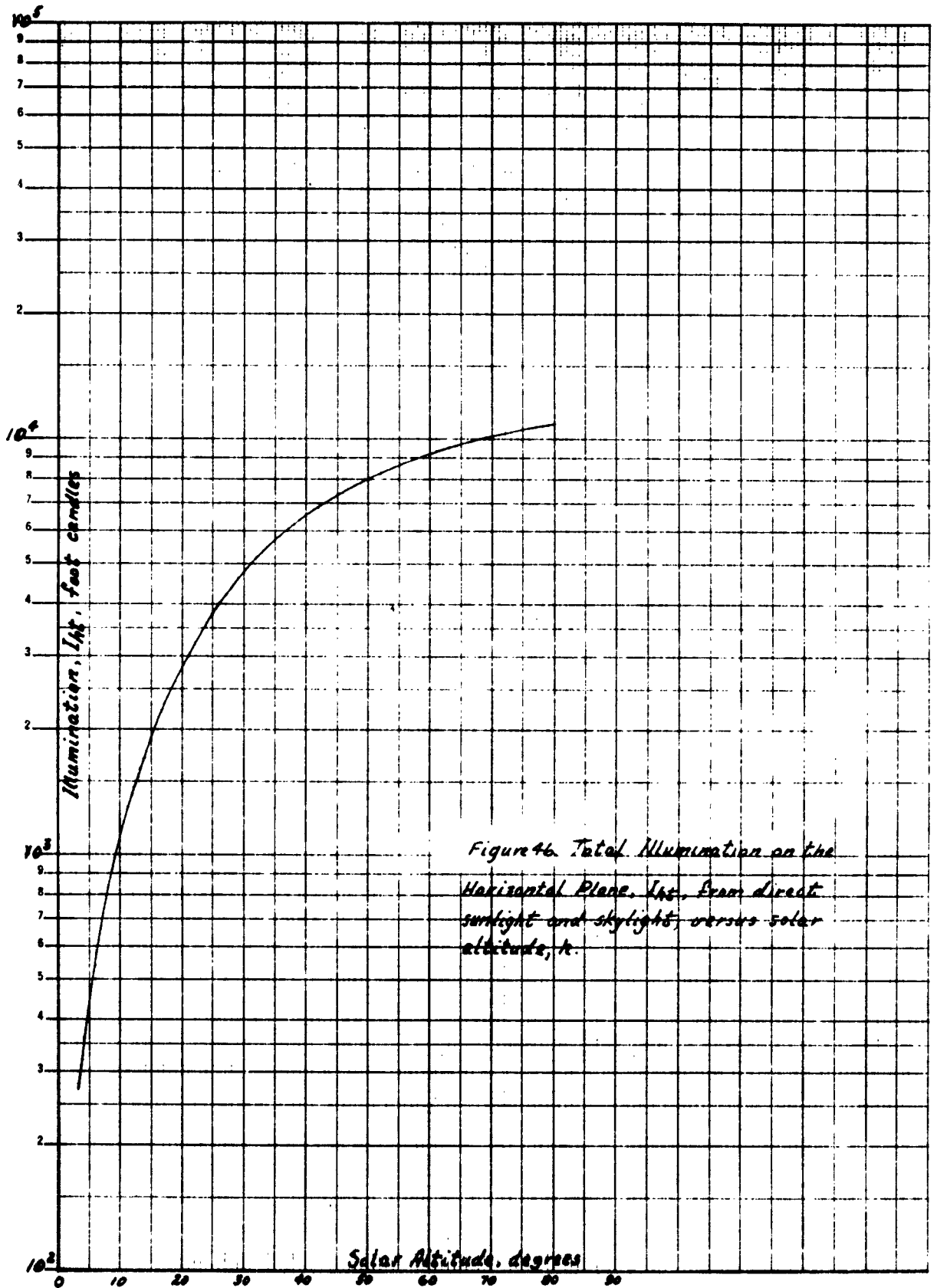


Figure 46. Total Illumination on the Horizontal Plane, *I<sub>h</sub>*, from direct sunlight and skylight, versus solar altitude, *h*.

found using figure 44, where T equals 5900°K. The above relationship becomes

$$E = \rho \frac{7.86}{\pi} \omega A_c (0.00147)(0.316)(0.137)^{-1} = 8.4 \times 10^{-3} \rho \omega A_c \text{ watts}$$

where the use of  $\pi$  assumes that the reflected energy is scattered according to the cosine law. Making the following further assumptions:

$$\rho = 0.2$$

$$\omega = 1.6 \times 10^{-5} \text{ steradian}$$

$$A_c = 200 \text{ cm}^2$$

$$E = 8.4 \times 10^{-3} \times 0.2 \times 1.6 \times 10^{-5} \times 200 = 5.3 \times 10^{-6} \text{ watt}$$

The quantity P, the noise equivalent power of the S-20 multiplier phototube, is (from the table given earlier)

$$P = \left[ 5.3 \times 10^{-18} (1.6 \times 10^{-14} + \frac{5.3 \times 10^{-6}}{2}) \right]^{1/2} = 3.7 \times 10^{-12} \text{ watt}$$

E in the above equation must be divided by 2 if the energy is chopped.

APPENDIX C  
EXPERIMENTAL DATA ON RANGEFINDING  
BY IMAGE-PLANE LOCATION

INTRODUCTION

A general description of the passive rangefinding technique adopted in the preliminary design was given in the section on Optical Ranging Methods. The discussion includes a theoretical development of the equations which relate the expected signal-to-noise ratio and the signal amplitude-focal position curve to the noise-equivalent range increment for systems of this type.

To verify these theoretical calculations, experiments have been performed in the laboratory using currently available equipment. This section provides a description of the experimental procedure, and an analysis of the data obtained. The results are in good agreement with theory, giving a further degree of confidence that the suggested approach can be applied to an effective terrain sensor for cross-country vehicles.

EXPERIMENTAL PROCEDURE--FIRST SERIES

The basic elements in the experimental setup are as follows:

1. A patterned target simulating the terrain to be sensed established at a known, fixed range.
2. An optical system to form an image of the target.
3. A chopper to modulate the radiant energy collected by the

optical system.

4. A detector (multiplier phototube) to form an electrical signal from this modulated radiant energy.
5. Electronics to process the electrical signals obtained from the detector.

The experimental procedure consisted of finding the variations in electrical output that resulted from changing the focus of the optical system. These variations are caused by the fact that the efficiency of chopping is a function of how well the target is imaged on the chopper. Further details on the experimental setup are given below.

#### Target

For simplicity, a high contrast target consisting of a 3-inch-wide black stripe on a white background was used. It was placed 18.3 feet from the objective lens of the optical system, and was illuminated by an ordinary household fluorescent lamp. The lamp was close to the target, but outside of the field of view of the optical system. The experiment was conducted in a darkroom laboratory, with no source of illumination other than the fluorescent lamp.

#### Optical System

The optical system consisted of an objective lens, a field stop,

and a relay lens. The objective was a good-quality photographic lens with 2 inch aperture, 90 mm focal length, and a minimum focal ratio of  $f/1.8$ . A circular field stop, 0.125 inch in diameter, was placed at the focus of the objective. The relay lens, a 15-mm-diameter triplet with 1-inch focal length, was placed 2 inches behind the field stop and 2 inches ahead of the chopper. The target image and field stop were thus made coincident on the chopper disk at unity magnification.

#### Chopper

The chopper was a disk of clear plastic approximately 5 inches in diameter, with 180 equally spaced radial spokes of constant width (1/64 inch). The portion of the disk centered 2 inches from the axis of rotation was used for chopping; in this region, the clear spaces are approximately 3-1/2 times the width of the opaque spokes. The disk was driven at 3600 rpm, to yield a chopping frequency of 10.8 kc.

#### Detector

The detector was an RCA Type 931-A multiplier phototube operated at 750 volts. It was positioned immediately behind the chopper disk to receive the modulated radiation.

#### Electronics

The output of the multiplier phototube was connected to a Spencer-Kennedy Laboratories Model 308-A Variable Electronic Filter. This is a two-section filter, and was operated as a bandpass filter with each high and low pass section set at 10 keps. The cutoff characteristics of the filters follow a 20 db per octave slope. The equivalent square bandpass of this filter combination is about 4.5 keps.

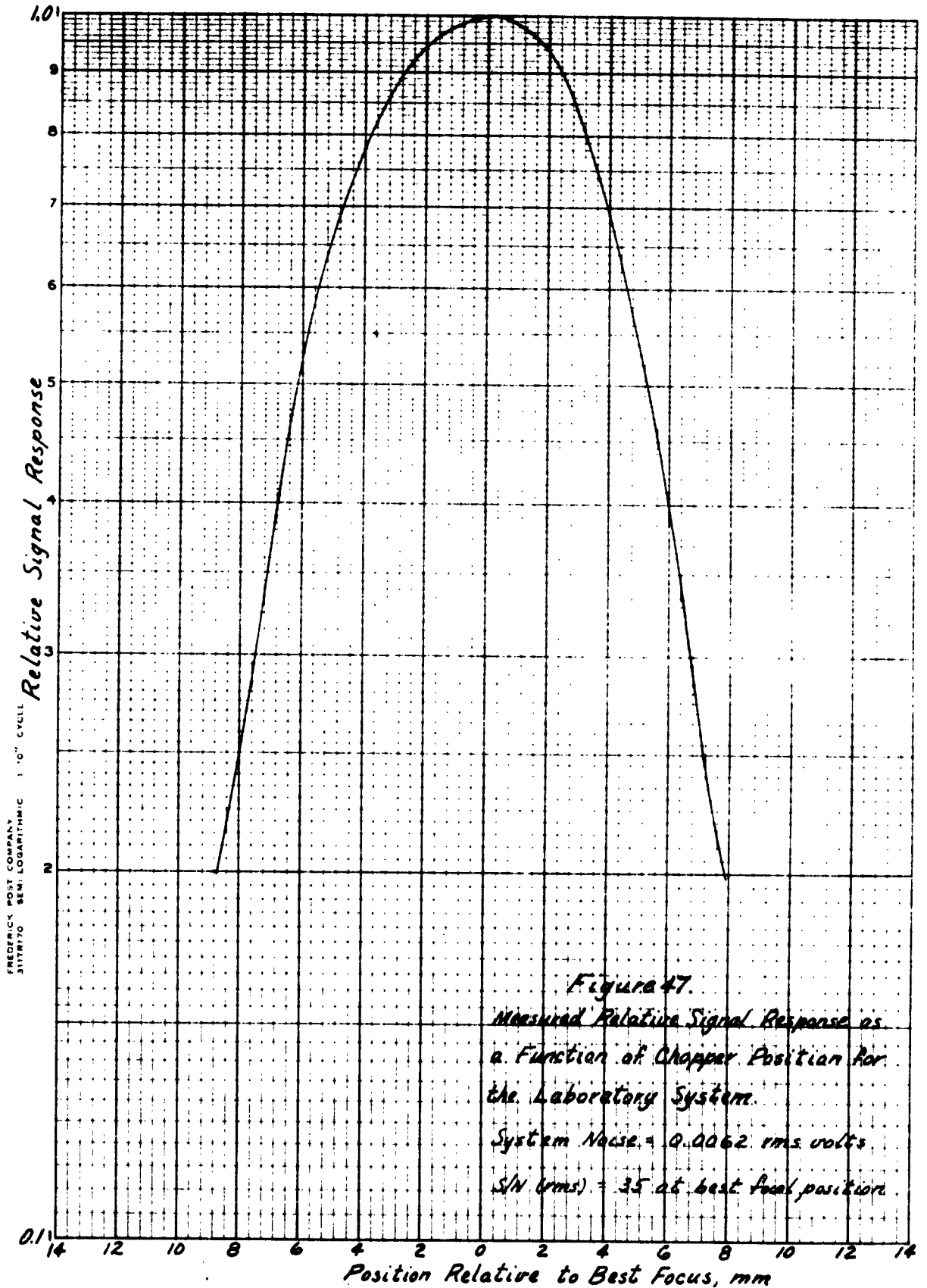
The output of the filter was connected to a Ballantine Laboratories, Inc. Model 300 Electronic Voltmeter, which was used to read the output voltage of the system.

#### MEASUREMENT PROCEDURE

As the first step in the experimental procedure, the system noise was determined. Since the experimental setup was not completely shielded from extraneous illumination, it was necessary to measure the system noise indirectly. (The only source of illumination in the room was the lamp used to illuminate the target, but a portion of its output was reflected into the multiplier phototube by stray paths which bypassed the primary optics.) The chopper was turned off, and the rms noise was measured. The entrance aperture of the objective lens was then shielded and the noise was measured. The rms system noise was then assumed to be the square root of the difference between the squares of these two measured noises.

Following the noise measurement, the chopper was turned on and the rms output signal was recorded. The objective lens was then moved along the optical axis in 1-millimeter steps and the resultant rms signal voltages were measured, resulting in the curve of Figure 47. A signal-to-noise ratio of 35 was obtained at the position of best focus.

Two characteristics of the curve are worth noting. One is the large peak at the position of best focus, and the other is the shape of the fall-off in signal as the image that is chopped becomes degraded.



### THEORETICAL CALCULATION OF S/N

Using the equations given in the section on the analysis of ranging by image plane location and Appendix B, the signal-to-noise ratio for a system of this type can be shown to be

$$S/N = m \left( \frac{\rho I \omega A_c}{\pi B K T} \right).$$

The factors involved in this equation are as follows:

$m$  - the r.m.s. fractional modulation of the field. In the experimental setup, the total field is  $(1/4)(\pi)(1/8 \text{ inch})^2$  and the approximate area of a spoke on the chopper within the field is  $1/64 \text{ inch} \times 1/8 \text{ inch}$ . Hence the fractional area modulated is  $1/2\pi$ . The estimated values of the reflectivity of the black and white portions of the target are 0.1 and 0.9, respectively. The average reflectivity of the portion of the target in the field of view is 0.5, and so the r.m.s. fractional modulation is

$$m = \frac{1}{2\sqrt{2}} \cdot \frac{1}{2\pi} \cdot \frac{0.8}{0.5} = 0.09.$$

$A_c$  - the area of the collecting optics. The entrance aperture is actually  $20 \text{ cm}^2$  (5 cm diameter); however, the diameter of the 15 mm relay lens is the aperture stop of the complete system. This 15 mm lens diameter, reflected back to the entrance aperture, corresponds to an aperture diameter of 26.6 mm, giving a value of  $A$  of  $5.5 \text{ cm}^2$ .

$\omega$  - the solid angular field of view as determined by the 1/8-inch

diameter field stop and 9-cm focal length:

$$\omega = \frac{\pi}{4} \times \left( \frac{.125 \times 2.54}{9} \right)^2 = 1.0 \times 10^{-3} \text{ steradian.}$$

$\frac{\rho I}{\pi}$  - the radiance reflected from the target, in watts/cm<sup>2</sup>-ster, in the spectral region of the detector. I is the illumination on the target. The value of  $\rho I/\pi$  was found to be 10 lumens/ft<sup>2</sup>-ster for the white portion of the target, as measured by a commercial light meter. It is difficult to determine the exact conversion factor between lumens and watts in this case, since specific data was not available on the spectral emission of the fluorescent lamp used. The generalized data available\* indicates that the total effective watts from the lamp in the visible region is approximately equivalent to the amount in the region within which an S-4 photocathode is sensitive. Thus for the white portions of the target, which occupied about half the total field,  $\rho I/\pi$  is approximately

$$10 \times \frac{.00147}{929} = 1.6 \times 10^{-5} \text{ watt/cm}^2\text{-ster.}$$

(The factor .00147 used above is the conversion factor from lumens to watts for the visible region - as discussed in Appendix B. The factor 929 is the conversion factor from ft<sup>2</sup> to cm<sup>2</sup>.) Hence the average value over the field is given by

\* Table 96, page 107, Smithsonian Physical Table, Ninth Edition, Published by the Smithsonian Institute, 1959.

$$\frac{\rho I}{\pi} = 1/2(1 + \frac{0.1}{0.9}) 1.6 \times 10^{-5} = 8.9 \times 10^{-6} \text{ watts/cm}^2\text{-ster}$$

B - the electrical bandwidth (4.5 kcps).

K - The coefficient that specifies the sensitivity of the multiplier phototube as expressed in the relationship for the noise equivalent power,  $P = (KE)^{1/2}$ , where E is the power on the detector from the target. This equation assumes that the dark noise contribution is negligible. This expression, as well as values of K for the S-11 and S-20 types of photocathodes, is developed fully in Appendix B. For the 931-A multiplier phototube, at a supply voltage of 750 volts, the following manufacturer's quoted values were used:

Cathode Radiant Sensitivity (S/G) = 30  $\mu$  amp/lumen.

Current Amplification (G) =  $1.1 \times 10^5$ .

The following values are also required:

$$\left. \begin{aligned} \eta(S-\lambda, 2870^\circ) &= .0170 \\ \eta(K-\lambda, 2870^\circ) &= .0249 \end{aligned} \right\} \text{Derived by the method of Appendix B.}$$

Thus

$$S/G = 30 \times 10^{-6} / (.00147) \times (.0170) \times (.0249)^{-1} = .030 \text{ amp/watt.}$$

Now

$$K = 2G_e/S = \frac{2 \times 1.6 \times 10^{-19}}{.030} = 10.7 \times 10^{-18} \text{ watt.}$$

t - the average transmission of the chopper; in this case it is about

$$t = 1 - \frac{1}{2} = 0.84$$

The calculated r.m.s. signal-to-noise ratio for the conditions of the experiment is therefore

$$S/N = 0.09 \left( \frac{5.5 \times 10^{-3} \times 8.9 \times 10^{-6}}{4.5 \times 10^3 \times 10.7 \times 10^{-18} \times 0.84} \right)^{1/2} = 99$$

This is a factor of 2.8 greater than the measured value of 35.

#### THE SIGNAL AMPLITUDE CURVE

Another factor which determines the accuracy with which the image plane can be located is the rate at which the detector output falls off as the chopper moves out of the plane of best focus. The expected shape of this curve can be calculated from the formula given previously. The shape of the curve,  $Q(\Delta)$  is given by

$$Q(\Delta) = 2\sqrt{2} mE \frac{J_1(y)}{y}$$

where

$$y = \pi k \sqrt{\theta^2 + \frac{(\Delta D)^2}{f^2}}$$

and  $m$  and  $E$  are constant,

$\theta$  is the optical blur,  
K is the spatial chopping frequency,  
 $\Delta$  is the displacement along the axis,  
D is the diameter of the optical system,  
f is the focal length of the optical system.

For the laboratory system,  $\theta$  can be neglected, and

K = 50 cycles - radian<sup>-1</sup>  
D = 26.5 mm  
f = 90 mm.

The resulting normalized curve is shown in Figure 48. The calculated width at the 3 db points is about 6.3 mm.

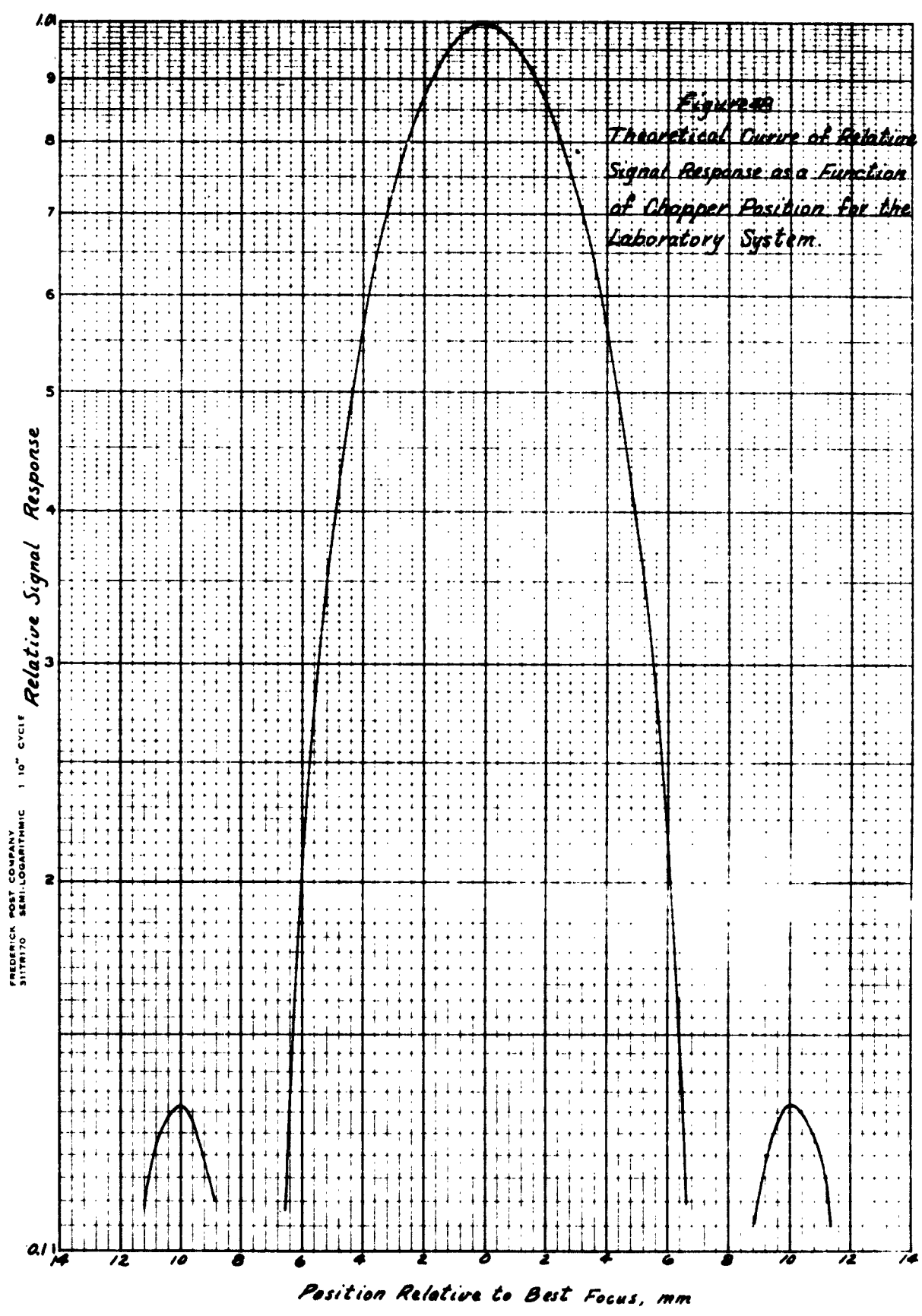
Since the experimental width is somewhat wider than this, additional experiments were performed to study the affect of various optical parameters on the shape of the curve.

#### EXPERIMENTAL PROCEDURE-SECOND SERIES

Essentially the same experimental equipment was used as before. The following additional equipment was used.

##### Target

In addition to the high-contrast target of a 3-inch-wide black stripe on a white background, a new target was used having a checkerboard pattern. This consisted of 1.5-inch-wide horizontal and vertical stripes of black tape on a white background with spacing between the stripes of 1.5 inches. This resulted in a pattern of white squares and black



FREDERICK POST COMPANY  
 3117B170 SEMI-LOGARITHMIC 1 10<sup>4</sup> CYCLE

Position Relative to Best Focus, mm

squares in a ratio of 1 to 2. Essentially, this pattern represented a more detailed target than the one used previously.

### Chopper

In addition to a spoke chopper, another chopper with a pattern composed of randomly spaced black dots of approximately 1/40 inch in diameter, was used. The average spacing between dots was between one and two dot diameters.

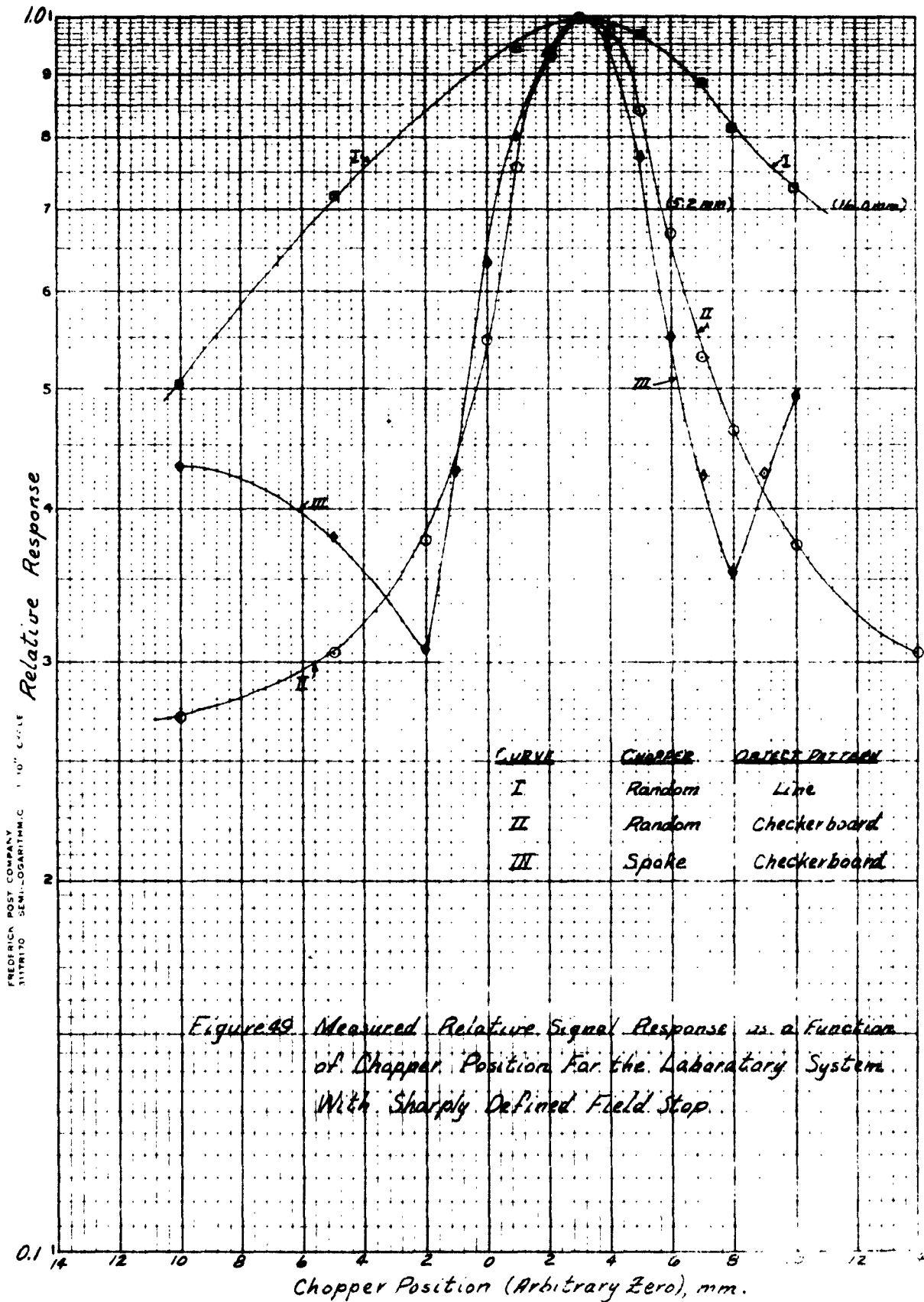
### Measurement Procedure

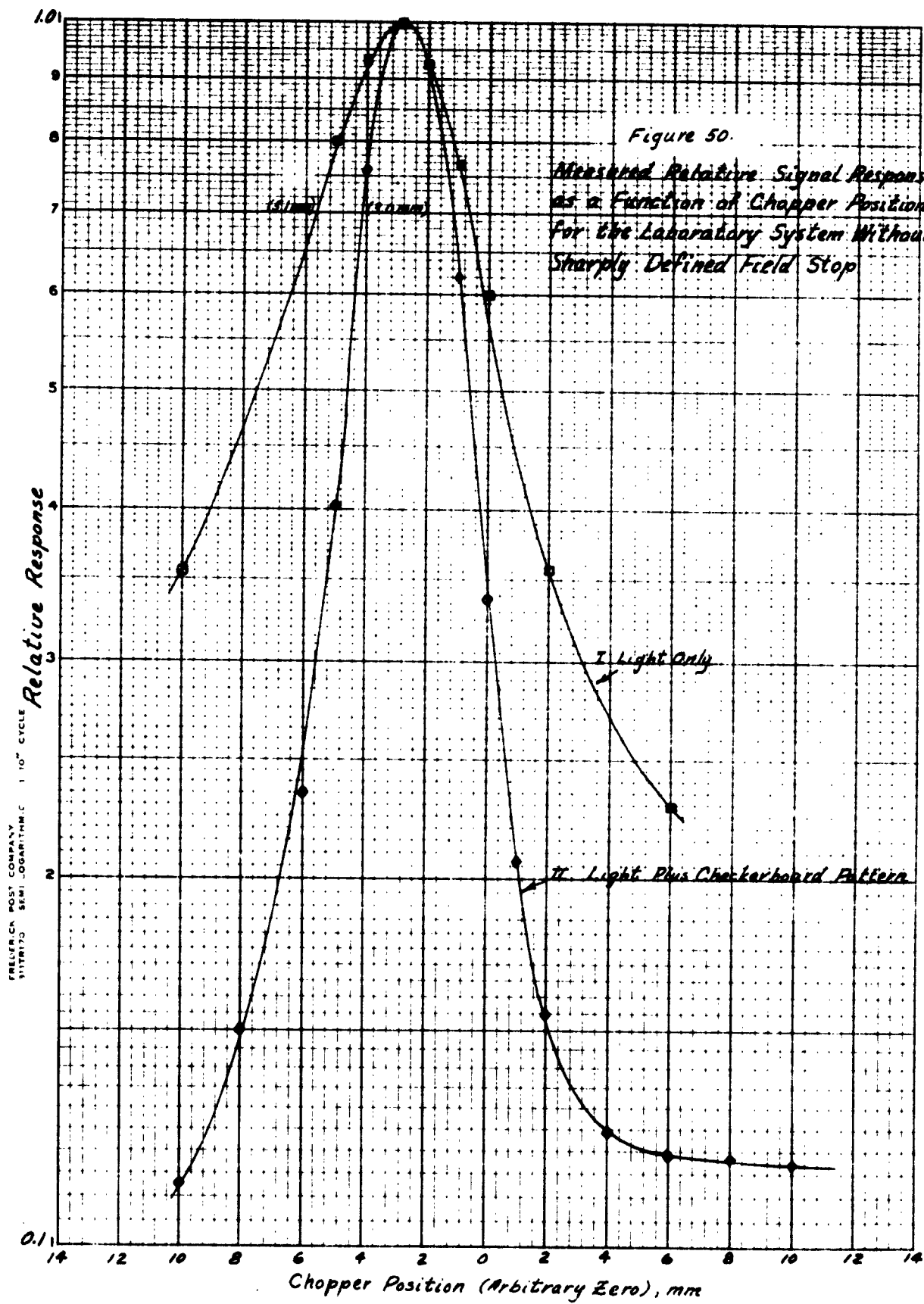
The rms output signal was recorded as the objective lens was moved along the optical axis in one-millimeter steps for various target and chopper combinations. Also, other data was obtained by chopping the image both with and without a field stop. These data are plotted in the form of curves normalized to their peak values.

### RESULTS OF SECOND SERIES OF EXPERIMENTS

Figure 49 gives the results of three measurements. Curve I shows the shape of the signal using the new chopper with random dots against the line target. Curve II represents the results using the random chopper and checkboard-patterned target. Curve III represents the results using the spoke chopper and line target. Measurements for all three curves were made using a circular field stop, 1/8 inch in diameter.

Figure 50 shows two curves obtained with no field stop. These experiments were performed in a dark room with a fluorescent lamp as the only source of illumination. Here no actual field stop with sharp edges was used. The edges of the field of view are determined by the falling-off





of illumination provided by the fluorescent lamp against the background. The lamp was enclosed in a shield which tended to direct the light in one direction.

#### DISCUSSION OF RESULTS OF BOTH SERIES

The values of measured and calculated signal-to-noise ratio are considered to compare favorably, and indicate that no significant considerations were neglected in the theoretical performance calculations on the passive ranging system. Closer agreement would have been desirable, but is unrealistic to expect for the following reasons:

1. The actual sensitivity of the off-the-shelf multiplier phototube (Type 931-A) used was not determined. Median values from the manufacturer's handbook were assumed. A different multiplier phototube of the same type could easily have had sufficiently differing characteristics to have affected the results by a factor of 2.
2. The measurement of the target radiance by an uncalibrated light meter yielded a value that could be questioned, certainly, to an accuracy of 50%.
3. The chopper used had slightly irregular line spacing. This chopper was hand-made for the experiment, and extreme precision in its fabrication was not warranted by the accuracy goals adopted in the experimental design.
4. There may have been other contributing factors, also, such as inaccuracies in the assumed values of the reflectivities of the black and white portions of the target, and imperfect optical

**alignment.**

In discussing the shape of the signal curve, it is convenient to denote the width of each curve by the distance between the 3 db points (the places where the curves are down .707 from their peak values). These "widths" are called out in Figures 49 and 50.

Curve I of Figure 49 shows a wide peak of 15.8 mm. This may be compared with the width of the curve in Figure 47, of 8.7 mm. This latter curve was obtained with the same line target and 1/8 inch field stop but the spoke chopper was used. In either case, the fall off from the peak is more gradual than expected, and it can be concluded that chopping of the field stop, which always remains in focus as the objective lens is moved along the optical axis, is contributing to the total signal.

Curves II and III show much smaller widths of about 5.0 mm, slightly narrower than the theoretical curve. Apparently the checkerboard target resulted in significantly more image chopping than did the single line target. Thus while field chopping still exists, it is at a much lower level than the image chopping and the shape of the curve around the peak represents a better picture of the fall off of image chopping. Note the "wings" on curve III which suggest the lower amplitude wings on the theoretical curve.

Curves I and II of Figure 50 show this effect even better. There was no definitive field stop and the target was the shade of a lamp seen against a high contrast circle of light produced on a white background.

Again, a width of about 5.0<sup>mm</sup> was obtained. Against a checkerboard chopper pattern a width of about 3.0 mm resulted. It is difficult to determine how this additional sharpness came about. It would seem that the use of the checkerboard pattern provided a higher image chopping signal, thus effectively lowering some field chopping which is still present. Another reason for the discrepancy is the possibility that the width of the curve, if there is negligible field chopping, does depend to some degree on the detail in the image.

#### CONCLUSIONS

These experiments indicate close agreement between the theoretical signal-to-noise ratio and output amplitude curve and values obtained in practice. They also demonstrate that in the design of a passive ranger based on the location of best focus, field chopping should be minimized. This can be effected successfully by various means. A simple approach should be the use of a field stop that is defined by shaded edges. Another effective means is the use of a field stop and a spoke-type chopper of just the right size so that the edge of one line on the chopper reticle enters the field of view as another leaves. For example, the field stop could be a portion of a sector of the circular chopper, bounded by two arcs concentric with the chopper circle and of smaller radius than the chopper and by two radii of the circle spaced to enclose the same number of black and white portions of the chopper.

Another important consideration in the reduction or elimination of field chopping is the nature of the optical blur. The lens used in the

experiments described gave a good quality image over a wide field angle, such that the field stop was always in good focus. The use of an optical system with good resolution near the axis and poor resolution near the edge of the field would reduce field chopping materially. A parabolic mirror should be ideal for this application.